ISBN 978-82-326-0586-6 (printed version)
ISBN 978-82-326-0587-3 (electronic version)
ISSN 1503-8181

Doctoral theses at NTNU, 2014:337

Marit Irene Kvittem

Modelling and response analysis for fatigue design of a semi-submersible wind turbine

NTNU
Norwegian University of Science and Technology
Faculty of Engineering Science and Technology
Department of Marine Technology

NTNU – Trondheim
Norwegian University of
Science and Technology

Marit Irene Kvittem
Doctoral Thesis

Doctoral theses at NTNU, 2014:337

NTNU

NTNU – Trondheim
Norwegian University of
Science and Technology

Marit Irene Kvittem

Modelling and response analysis for fatigue design of a semi-submersible wind turbine

Thesis for the degree of Philosophiae Doctor

Trondheim, November 2014

Norwegian University of Science and Technology
Faculty of Engineering Science and Technology
Department of Marine Technology

NTNU – Trondheim
Norwegian University of
Science and Technology

NTNU
Norwegian University of Science and Technology

Thesis for the degree of Philosophiae Doctor

Faculty of Engineering Science and Technology
Department of Marine Technology

ISBN 978-82-326-0586-6 (printed version)
ISBN 978-82-326-0587-3 (electronic version)
ISSN 1503-8181

Doctoral theses at NTNU, 2014:337

Printed by Skipnes Kommunikasjon as

Abstract

Offshore wind is seen as part of the solution for reducing the world's dependency on non-renewable sources with CO_2 intensive production processes. Developing wind turbines that float will enable us to harness wind in deep waters, where the winds are strong and less turbulent than over land. It also means that wind farms can be installed in sites where there are fewer conflicts of interest than onshore.

Both wind turbines and floating platforms are well known technologies, but combining them can introduce unexpected interaction effects. A floating wind turbine will experience large loads from wind, waves and rotating blades. These loads will be influenced by each other to a larger extent than for fixed wind turbines, and the interaction needs to be considered in order to predict the loads accurately. By coupling well known aero- servo-elastic and hydro-elastic codes, which was done as a part of this thesis, the interaction effects could be accounted for.

The large, fluctuating loads experienced by a floating wind turbine will cause fatigue damage to the structure, and could be an important design driver. Accurately predicting the fatigue life requires simulating a large number of load cases, and it also requires long simulation durations due to slowly varying loads and stochastic uncertainty. This thesis focuses on methods to reduce the simulation time for fatigue life prediction.

Using a catenary moored, three-column semi-submersible wind turbine with the NREL 5MW turbine mounted on one of the columns as a case study, the following aspects of FWT fatigue analysis were investigated:

- Frequency domain versus time domain analysis.
- Simulation length, number of seeds and bin sizes for selection of environmental conditions.
- Misaligned wind and wave directions.
- Morison versus potential theory for hydrodynamic modelling.

A frequency domain method for finding the variance spectrum for tower base bending moment in moderate environmental was developed and compared to results from coupled time domain simulations. The results showed that applying a frequency domain method including an approximation of dynamic excitation of the first flexible bending mode of the tower and blades, could predict bending moment standard deviations with reasonable accuracy.

The necessary simulation length can be up to 3-6 hours in extreme value analysis for compliant offshore platforms, but a long term fatigue analysis showed that reasonable accuracy can be obtained using shorter simulation lengths and fewer random seeds. It was also indicated that assuming wind and waves to come from the same direction will give a conservative fatigue estimate.

In all the case studies, fatigue was calculated for nominal stress. As the purpose was to study the simulation parameters affecting fatigue life, and not the fatigue life itself, it was assumed that the hot-spot stress amplitudes for the different load components are proportional to the nominal stress.

Proper representation of wave loads could be obtained using Morison's equation, provided that the inertial coefficients were determined separately for each sea state.

Acknowledgements

The research was performed with support from the Norwegian Research Council and industrial partners through the PhD and post doc programme Norwegian Research Centre for Offshore Wind Technology (NOWITECH), at the Centre for Ships and Ocean Structures (CeSOS) at NTNU.

I would like to thank my supervisor, Professor Torgeir Moan, for giving me the opportunity to work with offshore wind turbine research. I have appreciated our discussions, and his perspectives have always provided valuable input to the work as it progressed.

Thanks should also be extended to Adjunct Associate Professor Zhen Gao, for sharing his insights in the field of hydrodynamics and fatigue, and for always showing a genuine interest in helping with big and small questions. Harald Ormberg and Elizabeth Passano from Marintek deserve gratitude for their work with developing Simo-Riflex-AeroDyn, and also Tore Holmås and Reza Taghipour for help with the Usfos+VpOne code in the initial phases of the PhD period. Next, I would like to thank the administration at CeSOS and Institute of Marine Technology for their work to keep everything sailing smoothly.

I had several fruitful discussions, joint projects and out-of-work experiences with my fellow PhD candidates, so great thanks to Erin Bachynski (also for agreeing with me that it was OK to have one more beer on Saturday night even if we were going to work on Sunday morning), Chenyu Luan, Yihan Xing, Madjid Karimirad, Mahmoud Etemaddar, Zhiyu Jiang, Lin Li, Valentin Chaubaud, Morten Pedersen, Wenbin Dong and many other colleagues at CeSOS and the department of Marine Technology at NTNU. A special thanks to Zhenju Chuang, who sisterly shared the confined space called office with me for large parts of my time at MTS (and persistently tried to teach me the basics of Chinese).

I would like to express my gratitude to my parents and sister for their encouragement, and last, but not least to Jabus for being the highlight of my day, every day (and for help with the aerodynamics).

Contents

Nomenclature

Abbreviations

BEM blade element momentum

COD co-directional

DLC design load case

DLL dynamic linked library

DOF degree of freedom

FD frequency domain

FE finite element

FLS fatigue limit state

FWT Floating wind turbine

LWT land based wind turbine

MBS multi body simulation

Mor. Morison

MSL mean sea level

MUL multi-directional

MWL mean water level

NSS normal sea state

NTM normal turbulence model

NWLR normal water level range

NWP normal wind profile model

PDF probability density function

PF potential flow

QS quasi-static

RAO response amplitude operator

SCF stress concentration factor

SDOF single degree of freedom system

SSWT single semi-submersible wind turbine

TD time domain

TLP tension leg platform

ULS ultimate limit state

UNI uni-directional

Greek characters

$\boldsymbol{\kappa}(t)$ retardation function

λ wave length

ω circular frequency

ρ_a air density

ρ_w seawater density

σ axial stress

τ time lag or shear stress

Ω rotor speed

Latin characters

a' radial induction factor

a axial induction factor

d cylinder diameter

$\mathrm{d}D$ drag force

j	stress range bin no. j
$\mathrm{d}M$	pitch moment
m	slope parameter for S-N curve
n_i	number of stress cycles
$\mathbf{r}$, $\dot{\mathbf{r}}$, $\ddot{\mathbf{r}}$	FEM global nodal displacement/velocity/acceleration vector
t	time
u,$\dot{u}$	wave particle velocity/acceleration
$\mathbf{u}$	wave particle velocity vector
x,$\dot{x}$,$\ddot{x}$	local body displacement/velocity/acceleration
$\mathbf{x}$, $\dot{\mathbf{x}}$, $\ddot{\mathbf{x}}$	body motion/velocity/acceleration vector
$\mathbf{A}$	added mass matrix
A	outer area or cross section area of cylindrical cross section
$\mathbf{B}$	linear damping matrix
$\mathbf{C}$	restoring matrix
C_d	quadratic drag coefficient
C_m	added mass coefficient
C_q	quadratic drag coefficient
$\mathbf{C}^S$	FEM global damping matrix
$C_X(\tau)$	correlation function for process X
D	accumulated fatigue damage
D	diameter cylindrical cross section
$\mathbf{F}$	force vector
$\mathbf{A}^\infty$	added mass matrix high frequency limit
$\mathbf{F}^D$	diffraction force vector
$\mathbf{F}^{FK}$	Froude Krylov force vector
$\mathrm{d}F$	Horizontal Morison force per unit length
$\mathbf{F}^{moor}$	force vector from mooring
$\mathbf{F}^{turb}$	force vector from turbine
$\mathbf{F}^{wave}$	wave force vector
$\mathbf{F}^{wind}$	wind force vector
$\mathbf{M}^H$	FEM global added mass matrix
H	wave height
H_s	significant wave height
K	material parameter for S-N curve
$\mathbf{K}^S$	FEM global stiffness matrix
$\mathrm{d}L$	lift force
$\mathbf{M}$	mass matrix
$\mathbf{M}^S$	FEM global mass matrix
M_x	torsional moment
M_y, M_z	bending moment
N_i	number of stress cycles to failure
N_{bins}	number of stress range bins
I_p	polar moment of area
I_y,I_z	second moment of area
N_x	axial force
$\mathbf{R}^{EXT}$	FEM external forces
S	stress range
$S_X(\omega)$	variance spectrum for process X
U_{rel}	relative velocity
T_p	wave peak period
U	mean wind speed
V_y, V_z	shear force

Chapter 1

Introduction

The current chapter gives an overview of the motivation, research context, objectives and scope of the work, lists the papers that form the basis of the thesis and the contributions to the research community. The remaining chapters are devoted to:

Chapter 2:	More about the background of the investigations and a review of previous work in the field.
Chapter 3:	Theory behind modelling and response analysis analysis for fatigue design of floating wind turbines.
Chapter 4:	Results from the case studies performed as a part of the thesis.
Chapter 5:	Conclusions from the case studies and suggestions for further work.

The thesis consists of a collection of 4 papers, which are appended in App. A.

1.1 Motivation

The wind resource is renewable and the process of harnessing wind energy involves very small CO_2 emissions compared to other sources of electrical power. This is why wind energy is seen as an important contributor to reaching the European Union's Renewables Directive; at least 20% of the member countries' total energy consumption should be covered by renewable sources of energy within the year 2020. Limitations in available wind farm sites on land pushes the industry to go offshore, in fact, offshore wind is currently one of the fastest growing maritime sectors [3].

In deep water (> 45m), it is expected that floating wind turbines (FWTs) will be less expensive than bottom supported turbines [79]. A floating substructure also means that wind farms can be installed farther from shore, and thus eliminate problems with visual contamination and noise. Another important advantage of turbines far from shore is stronger and less turbulent wind. Floating wind turbines are comparable to other offshore wind

turbines when it comes to environmental impact, and they have a much smaller impact on global warming than for example a natural gas power plant [103]. Among countries that have most of their offshore wind resources in deep water (more than 100 meters) are the US, Japan, Norway and Portugal [69]. However, FWTs is a young field of research, and no commercial turbines or parks with more than one unit have been installed at the time of writing.

Locating wind turbines in deep water areas with strong wind will necessarily impose large, irregular loads from wind, waves and current on the turbine and its support structure. Due to difficult access, inspection and repair is expensive, and high reliability of the FWT is required for it to be economically feasible. Also, since wind parks consist of several units with the same design and fabrication, the turbines are vulnerable to "common cause" failures. This is why precise prediction of extreme load effects and fatigue damage is important. Numerical modelling and analysis as well as wave tank and prototype testing can be used for this purpose, preferably all three together, in the concept development phase.

Floating wind turbines have to be designed to fulfil criteria with respect to both function and safety. Sufficient resistance of the material, connections and other components has to be ensured, in addition to floater stability. This is covered by the Ultimate Limit State (ULS) criterion, the Fatigue Limit State (FLS) criterion and the Accidental Limit State (ALS) criterion. Functional criteria are covered by the Serviceability Limit State (SLS), which involve requirements to for instance power production, corrosion protection and nacelle accelerations. The focus in this thesis will be on motion and fatigue failure.

Fatigue Limit State (FLS) refers to failure during cyclic loading, and the fatigue life is defined as the predicted time before failure due to fatigue. Wind turbines in offshore environments will experience cyclic loading and dynamic resonance effects from wind, waves and rotating machinery, and thus fatigue must be addressed. In order to give a realistic estimate of the fatigue life, stress histories must be predicted for all relevant environmental conditions that can be experienced by the FWT throughout its lifetime. This is a challenging task, due to several causes:

- Simulation tools for FWTs are in the developing stage.
- There is limited knowledge of the load effects on FWTs and the implications for fatigue.
- A large number of design load cases and environmental conditions have to be included in the FLS analysis.
- The return periods typically used as basis for wind- and wave statistics are different.
- Time domain analysis are recommended due to non-linear effects and coupling between response to wind and wave loading, and time domain analysis can be very time consuming.

Since FWTs are new to both the research community and the industry, so far only limited

FLS studies have been performed. This thesis focuses on the establishing and applying numerical analysis tools in the FLS design of floating wind turbines, seeking efficient methods to predict the fatigue life.

1.2 Research context

This research was performed as a part of the PhD and post doc programme Norwegian Research Centre for Offshore Wind Technology (NOWITECH), work package 3 - *Novel substructures for offshore wind turbines*. The work was carried out at Centre for Ships and Ocean Structures (CeSOS) at NTNU in Trondheim.

1.3 Objectives

Response analysis for FLS design of FWTs has to cover many design load conditions (DLC), and within each DLC many environmental conditions. Stress analysis for FLS involves modelling non-linear and highly dynamic responses to both deterministic and stochastic loads, and requires sophisticated analysis tools and long simulation time. The author is not aware of any full FLS design of a FWT to this date (a review is given in Chap. 2), which is presumably because it is such a comprehensive task. For this reason it is important to assess the necessary level of refinement of the analyses, i.e. modelling details, number of load cases and analysis methods. Also, since there are many limitations to how much detail numerical models can include in simulation tools, it is important to check the validity of different theories and compare them.

Two questions are put forward here, where RQ1 covers a broad aspect of topics and RQ2 is partly a sub-question of RQ1. The underlying objective of these questions is to look at areas where simplifications of the response analysis can be made, without compromising the quality of the fatigue predictions. The following research questions form the basis for the thesis:

- RQ1: How should loads and structural response be modelled in order to properly predict the fatigue life of a floating wind turbine?
- RQ2: Can simplifications in the analysis be made in order to make the FLS analysis more efficient?

At the time this project started, there were no standards or guidelines for design of FWTs. During the course of this project, a few guidelines have been published [1, 27], but these reflect the lack of experience with mass production of FWT units and long term operation and maintenance of FWT farms. The reason for this is simply that the development of FWT is still in the research stage; only a couple of prototypes exist world wide, and no commercial wind farms using floating foundations for turbines have been installed yet.

This thesis aims to contribute to design guidelines, by studying the global mechanisms that cause fatigue and by trying to come closer to defining a set of requirements for FLS design.

1.4 Scope

The research questions were investigated using a semi-submersible wind turbine as the basis for case studies, and focus was kept on fatigue in the support structure. The detailed studies described in the papers cover:

- Requirements for hydrodynamic modelling. Morison versus potential theory with diffraction for calculation of wave forces on a SSWT.
- Effect of simulation length, stochastic sample and bin size for selection of environmental conditions for response analysis for FLS design.
- Effect of misaligned wind and waves in fatigue analyses.
- Linearised frequency domain analysis versus non-linear time domain analysis for fatigue damage calculation.

A part of estimating fatigue damage is developing a numerical model to perform the response analyses with. Development of FWTs was at an early stage, and no computer codes suitable for the purpose existed at the beginning of this project. Thus, developing a numerical tool and building a model in this also became part of the scope of this project.

The title of the thesis is *Modelling and response analysis for fatigue design of a semi-submersible wind turbine* since the main focus is on the global dynamic analyses. Thus, no local stress concentration factors (SCF) have been used in the investigations.

A semi-submersible floater with a single wind turbine (SSWT) placed on one of the three columns was used in the study. The columns are connected by braces and four catenary mooring lines. The word “turbine" is used throughout the thesis to describe the tower and the rotor-nacelle assembly.

1.5 Papers and declaration of authorship

The following papers [57, 59, 8, 60] form the scope of this thesis.

P1 Marit I. Kvittem and Erin E. Bachynski and Torgeir Moan: *Effects of hydrodynamic modelling in fully coupled simulations of a semi-submersible wind turbine*, Elsevier Energy Procedia, vol 24, p.351-362, 2012

Relevance to this thesis: This paper presents the first analyses performed with Simo-Riflex-AeroDyn. It also compares the response of a SSWT to Morison type wave forces and the response to potential theory forces including diffraction.

My contribution: This paper is the result of a cooperation with Erin E. Bachynski. I laid out the basic structure of the coupling between Riflex and AeroDyn, did some contributions to the programming and testing of the software and performed the wave-only analyses. The coupled analysis was a collaborative effort.

P2 Marit I. Kvittem and Torgeir Moan: *Time domain analysis procedures for fatigue assessment of a semi-submersible wind turbine*, under review for Journal of Marine Structures, 2014

Relevance to this thesis: The paper describes a long-term fatigue analysis of a SSWT tower and braces, focusing on the effect of simulation duration, number of realisations and bin size for selection of environmental conditions for FLS design.

My contribution: I performed a new design of a SSWT based on the WindFloat concept to obtain more detailed information than what was available. All the analyses and the post processing of the results were carried out by me.

P3 Erin E. Bachynski, Marit I. Kvittem, Chenyu Luan and Torgeir Moan: *Wind-wave misalignment effects on floating wind turbines: motions and tower fatigue damage*, to be published in Journal of Offshore Mechanics and Arctic Engineering in November 2014

Relevance to this thesis: The paper compares the effect of misaligned wind and waves on short term fatigue damage for four different FWT concepts; a spar, a TLP and two SSWT concepts.

My contribution: The study was a cooperation between Erin E. Bachynski, Chenyu Luan and myself. The paper was initiated and written by E. E. Bachynski. C. Luan and I participated in determining the analysis methodology and discussing the results. I performed the analyses for one of the SSWT concepts.

P4 Marit I. Kvittem and Torgeir Moan: *Frequency versus time domain for fatigue analysis of a semi-submersible wind turbine*, accepted for publication in Journal of Offshore Mechanics and Arctic Engineering 2014
Relevance to this thesis: The paper describes a linearised frequency domain method to estimate tower base bending moment and fatigue damage for a SSWT and compares the results to non-linear coupled wind- and wave simulations.
My contribution: I developed a methodology to calculate bending moments from a frequency domain model of platform motions and to represent flexible dynamics of the turbine and performed the analysis.

1.5.1 Additional papers

The following papers [58, 61, 7, 77] are related to the work with FWT analysis, but are not included as a part of this thesis. The reasons for not including the papers are that they fall outside of the main topic of the thesis or that they are seen as preliminary studies to the more complete papers 1-4. Since the papers still could be of interest to the FWT research community, abstracts for the secondary papers are given in App. B.

P5 Marit I. Kvittem, Torgeir Moan, Zhen Gao and Chenyu Luan: *Short-term fatigue analysis of semi-submersible wind turbine tower*, Proceedings of the 30th International Conference on Ocean, Offshore and Arctic Engineering, Rotterdam, The Netherlands, 2011

P6 Marit I. Kvittem and Torgeir Moan: *Effect of mooring line modelling on motions and structural fatigue damage for a semi-submersible wind turbine*, Proceedings of the twenty-second International Offshore and Polar Engineering Conference, Rhodes, Greece, 2012

P7 Erin E. Bachynski, Mahmoud Etemaddar, Marit I. Kvittem, Chenyu Luan and Torgeir Moan: *Dynamic analysis of floating wind turbines during pitch actuator fault, grid loss, and shutdown*, Elsevier Energy Procedia, vol 35, p.210-222, 2013

P8 Torgeir Moan, Zhen Gao, Madjid Karimirad, Erin E. Bachynski, Mahmoud Etemaddar, Zhiyu Jiang, Marit I. Kvittem, Made Muliawan and Yihan Xing: *Recent developments of the design and analysis of floating wind turbines*, ISCOT: Developments in fixed & floating offshore structures, Busan, South Korea, The Royal Institution of Naval Architects, 2012.

1.6 Main contributions

The main contributions of this thesis to the floating wind turbine research community are listed in this section. The relations between research questions, papers and contributions are illustrated in Figure 1.1.

C1 A numerical tool for coupled analysis of floating wind turbines. Existing softwares Riflex and AeroDyn were coupled through a dynamic linked library (DLL).

The DLL developed by PhD candidate Erin E. Bachynski and the author provided a coupling between state-of-the-art simulation tools and the possibility of performing analysis with a turbulent wind field, where turbine and platform response is fully coupled. The performance of the tool was verified for a land based turbine and a spar wind turbine with good agreement with other wind turbine analysis codes [84].

C2 Development of a simplified method to assess fatigue damage for the tower base of a SSWT based on linear frequency-domain methods.

The linearised frequency domain analysis developed to calculate variance spectra for tower base bending moment gave bending moments with reasonable accuracy for a limited selection of intermediate environmental conditions. A generalised degree of freedom model applied to account for excitation of the first flexible mode of the turbine increased the accuracy. Applying the bending moment model for calculation of fatigue gave increased errors due to the exponential relationship between stress ranges and fatigue damage in a Wöhler curve approach.

C3 Knowledge about the effect of diffraction forces for a SSWT with column diameters of 10 m and heave plates, and a proposed method to numerically determine the added mass coefficients in the Morison type forces.

It was found that for the SSWT studied in the thesis, the relative importance of viscous forces and diffraction forces is comparable to what can be found for a fixed cylinder, provided that the correct inertial coefficients in the Morison formulation are applied. For a fixed cylinder, diffraction effects become important for diameter to wavelength ratios above 0.14. Inertial coefficients had to be chosen based on the wave period for short waves, and could not be assumed to be the same for every wave condition. Analytical force transfer functions for including dynamic pressure in Morison models for a three column semi-submersible were derived and applied with success.

C4 Investigations of required simulation lengths, number of realisations and bin size for selection of environmental conditions for FLS design of FWTs.

The accuracy of using shorter than 3 hour simulation length and fewer than 10 stochastic seeds for response analysis for long term fatigue damage for a semi-submersible was studied. Fatigue damage in the tower base was found to be less sensitive to simulation length than in the main beams, pontoons and braces, but calculating damage based on 1-hour simulations gave less than 4% error compared to using the 3-hour simulations. Reducing the number of random seeds also gave acceptable accuracy compared to using 10 random samples.

C5 Knowledge about the effect of applying wind and waves from different directions on motions and in FLS design of different concepts of FWTs.

Wind and waves coming from the same direction gave higher fatigue damage than the misaligned cases. Even though increased wave induced motions were observed for misaligned cases, the fact that wind and wave forces acted around different axes gave a better distribution of stress around the circumference of the tower and thus reduced the fatigue damage. The concept comparison showed that a semi-submersible with large mass performed best with respect to motions and fatigue damage compared to a semi-submersible with less inertia, a TLP and a spar buoy.

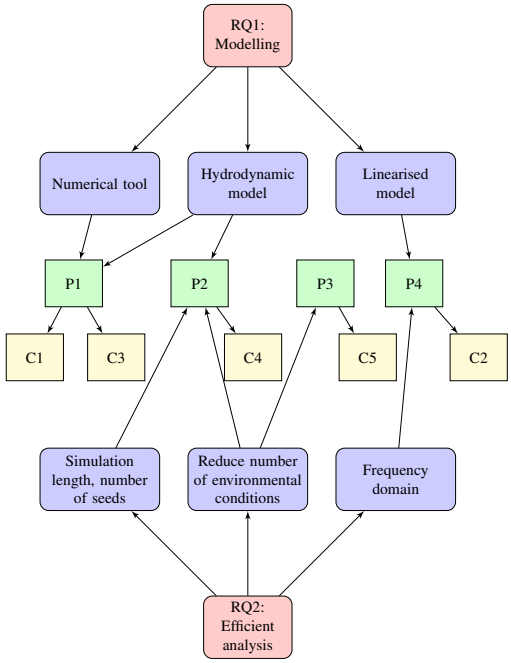

Figure 1.1: Relations between research questions, papers and contributions.

Chapter 2

Background

The general background for the investigations is described in this chapter. A brief introduction to the various types of foundations for floating wind turbines is given, followed by a review of the state-of-the-art in the field of design and modelling of floating wind turbines, with emphasis on fatigue design and numerical simulation tools.

2.1 Floating wind turbine concepts

Development of floating concepts is still at an early stage. There are currently three full scale prototype floating wind turbines in operation; Hywind spar in Norway [69, 96], WindFloat semi-submersible in Portugal [69, 93, 92] and a downwind semi-submersible off the coast of Fukushima, Japan [83]. There are also a number of concepts installed in smaller scale in wave basins and in full scale environments [69].

In principle, most proposed concepts combine known technology for onshore turbines mounted on floating substructures known from offshore oil and gas technology. Some of the suggested floating support structures are [99]:

- Ballast stabilized spar-buoy with catenary mooring with one turbine (Hywind)
- Single tension leg moored spar with one turbine (Sway)
- Multiple tension leg moored semi-submersible with one turbine (Blue H, Pelastar)
- Semi-submersible with catenary mooring and one or multiple turbines (WindFloat, Winflo, HiPR Wind, WindSea)

While most proposed concepts use horizontal axis upwind turbines, some use less traditional turbine technology, like two-bladed rotors (Winflo) or vertical axis turbines (Vertiwind). There are also concepts that combine wave energy converters with wind turbines on floating platforms (Pelagic Power, Poseidon).

(a) Winflo

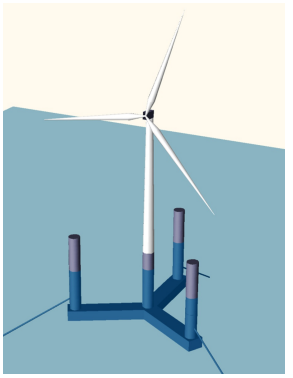

(b) CSC

(c) Hywind

(d) Pelastar

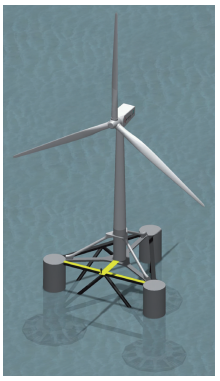

(e) HiPRWind

(f) WindFloat

Figure 2.1: Floating wind turbine concepts. Images were downloaded from project web pages [88, 21, 4, 96] or received from project owners (Principle Power and CSC braceless semi-submersible from NTNU).

Due to the cost of a floating foundation, it is expected that floating platforms must support turbines with an effect larger than what is normal for onshore and offshore bottom fixed turbines today. Although the full scale prototypes do not carry turbines larger than 2.3 MW, it is normal to assume at least 5 MW for commercial installations. In 2009 Jonkman et. al [49] developed data for a generic 5 MW horizontal axis upwind turbine (NREL 5 MW baseline turbine), which has been widely used in the research community for analysis of offshore wind turbines. In the IEA Offshore Code Comparison Collaboration Phase IV (OC3) [42], where numerical aero-hydro-servo-elastic codes were compared in analysis of a spar wind turbine, a tower suited for floating wind turbines was developed. This tower is 10 m shorter than the original NREL 5 MW turbine, and is assumed to be mounted 10 m above sea level, to maintain a hub height of 90 m.

2.1.1 Semi-submersible wind turbines

A semi-submersible platform achieves stability by water plane stiffness, but also to some extent by ballast in the columns or pontoons. Compared to a spar buoy, that obtains stability by having a deep draught ballasted substructure, it has a significantly lower draught, and is thus a more flexible concept when it comes to suitable water depths, installation and transport. A spar WT either needs deep harbours and seaways to be towed from the yard to the installation site, or a more sophisticated transportation- and installation method than what exists today. The shallow draught of a semi-submersible makes it suitable for intermediate water depths, and for shallow water assembly yards.

The case studies in the thesis were carried out for a three-column SSWT with the NREL 5MW on the OC3 Hywind tower [42] placed on one of the columns, a concept inspired by the generic WindFloat [93] (see Figure 2.1). The station keeping system for the generic WindFloat consists of four catenary mooring lines anchored to the seabed, where two of the mooring lines are connected to the column with the turbine, and one mooring line is connected to each of the other two columns.

The WindFloat platform has an active ballast system to keep the turbine upright (see Figure 2.2) and thus maximise power output as the wind direction and intensity change. This is done by pumping water ballast between the columns, and the system has a reaction time of 20 minutes to significant changes in the mean wind speed and direction.

Another semi-submersible WT that has been frequently used in FWT studies, for instance in IEA Offshore Code Comparison Collaboration Phase II (OC4) [91], is the DeepCwind concept. Compared to WindFloat and the semi-submersible studied in this thesis, it also has three main columns and catenary moorings, but the turbine is placed on an additional central column, and the displacement is close to three times higher. The DeepCwind concept was used in the study of misaligned wind and wave conditions in Paper 3 [8] , together with the SSWT used in Papers 1-4 [57, 59, 8, 60] and two other concepts.

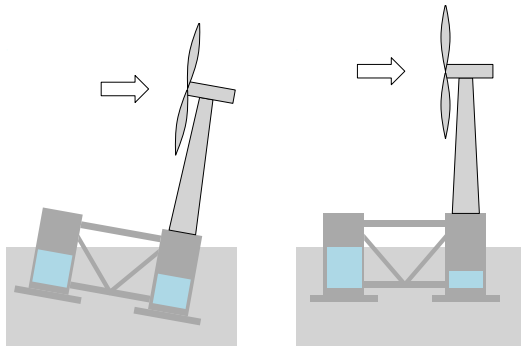

(a) Unballasted platform with turbine in operation.

(b) Ballasted platform with turbine in operation.

Figure 2.2: Illustration of ballast system.

2.2 Design and analysis of floating wind turbines

2.2.1 Design load cases

Since the field of floating wind turbines is new, only design of prototypes has been performed. This means that designs may not be optimised designs, since the prototypes are built to gain experience. Also, since there were no guidelines or standards that applied to FWTs until recently, there was no defined set of load cases to run through in a design process.

As mentioned in Chap. 1, FWTs have to be designed after Ultimate Limit State (ULS), Accidental Limit State (ALS), Fatigue Limit State (FLS) and functional requirements (often grouped under Serviceability Limit State). The largest load experienced under harsh environmental condition is normally defined under ULS, whereas loads due to accidental events, for instance ship collisions or explosions, fall under the definition of an ALS. FLS covers accumulated crack growth under cyclic loading in normal environmental conditions.

The IEC 61400-3 standard for bottom fixed offshore wind turbines specifies a minimum set of design load conditions for ULS and FLS. These consist of the conditions power production, power production plus fault, start up, normal shut down, emergency shut down, parked, parked plus fault and transport assembly and repair. For each of these conditions, a subset of load conditions with the wind and wave condition and directionality, currents, water level, limit state and partial safety factor for each of the load conditions in the subset. For the full table of load cases, refer to [40, Chap. 7]. The load cases valid for FLS are shown in Table 2.1. All the requirements for bottom fixed wind turbines are not necessarily relevant for FWT design, while additional requirements apply in the DNV Offshore

Standard [27], for example requirements with regards to stability, mooring and anchoring. The compliant nature of an FWT means that the recommended values for parameters like length of extreme operating gust, wind and wave return periods or wave spectrum can not be transferred directly from bottom fixed design codes. Other design load cases than those specified in the IEC standard [40] may be governing.

Table 2.1: Design load cases in IEC [40] relevant for fatigue limit state.

Name	DLC	Wind	Wave	Wind/wave dir.	Current	Water level
Power production	1.2	NTM	NSS joint PDF	COD, MUL	No current	NWLR or $\geq$ MSL
Power production plus fault	2.4	NTM	NSS $H_s = E[H_s\|V_{hub}]$	COD, UNI	No current	NWLR or $\geq$ MSL
Start up	3.1	NWP	NSS(or NWH) $H_s = E[H_s\|V_{hub}]$	COD, UNI	No current	NWLR or $\geq$ MSL
Normal shutdown	4.1	NWP	NSS(or NWH) $H_s = E[H_s\|V_{hub}]$	COD, UNI	No current	NWLR or $\geq$ MSL
Parked	6.4	NTM	NSS joint PDF	COD, MUL	No current	NWLR or $\geq$ MSL
Parked plus fault	6.4	NTM	NSS joint PDF	COD, MUL	No current	NWLR or $\geq$ MSL
Transport, assembly, maintenance and repair	6.4	NTM	NSS joint PDF	COD, MUL	No current	NWLR or $\geq$ MSL

Jonkman [51] ran through the ULS DLCs for power production in the IEC 61400-3 standard for one FWT (barge) and one land based wind turbine (LWT), and compared the results. No capacity evaluation was performed, but quantification of the ratio between floating and land based response parameters showed that design loads were expected to be higher for the barge FWT than for the LWT. Pitch motion and inertia loads were pointed out as the driver for these differences. He also showed that the design driving load conditions are not necessarily the same for FWTs and LWTs; i.e. the normal turbulence models

were worse than the extreme operating gusts for the barge, whereas it was vice versa for the LWT turbine.

A more comprehensive concept comparison running through both ULS and FLS for the normal operational conditions of the IEC-standard for six different FWT concepts was performed by Robertson and Jonkman [90]. The conclusion was the same as in [51], that increased pitch and roll motions increase the design loads.

Karimirad and Moan [54] compared tower forces for a spar FWT in the operational condition with maximum thrust force, to idling conditions in a harsh environment, and found that the forces can be 2.3 times higher for the harsh environment condition, due to large wave induced response in harsh sea states. Jiang et. al. [44] compared turbine transient loads due to blade pitch system fault, grid loss, and shutdown events for a spar and for a land based turbine. The work indicated that the increase in tower and blade forces during a fault event was smaller for a FWT than for a LWT.

2.2.2 Fatigue limit state for floating wind turbines

Fatigue damage is known to be a problem for bottom fixed offshore wind turbine substructures, and is also expected to be significant for floating wind turbines (FWTs). Adequate fatigue strength should be ensured by design as well as by inspection and repair. Wind parks consist of units with similar designs, and are thus vulnerable to “common cause" failures, which means that the economic consequences of poor fatigue design are serious. It is important, therefore, to make good fatigue estimates early in the design process.

How comprehensive a fatigue damage analysis of a structure is, depends on the number of load cases, the nature of the structural response to varying loads, the level of stochastic uncertainty in the load models, the complexity of the detailed geometry and the response analysis tool.

Unlike structural failure during extreme load conditions, fatigue cracks can also grow under benign environmental conditions, which means that every event that can possibly cause crack- initiation and growth must be included in the analysis. For a traditional offshore structure, that does not have significant dynamic response to turbulent wind, environmental conditions for fatigue analyses are taken from scatter *tables* of two parameters; significant wave height and wave peak period. When wind is introduced as a third parameter, environmental conditions are found in a scatter *block*, which dramatically increases the number of load cases. Other parameters that further increase the number of load cases necessary for fatigue analysis are wind- and wave directions, current and operational state of the turbine.

To make accurate predictions, fully coupled time domain analyses should be performed, but this is a challenging task. Firstly, at the beginning of this project, the number of available and suitable analysis tools was limited. Secondly, such analyses are quite time consuming, and a fatigue analysis ends up altogether being an extremely time consuming

process. This is why it is important both to assess the validity of the theories available in computer codes today and to investigate the impact of measures for reducing the computation time for fatigue analysis.

There has been a couple of FLS studies for FWTs so far. As mentioned in the previous subsection, Robertson and Jonkman [90] found that floater motion gave increased fatigue damage compared to the land based case. This effect was particularly visible for fatigue damage in the tower base. Haid et. al [35] studied the effect of simulation length on fatigue and ultimate loads for the OC3 spar buoy wind turbine, and concluded that the fatigue damage in the tower, blades and mooring system was more sensitive to the treatment of residuals in rainflow cycle counting than to simulation length. Recent studies of a spar FWT by Jiang et al. [45] showed that the contribution to blade, tower and mooring line fatigue damage in transient fault conditions can be minimal if the appropriate shutdown procedure is used.

A structural analysis including fatigue of the WindFloat platform was presented in [5, 92]. An analysis covering 12 different sea states gave a fatigue life of 36 years for a stress concentration factor (SCF) of 2.0 for the braces in the platform and a fatigue life of 15 years for an SCF of 6.0 for the tower base. No SCF based on weld geometry was determined in these analyses, but a sensitivity study calculating fatigue based on different SCFs was performed. These calculations did not include the cyclic rotor loads from turbulent wind and rotating blades, but the study showed that fatigue may be a critical limit state for floating wind turbines.

The FLS studies that have been performed so far, do not contain the full number of environmental conditions that the IEC-standard specifies. In [90, 75, 35] only one set of waves is combined with each wind speed, whereas the standard specifies that a bin sizes of 2 m/s wind, 0.5 m for wave heights and 0.5 s for wave period shall be applied to the joint probability distribution [40].

Frequency domain analysis for fatigue

Fatigue analysis for wind turbines is normally performed in the time domain. For a semi-submersible WT, interaction between rotor and platform motion and non-linearities due to viscous forces, catenary mooring lines and large deflections make time-domain analysis necessary. However, the solution process of a non-linear time domain finite element system with many degrees of freedom is very time consuming, and is not ideal for long term fatigue analysis, which requires consideration of many environmental conditions. Frequency domain methods are significantly faster and are also recommended in guidelines [24] for fatigue analyses of oil platforms subjected to wave loads.

Frequency domain methods have also been applied in the fatigue analysis of bottom fixed offshore WTs. Kühn [55] investigated simplified analysis methods for fatigue calculation for offshore bottom fixed monopile turbines, where the wave response was performed by linear spectral analysis. Van der Tempel [100] performed support structure response anal-

yses in the frequency domain with spectral analysis for both wind and wave response, and got acceptable accuracy compared to time domain simulations and full scale measurements. In these studies, the wave and wind loads were treated separately, which can be a valid assumption for a fixed, but not necessarily for a floating wind turbine, since there is a stronger interaction between wave- and wind induced responses. Both Kühn and Van der Tempel emphasized the importance of including the aerodynamic damping due to an operating turbine in simplified modelling.

A couple of studies have used frequency domain for FWT analysis. Bachynski [9, 6] applied the procedure of Wayman et. al [102], added a wind response model, and studied the applicability of frequency domain methods in the early concept development phase of tension leg platform wind turbines. The conclusion of these studies was that the accuracy was too low to use for concept development, since they gave a poor representation of low-frequent response and since flexible modes of tendons, tower and blades were not considered. The wave frequency motions and accelerations were captured quite well.

A comparison between frequency and time domain wave response analyses for a barge type floating wind turbine was conducted by Philippe et al. [86], with good results for surge, pitch and heave motions. Other studies applying frequency domain analysis for floating wind turbines have been reported in [14, 67, 101].

The above mentioned studies for FWTs did, however, not consider fatigue. Although the frequency domain method has limitations, in particular for FWTs, it can be a useful tool in performing early stage design assessments. Such an approach can be easier to understand than numerical models for time domain analysis, and makes isolating the effect of different physical factors easier.

2.2.3 Model tests

A first step in design is to have an analysis tool that can be used to run all the necessary load cases. Such a tool needs to be verified in order to be suitable for design, both against scaled model tests and full scale measurements. However, since the hydrodynamic Froude scaling, geometric similarity and the aerodynamic Reynolds scaling are difficult to match in the same model, scaling up the results properly is difficult. However, efforts have been made to get reasonable scale models [34, 19].

A 1:47 scale model test for the Hywind concept was performed in the Marintek ocean basin. These model tests were first compared to Simo-Riflex coupled to a simplified thrust force model by Nielsen et. al. in 2006 [81]. In 2007 Skaare et al. [95] compared these model tests to a model with state-of-the-art aerodynamics by using Simo-Riflex coupled to Hawc2, with good agreement.

In a paper by Goupee et al. [34], a concept comparison of three concepts of FWTs (spar, TLP and semi-submersible) is performed with scaled model tests (1:50) in the Marin ocean basin. The University of Maine DeepCwind program followed up these model tests

by using them for calibrating simulations in Fast [19, 97]. The semi-submersible used in these studies was the DeepCwind platform.

2.2.4 Software for dynamic response analysis of floating wind turbines

Numerical analysis tools that have been applied in FWT research so far has been developed from existing tools, either software for land based turbines or software for offshore structures. Other tools have been developed from scratch, but do not contain as many features, and still have a way to go on validation. The most widely used software is described below. During the course of this thesis, a number of codes under development have emerged; Table 2.2 shows the current status, as of December 2013, of a selection of available computer codes. At the beginning of this project, none of the existing computer codes were found sufficiently sophisticated to model the SSWT in this project, so a new tool was developed. This will be further described in Sec. 3.1.4.

A code-to-code comparison for FWT software is currently beeing performed in the IEA Task 30 - OC4 Phase 2 [89], for a semi-submersible wind turbine. Task 23 [50] did the same for a spar FWT. Worth mentioning is also the Upwind project, where the capabilities of the FWT softwares that were available in 2010 [18] were summarised.

Two computer codes for dynamic response analysis of FWTs that originate from wind turbine software (Fast and Hawc2) and two that originate from offshore structures analysis software (Simo-Riflex and Usfos) are described below. The descriptions contain the history of development and the status of capabilities of their released version as per December 2013.

Fast

Fast is an open source, publicly available aeroelastic simulation code for two- and three-bladed horizontal axis turbines [43] developed at the National Renewable Energy Laboratory (NREL). It can be coupled to the commercially available FE structural solver Msc.Adams. The aerodynamic forces are calculated by the module AeroDyn, which provides a BEM with various corrections (see [78]) and a GDW option. The structural dynamics are described by a combination of multibody dynamics and modal superposition of pre-calculated mode shapes with small deflections. The number of global degrees of freedom (DOFs) for the entire system in Fast (when it is not coupled to ADAMS) is limited to 24 for a three-bladed turbine. This means, for instance, that the tower lacks the axial and twist DOF, and the blades lack the twist DOF.

In 2004, Withee [104] developed a model for coupled analysis of hydrodynamic and aerodynamic loads using Fast and structural solver Msc.Adams and wave forces based on slender body theory. The hydrodynamic module was later expanded in a cooperation between

Table 2.2: Selected computer codes for analysis of floating wind turbines and their current features as of December 2013 [43, 66, 73, 78, 89]. See the Nomenclature for abbreviations.

Name	Company	Structural model	Aero. model	Hydro. model	Mooring model	Comment
Simo-Riflex	MARIN-TEK	FE	BEM	PF+ Mor.	FE	Currently no yaw bearing. no nacelle drag
Fast	NREL	Modal	BEM+ GDW	PF+ Mor.	QS	No dynamic wake correction for BEM
Usfos+ VpOne	Sway	FEM	BEM	Mor.	FE	
Fast+ OrcaFlex	NREL	FEM	BEM	PF+ Mor.	FE	De-coupled aero- and hydrodynamics
3DFloat	IFE	FEM	BEM	Mor.	FE	No dynamic stall model
Hawc2	DTU	MBS	BEM	Mor.	MBS	

Massachusetts Institute of Technology (MIT) and NREL to include large volume body dynamics, by applying input generated by potential theory software Wamit. This module was included as a Fast module and named HydroDyn. HydroDyn applies the wave forces in the 6 platform DOFs in Fast. A quasi-static non-linear mooring line model, based on look-up tables, was added later [52].

Simo-Riflex

Simo [72] is a simulation tool for floating structures, developed by Marintek and extensively used in the offshore industry. Coupled to Riflex [73], a finite element solver for slender marine structures, they form a software package for non-linear time domain simulation of offshore structures.

The first development of Simo-Riflex with a wind turbine module considered the tower and blades as rigid [32]. Later the wind turbine model was incorporated with flexible elements in Riflex [85, 70], but there were no options for turbulent wind or external control. At the time of writing Simo-Riflex has fully coupled aero-hydro-servo-elastic capabilities, however with the limitations described in Table 2.2. The development performed in relation to this thesis is more thoroughly described in Sec. 3.1.4.

Usfos - VpOne

Usfos [37] is a non-linear static and dynamic FE solver tailored for space frame structures. With a beam element turbine model, coupled to an aerodynamic BEM solver, the software package Usfos-VpOne provides coupled offshore wind turbine analyses. It has been used in the development of the Sway concept [38], and Karimirad et. al. [53] did validation efforts of the Usfos-VpOne for a floating spar-type TLP.

The initial plan was to work with VpOne for a semi-submersible. It was, however, found that since a semi-submersible can fall under the definition of a large volume structure, and since there can be hydrodynamic interaction between the members of the platform, the slender body theory available in Usfos was unfit for the purpose.

Hawc2

Hawc2[66], developed by Risø, has the state-of-the-art capabilities in aerodynamics for land based wind turbine design. The structural model consists of multibody dynamics combined with a linear finite element formulation [18]. Early developments for FWTs included a coupling to Simo-Riflex, but Hawc2 has later been developed to have FWT simulation options as a stand-alone program. Wave forces assume slender body theory and the mooring line model is a quasi-static non-linear force-displacement relationship, however, a FE mooring line model is under development.

Earlier versions of Hawc2 for slender FWTs lacked the dynamic pressure formulations, as can be seen in a code-to-code-comparison between Simo-Riflex and Hawc2 [54], but this has been added later.

Chapter 3

Modelling of floating wind turbines

Structural analysis of FWTs for design in all limit states require dynamic structural analysis, where aerodynamic and hydrodynamic loads and interaction with the controller need to be accounted for. The theory behind the global response analysis methods applied in the case studies is described in this chapter.

3.1 Structural dynamics of FWTs

A floating wind turbine in operation will be experience time varying environmental loads and periodic load variations associated with rotating blades. These loads can cause significant dynamic effects, and a static approach when determining the load effects is not sufficient. Waves, wind and rotating blades cause cyclic loads on the FWT, and cyclic loads can cause fatigue damage in the structure. Secondary effects of currents, i.e. vortex induced vibrations or motions, also cause cyclic loading, but it has not been considered in the case studies.

3.1.1 Equation of motion

The linear equation of motion for a submerged rigid body with 6 degrees of freedom and external forces can be expressed in the frequency domain as in Eq. 3.1 [80]. $\mathbf{F}(\boldsymbol{\omega})$ forces can represent wave forces, mooring forces or other external forces.

$$\big(\mathbf{M} + \mathbf{A}(\omega)\big)\,\ddot{\mathbf{x}}(\omega) + \mathbf{B}(\omega)\dot{\mathbf{x}}(\omega) + \mathbf{C}\mathbf{x}(\omega) = \mathbf{F}(\omega) \tag{3.1}$$

For non-linear systems, solution of the equation of motion must be performed by iteration in the time domain. Equation 3.1 can be transformed to a non-linear time domain model (Eq. 3.2) by using the Cummins equation, which introduces an impulse-response (memory) function into the equation of motion [80, chap.14]. This Duhamel integral is called

the retardation function, is denoted by $\boldsymbol{\kappa}(t)$ and accounts for frequency dependent added mass and linear radiation damping in the time domain.

$$(\mathbf{M} + \mathbf{A}^{\infty})\,\ddot{\mathbf{x}}(t) + \int_0^t \boldsymbol{\kappa}(t-\tau)\dot{\mathbf{x}}(\tau)\,\mathrm{d}\tau + \mathbf{C}\mathbf{x}(t) = \mathbf{F}(t) \tag{3.2}$$

3.1.2 Non-linear FEM

Finite element analysis (FEM) is a numerical method that, when applied in structural analysis, approximates the solution of the differential equations for displacement by dividing the structure into smaller elements with a reduced number of displacement patterns.

Non-linear FEM refers to solution methods that take the effects of large displacements, non-linear material behaviour or changing boundary conditions into account. These effects introduce a memory effect, and traditional structural mechanics principles like superposition of loads and responses are no longer valid. Non-linear formulations of loads also introduce non-linearities, but these are not addressed in this section.

In floating wind turbine modelling, the relevant non-linearities are related to geometric structural non-linearities, i.e. the effects of large displacements, and quadratic load formulations in the thrust and drag forces. The current section briefly addresses the geometric non-linearities and the solution methods inherent in structural FEM solver Riflex.

The non-linear equation for dynamic equilibrium of a system of finite elements can be expressed by global matrices that contain the mass, damping and stiffness properties of the finite elements (Eq. 3.3) [73]. External forces can typically be weight, buoyancy, forced displacements from attached bodies ($\mathbf{x}$,$\dot{\mathbf{x}}$ and $\ddot{\mathbf{x}}$ in Eq. 3.2), viscous drag and wave acceleration terms from Eq. 3.6 and wind forces from AeroDyn.

$$\left(\mathbf{M}^S + \mathbf{M}^H\right)\ddot{\mathbf{r}}(t) + \mathbf{C}^S\dot{\mathbf{r}}(t) + \mathbf{K}^S\left(\mathbf{r}(t)\right) = \mathbf{R}^{EXT}\left(\mathbf{r}(t), \dot{\mathbf{r}}(t)\right) \tag{3.3}$$

Geometric non-linearities can be particularly important for wind turbines with large deflection of the blades and in mooring lines. The non-linear dynamic solver applies implicit integration for increments of time; a Newmark-β method, to find the dynamic equilibrium at every timestep [73]. The parameters in this method control the accuracy, numerical stability and numerical damping of the integration method [17]. This displacement driven method allows unlimited displacements, but assumes small strains.

3.1.3 Coupled analysis

If an FWT is regarded as separate components; the floating platform and the wind turbine, response analysis can be performed with software and analysis methodologies that

are well known within the respective offshore- and wind industries. Handling the substructure and the wind turbine separately is often done for bottom fixed offshore wind turbines. However, when considering a floating platform, moorings and a flexible turbine separately, important coupling effects can be ignored.

The submerged part of a floating platform is normally analysed by rigid body dynamics. Moorings are modelled by flexible, slender FEM. The solvers are thus separate, and individual analysis of the floater and the moorings will not include the interaction between the two. For coupled analysis, information must be passed between the two solvers at every time step of the analysis.

For a floating wind turbine, coupling effects are important. Coupling effects in this context are:

- Aerodynamic damping from the rotor on floater motion
- Platform motions influence the wind force
- Mean position of the platform influences wind force and mooring force
- Mooring line dynamics (inertia and damping) influences platform motion

In a coupled analysis, the rigid body and the flexible elements are connected at common nodes. The motion equilibriums for the flexible element system and the rigid body are solved individually, but simultaneously, in time domain, exchanging external forces and displacements at every timestep [74]. Iteration is used at every timestep to achieve equilibrium for both equations.

The force vector ($\mathbf{F}(t)$ in Eq. 3.2) for a rigid platform with catenary mooring lines and a turbine in a coupled model, contains non-linear restoring, inertia and damping from the mooring lines, wave forces, wind forces and inertia and damping forces from the turbine (Eq.3.4). All the forces are functions of platform motions, velocities and acceleration, in addition to time. If one assumes 1st order wave excitation, wave forces are only a function of time. As mentioned in the previous section, $\mathbf{R}^{EXT}$ in Eq. 3.3 contains forced displacements, velocities and accelerations from the rigid platform in the coupled solution.

$$\mathbf{F}(t) = \mathbf{F}^{moor}(t) + \mathbf{F}^{wave}(t) + \mathbf{F}^{wind}(t) + \mathbf{F}^{turb}(t) \tag{3.4}$$

3.1.4 Development of a new analysis tool

At the start of this project, none of the software listed in Sec. 2.2.4 could provide a sufficiently sophisticated combination of structural model, hydrodynamics and aerodynamics to model a semi-submersible wind turbine. The Fast [43] package was the most complete option, but it did not include a dynamic mooring line model or the option of vertical Morison members. The SSWT used in the studies throughout this thesis has catenary mooring lines and heave-plates, which makes these features important.

Another option existed, namely Marintek's Simo-Riflex windturbine code. At the time, it was being extended from representing the tower and blades as rigid to flexible structures using FEM, i.e. going from a Simo-model of the turbine to a Riflex model. However, the in-house blade element momentum (BEM) model was not validated, external controllers were not possible and only constant wind could be applied. Nevertheless, since coupled analyses with Simo-Riflex had been successfully performed by the offshore industry for analysis of floating structures for years, and since close cooperation with Marintek was possible, it was decided to develop this tool further. The open source aerodynamic Fast-module AeroDyn [62], developed by NREL, is a stand-alone code that had earlier been coupled to structural analysis software Msc.Adams [63] and SimPack [36]. AeroDyn was found suitable for coupling to Riflex, since it is a widely used and validated code that can read turbulent wind fields generated by TurbSim [48].

In cooperation with Elizabeth Passano and Harald Ormberg from Marintek, PhD candidate Erin E. Bachynski and the author developed a dynamic linked library (DLL) that at the beginning of every timestep passes nodal positions, orientations and velocities from Riflex to AeroDyn and sends the aerodynamic nodal loads from AeroDyn back to Riflex.

Simo-Riflex-AeroDyn

The fully coupled aero-hydro-servo-elastic simulation tool Simo-Riflex linked to AeroDyn comprises all the aerodynamic features of AeroDyn [78]. The module receives nodal velocities, orientations and positions from Riflex through the DLL, reads the local wind velocity from a turbulent wind field box generated by TurbSim (or a defined constant wind speed), iterates to find the induction factors, calculates the element loads based on BEM (see Sec. 3.2.2), and returns the forces as nodal blade loads back to Riflex through the DLL. Figure 3.1 illustrates the role of the DLL in this procedure. Validation work for Simo-Riflex-AeroDyn is presented in [84] and in Paper 1 [57].

AeroDyn and DLL features worth mentioning are:

- Tower shadow model
- Tip, root and hub loss (Prandtl)
- Skewed inflow correction (Pitt-Peters)
- Generalised dynamic wake (GDW) option (dynamic inflow)
- Dynamic stall (Beddoes-Leishman)
- Wind shear

In Riflex, the tower and blades are modelled as lines of beam elements between supernodes. The lower tower node is connected through a master-slave DOF to the rigid body in Simo. There is also a master-slave dependency between the tower top and the shaft. The shaft is modelled as two beam elements with high stiffness, and the connetion between

them is the rotational spring in which generator torque is applied. The same type of connection is used for the pitch actuators in the nodes between the hub element nodes and the first blade nodes. The hub elements are also modelled as beams with high stiffness, and they are rigidly connected to the low speed shaft. Figure 3.1 shows the layout of the Riflex turbine model.

The blade elements are defined by their structural properties in Riflex, including structural twists around the blade axis. Modelling of centres of gravity that are eccentric to the structural axis is, however, not possible. Aerodynamic properties, i.e. aerodynamic coefficients and aerodynamic twist, are specified in AeroDyn.

The masses and inertias of the hub and the nacelle are modelled by rigid bodies connected by a master-slave connectivity to the low speed shaft and the tower top, respectively.

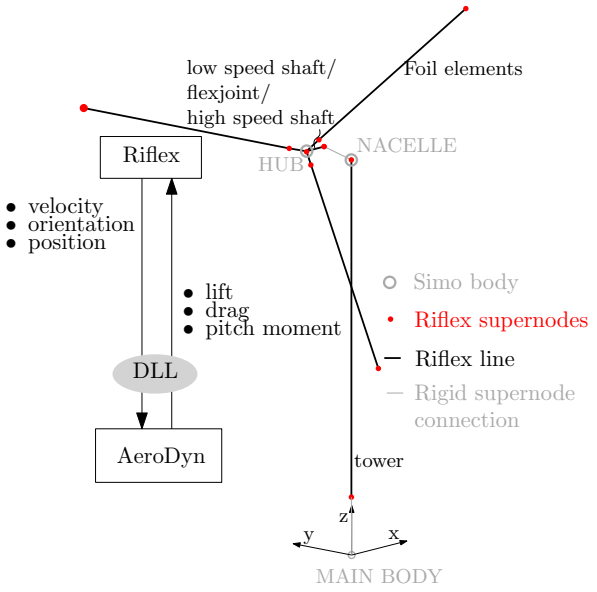

Figure 3.1: Illustration of beam element model for the turbine in Riflex.

During the course of this project, Riflex was opened for the possibility of using external pitch and torque control algorithms written in Java. The rotor speed and blade pitch angles are received from Riflex and the controller feeds back the actuator torque and blade pitch angle.

3.2 Load Modelling

3.2.1 Hydrodynamic loads

Hydrodynamic loads from surface waves on floating structures are normally calculated based on one out of two theories: Morison's formula or potential flow theory.

Morison's formula is a semi-empirical formula assuming that the size of the structure is so small that it does not affect the waves, thus it is best suited for slender structures. In this thesis, "potential theory" refers to solution of the velocity potential for a linearised boundary value problem where the wave forces are found by pressure integration around a rigid body [30]. In the case studies, the potential theory forces were obtained using panel method software Wadam [23]. The potential theory solution (see Eq. 3.5) contains one force component from the undisturbed wave field (Froude-Krylov) and a diffraction component that accounts for the flow disturbance due to the presence of the body . The potential flow solution approaches the Morison solution for a cylinder when the wave-length to diameter ratio is large and non-linear viscous effects are negligible.

$$\mathbf{F}^{wave} = \mathbf{F}^{FK} + \mathbf{F}^{D} \tag{3.5}$$

Figure 3.2 shows a theory validity diagram for a fixed cylinder with a diameder d, and indicates which effects are important for various wave-height-to-diameter and diameter-to-wave-length ratios.

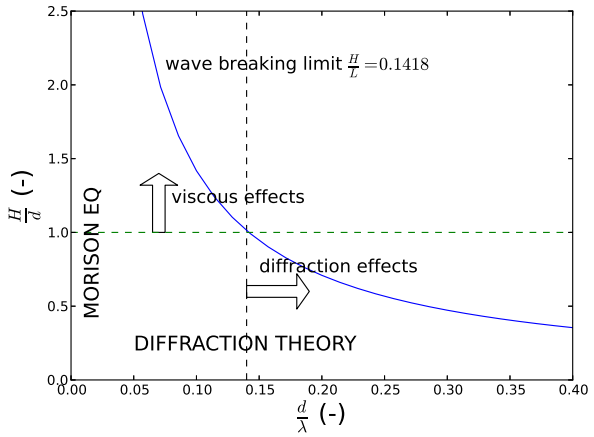

Figure 3.2: Theory validity diagram for wave forces on a fixed cylinder [13].

The non-linear FEM-solver applied in the analyses (Riflex) calculates wave forces on slender members by Morison's formula (Eq. 3.6), whereas the floating rigid body (Simo)

was modelled with a combination of potential theory forces and the viscous drag term from Morison's formula. Equation 3.6 shows how the axial, lateral or transversal force, dF acting on a strip of the member, in its local coordinate system, are expressed in the simulations.

$$\mathrm{d}F = \rho_w A\dot{u} + \rho_w A C_m \left(\dot{u} - \ddot{x}\right) + \frac{\rho_w}{2} D C_d |u - \dot{x}| \left(u - \dot{x}\right) \tag{3.6}$$

Surface piecing floating bodies, i.e. the columns in a semi-submersible, will experience a vertical force resultant due to the unbalanced dynamic pressure at the base of the columns. This is not included in the Morison formulation, but has to be taken into account [16].

Paper 1 compares a model of a SSWT with pure Morison type forces to a model with potential theory forces. In a pure Morison model, as it is modelled in Simo, there was no way to account for the unbalanced dynamic pressure at the base of the columns in the program itself. An analytical force transfer function was therefore derived and added to the columns in the analysis. The derivation and verification of these transfer functions are shown in Appendix D.

3.2.2 Aerodynamic loads by BEM

Simple momentum theory considers the change in momentum in the wind flow over an actuator disc with area A_D. By applying conservation of momentum, an expression for the thrust force (T) and power (P) acting on the actuator disc can then be derived as a function of the far field wind velocity (U_∞). The theory described here is based on Burton et al.[15, Chap. 3].

$$\begin{aligned} T &= 2\rho_a A_D U_\infty^2 a(1-a) \\ P &= 2\rho_a A_D U_\infty^3 a(1-a) \end{aligned} \tag{3.7}$$

The blade element theory assumes that the forces on the blades can be calculated based on two-dimensional aerodynamic properties. Thus the forces are also only calculated for two dimensions. The forces on a 2D blade element depend on the effective wind velocity experienced by the element (relative velocity U_{rel}). The relative velocity is the combination of the tangential velocity ($\Omega r(1 + a')$) due to the rotating blade and the velocity at the rotor disc (axial velocity $U(1 - a)$). The angle between these two velocity components determines the inflow angle (ϕ). The angle of attack (α) is defined as the angle between U_{rel} and the chord c, and the sum of the angle of attack and the blade pitch angle (γ) is the inflow angle. Aerodynamic coefficients for each aerofoil type are based on experiments and expressed as a function of the angle of attack. Figure 3.3 shows the velocities and forces acting on an aerofoil. The lift (L) and drag (D) forces are defined as normal and parallel to U_{rel}, respectively. In addition, there is a pitching moment (M)

around the aerodynamic centre. The aerodynamic force per unit length on the rotor blades, referred to the aerodynamic centre, are defined by Eq. 3.8.

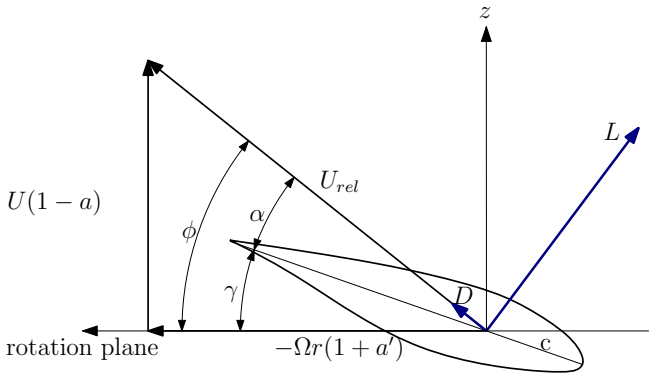

Figure 3.3: Definition of axes and forces on a 2D aerofoil.

$$\begin{aligned} \mathrm{d}L &= \frac{1}{2} C_l \rho_a c U_{rel}^2 \\ \mathrm{d}D &= \frac{1}{2} C_d \rho_a c U_{rel}^2 \\ \mathrm{d}M &= \frac{1}{2} C_m \rho_a A c U_{rel}^2 \end{aligned} \tag{3.8}$$

The axial induction factor is found by equating the trust force on all blade elements to the rate of change of axial momentum, and similarly for the tangential induction factor. The equations are solved by iteration.

The underlying assumptions of BEM theory introduce a number of inaccuracies. Assuming that the flow over the blades is always in equilibrium, disregards the dynamics of the wake. Also, pressure gradients in the span-wise direction of the blade, which can be important in a case with a highly loaded rotor (high tip speed ratios), are ignored. In numerical BEM solvers, various corrections are normally applied, for instance for tip loss, flow separation, dynamic stall and dynamic inflow.

3.2.3 Aerodynamic loads by GDW

In AeroDyn, a second option for aerodynamic load calculation is available, namely the generalised dynamic wake model (GDW). GDW was developed from helicopter theory and is based on the potential flow solution of Laplace's equation [78]. As the name implies, the method takes into account the dynamics of the wake, i.e. the transient condition

when the inflow angle changes. In GDW, tip loss, dynamic stall and dynamic- and skewed wake are inherent.

GDW is, however, not valid for highly loaded rotors, i.e. at low wind speeds. And neither GDW nor BEM accounts for the effect of large deflections on the blades on the aerodynamic forces.

In connection with the work with Paper 2, tower bending moments for different methods for calculating the aerodynamic loads was compared with wind-only simulations. BEM without dynamic wake correction, BEM with dynamic wake correction and GDW were compared. The differences were significant for the case where the 3P frequency interferes with the first fore-aft bending mode of the tower, i.e. where aerodynamic damping is important. The GDW method and the BEM method with dynamic wake correction gave rise to significantly higher damping than the BEM method without dynamic wake correction. This work is summarised in [56].

3.2.4 Thrust force on pitch regulated wind turbines

Wind turbine control systems ensure optimised power output and mitigation of loads under high wind conditions by changing the blade pitch angle (and thus the angle of attack of the aerofoils), the generator torque or the yaw position [15]. The turbine used in this thesis is a variable speed generator with active pitch control (pitch to feather). Variable speed control means that the rotational speed is controlled by varying the generator torque, to maximise the power output below rated wind speed. The active pitch control ensures that the aerodynamic torque is kept constant above rated wind speed. Since the blades are pitched out of the wind above rated wind speed, the thrust force reduces for higher wind speeds, and the maximum thrust force occurs at the rated wind speed.

The active pitch controller for the NREL 5MW uses proportional-integral (PI) control of the generator torque in the above rated - below cut-off region. This is a strategy that uses measurements and control system actions in a closed loop to obtain the desired torque [71, 49]. The loop can be described as a dynamic SDOF system with constants that determine the response characteristics of the controller. The control system constants from the OC3 Hywind spar study were applied [42] for the NREL 5 MW used in the investigations. This controller is tuned to avoid negative damping above rated wind speed due to the pitch motion of the OC3 Hywind platform. This was done by setting the control system natural frequency to 0.2 rad/s, which is outside of the wave frequency range and below the natural pitch frequency of the spar platform. 0.2 rad/s is above the natural pitch frequency of the SSWT (0.17 rad/s) in this study, but setting constants to get below this will give too much variation in the power production. Even though the controller natural pitch frequency could not be set a value below this limit, applying the OC3 Hywind constants gave less pitch motion than the onshore controller. The negative damping instability was not observed for this platform, probably due to the heave plates, which provide viscous damping for pitch motion.

3.3 Stochastic modelling of environmental loads

For engineering applications, the wind speed and the wave elevation create the basis for calculating environmental loads on an offshore structure. These have variations in long and short term, but the engineering approach is to assume stationary conditions for a certain period of time (long term), with small scale variations around the mean conditions (short term).

3.3.1 Long term distribution of wind and waves

Wind and wave statistics are normally based on wind speed, wave height, wave period and directional data recorded over several years at a specific location. The measured parameter is assumed stationary for a certain return period, and the mean value over this period forms the basis for long term statistics. For wind it is normally the 10 minute mean wind at 10 m above the ground that is measured [98]. Sea states of significant wave height (H_s) and wave peak period (T_p) can be assumed to be stationary for 30 minutes to 10 hours (normally 3 hours), and normal engineering practice is that the H_s and T_p data from measurements are fitted to a 3-parameter Weibull distribution [22].

The mean wind speed normally varies as a function of vertical distance to the surface and the terrain roughness. Profiles describing this are called wind shear profiles, and can be found in standards, e.g. the IEC standard [39]. For offshore wind, the surface roughness is low, and an exponential profile is frequently used.

Since environmental condition statistics require measurement records over sever years, not many joint wind and wave statistics are available. Johannesen et al. [47] fitted a 3-parameter Weibull distribution to wind and wave measurements from the northern North Sea during the period 1973-1999. This distribution has been applied to several offshore wind turbine studies, e.g. in [54, 105, 29].

In a study of combined wind and wave power units, Marina Platform [87], joint wind and wave distributions for five sites in European waters were established [68], based on hindcast data of 1-hour averaged sea states and wind. Figure 3.4 shows the long term joint probability distribution of mean wind, wave height and wave period for the Buoy Cabo Silleiro site, off the coast of Portugal. Since the WindFloat prototype is located in Portugal, environmental conditions from this site were chosen for the studies in papers 2-4.

The scarcity of simultaneously measured wind and wave data also means that there is even less information about the directional scatter of wind and waves available. The joint wind and wave distributions in [68], where the wind and waves were assumed uni-directional, were based on data that also contain direction [20]. However, a large number of data points per direction is needed in order to make a proper probability distribution that also covers direction. Figure 3.5 shows the occurrence of misaligned wind and wave

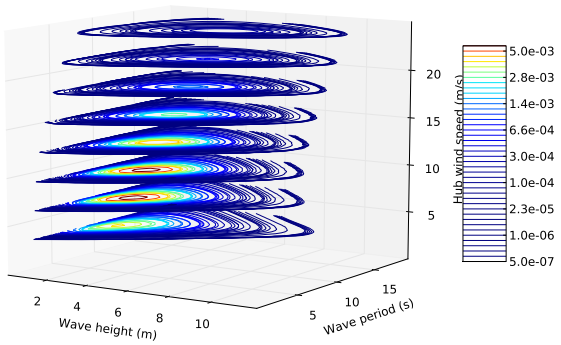

Figure 3.4: Joint wind and wave distribution.

conditions in the Buoy Cabo Silleiro site, and illustrates that considering multi-directional wind and waves in the design of FWTs may be necessary.

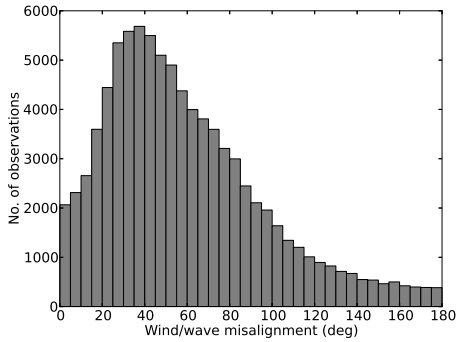

Figure 3.5: Observations of relative direction between wind and waves in the hindcast data for site 3 in [68]. The distribution includes observations in all directions.

3.3.2 Short term distribution of wind and waves

For simulations of response to stochastic loads, environmental conditions chosen from long term statistics are assumed to be stationary for the assumed return period. The short term random variations in wave elevation, or around the mean wind speed, are normally in the scale that gives structural dynamic response. For wind, variations around the mean wind speed is called turbulence, whereas the random wave elevation is often referred to

as irregular waves. The short term recordings of the random variations can be fitted to a Gaussian distribution. The individual maxima of this process are thus Weibull distributed [80].

The wind field can be described by three velocity components, where the longitudinal component varies around the mean wind speed, and the vertical and the transverse components are zero mean processes.

The short term variations are normally described in the form of spectra that describe the amplitudes and frequency content of the variations. A frequently used spectrum for the North Sea, for developing waves created by wind friction, is a modified Pierson-Moscowitz spectrum, referred to as the Jonswap spectrum [80]. A typical Jonswap spectrum is shown in Figure 3.6. Swell spectra, e.g. the Torsethaugen spectrum (wind sea and swell), can also be important to include in response analysis of FWTs, if relevant for the particular site conditions [27].

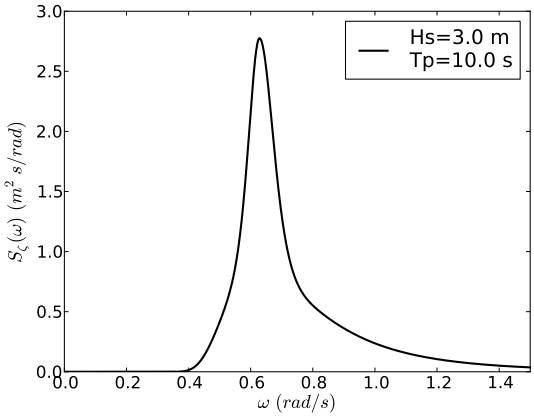

Figure 3.6: Joswap spectrum for distribution of wave frequencies for a wind sea state with H_s = 3 m and T_p = 10 s.

Spatial turbulence models that are frequently used in wind turbine design are the Mann turbulence model and the Kaimal spectral and exponential coherence model. Figure 3.7 shows an example of a Kaimal spectrum for 11.2 m/s (rated wind speed for the NREL 5MW), as given in [40]. The coherence model describes the spatial correlation of the longitudinal velocity component.

The Kaimal spectrum, which is recommended in the standard for offshore wind turbines [40] is based on onshore wind measurements. There is limited offshore wind measurement data available, but 14 month long recordings of wind speeds from a site outside of Frøya in Norway [2], showed more energy in the low-frequency range than the Kaimal spectrum and other land based spectra. This spectrum is probably more relevant for

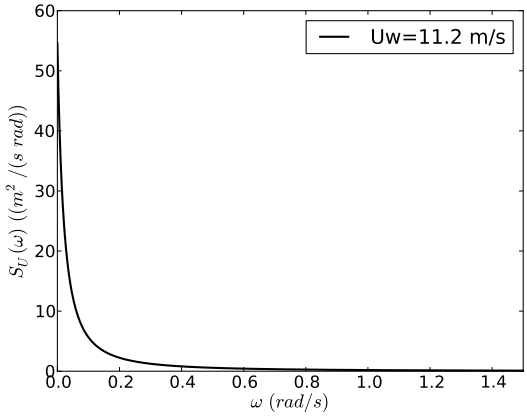

Figure 3.7: Kaimal spectrum for turbulent wind speed for a mean wind speed of 11.2 m/s.

FWTs, but it was not available in the turbulence generator for AeroDyn, thus the Kaimal spectrum was used in the case studies.

The timeseries of wave elevation or wind speed is generated by IFFT in both Riflex [73] and in TurbSim [48].

3.4 Response to stochastic loads

3.4.1 Variance spectrum and frequency-response function

Short term variations in stationary wind or wave conditions can be described as a linear combination of different frequency components. A useful way of defining the frequency content of a process X is by the variance spectrum, which is defined as the Fourier transform of the correlation function [80].

$$S_X(\omega) = \frac{1}{2\pi} \int_{\infty}^{\infty} C_X(\tau) e^{-i\omega t}\, \mathrm{d}\tau \tag{3.9}$$

For a linear relationship between a force ($F(\omega)$) and a process (wind speed or wave elevation), the variance spectrum for the force ($S_F(\omega)$) can be expressed by the variance spectrum for the wind- or wave load through a complex transfer function (H_{XF}), as shown in Eq. 3.10. Here, $S(\omega)$ denotes the one-sided variance spectrum.

$$S_F(\omega) = |H_{XF}(\omega)|^2 S_X(\omega) \tag{3.10}$$

3.4.2 Variance spectrum from timeseries

In this thesis, spectral estimates directly from timeseries were determined by Fourier transform. Depending on the application, e.g. whether or not smoothing would introduce errors, different procedures were chosen.

The Cooley-Tukey direct fast Fourier transform (FFT) algorithm provides an efficient way to estimate the variance spectrum from long signals. However, the procedure requires some tapering to give a good estimate of the variance spectrum. One method is computing the autocorrelation function of the timeseries by inverse FFT, apply a taper window function, e.g. a Hanning window, to the autocorrelation estimate and apply FFT to the tapered autocorrelation function. This procedure is described in detail by Bendat and Piersol[12, chap. 5].

3.5 Fatigue in steel

Fatigue damage in metals is fracture that occurs due to cyclic stress variations even if the stress level is below the yield stress of the material. The cause of the fracture is microscopic imperfections that cause high local stress and gradual crack growth. For steel, imperfections and microscopic cracks are most likely to be found in welds, thus the weld is the weak point from a fatigue damage point of view. The cracks grow until the remaining cross section area does not have enough capacity, and the whole member or joint fails.

A fatigue process is normally classified as high cycle or low cycle fatigue. High cycle fatigue has more than 10^4 load fluctuations during the lifetime, but has a lower stress level, whereas low cycle fatigue has a lower number of cycles, but has stresses into the plastic deformation range [65]. This thesis only addresses high cycle fatigue, since stress levels above the yield stress is defined as structural failure and since the number of cycles during the life of an FWT is high.

Fatigue damage estimation is performed based on long term stress distributions and a material response model. For the material response model, either fracture mechanics, that considers the different phases of crack growth and the local stresses in the crack (e.g. Paris' law), or an S-N curve approach can be applied. The latter was used in the case studies, and the method is described below.

3.5.1 Fatigue damage calculation by S-N curves

The most common engineering approach to high cycle fatigue in steel welds is to assume that the mean of the varying stress is insignificant and that it is purely the stress variation that causes cracks to grow. The method is based on laboratory tests, where specimens are subjected to stress ranges of varying amplitude (S) until it reaches failure. The Wöhler

approach assumes that the number of cycles until failure (N) has a linear relationship (with slope m) with the logarithm of the stress amplitude (S) (see Eq. 3.11).

$$N = KS^{-m} \tag{3.11}$$

This relationship is normally referred to as an S-N curve. S-N curves for offhore welded steel structures can be found in [25]. In beneficial conditions, e.g. where the structure has corrosion protection or for structural parts in air, a higher number of stress cycles with small amplitudes can be allowed, and the S to log(N) relationship can be described with a bi-linear curve, as shown in Figure 3.8.

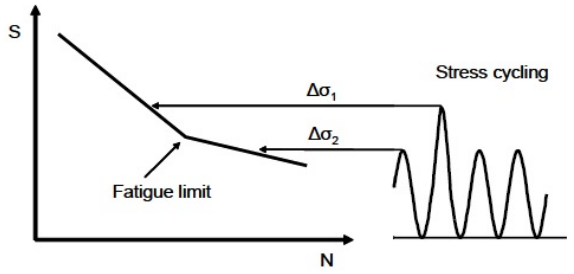

Figure 3.8: Typical bi-linear S-N-curve with an illustration of cyclic stress [25].

From a global FE model, only nominal stresses in the base cross sections can be obtained. However, S-N curves refer to hot spot stress, which means the concentrated stress around a sudden change in geometry, e.g. a weld toe. In a full fatigue analysis, there are different ways of accounting for stress concentrations. Either, local analyses are performed to determine hot spot stress directly, or so called Stress Concentration Factors (SCF) can be applied to the nominal stress. The use of SCFs is most suitable for simple joints, and can involve different SCFs for different stress components. Since no weld geometry was considered in this thesis, no evaluation of hot-spot stress was performed. Reference is, however, made to Fredheim [31], whp performed a local hot spot stress analysis for a semi-submersible windturbine.

The fatigue damage for a long term stress range distribution can be found using the Miner-Palmgren hypothesis (Eq. 3.12), which assumes that each stress fluctuation contributes with linearly accumulated partial damage. The accumulated damage is found by adding the contributions from each stress level.

$$D = \sum_{j}^{N_{bins}} \frac{n_j}{N_j} \tag{3.12}$$

where n_j is the number of stress cycles in the time history and N_j is the number of cycles to failure according to the S-N curve. Failure occurs when D = 1.

3.5.2 Cycle counting algorithms

The nominal stress histories of structural members can be achieved from frequency domain estimates, or directly from stresses from time domain FE analyses.

To be able to calculate the damage from stress histories using S-N curves, counting of cycles and stress levels must be performed. Different methods for cycle counting are available: Range counting, peak-valley counting or level crossing method, but the cycle counting method that gives the best results for fatigue analyses for wide banded stress histories is the Rainflow counting method [76]. The Rainflow counting algorithm applied in papers 2-4 uses the Rychlik [94] adjustment. Rychlik introduced a toplevel-up cycle counting method, that is equivalent to the original Rainflow counting mehtod. The stress ranges obtained by cycle counting are paired in cycle pairs and sorted into bins based on the stress range.

Frequency domain methods for fatigue estimation use the fact that the stress amplitudes are directly related to the variance of the process. For a narrow banded Gaussian process, stress amplitudes will be Rayleigh distributed and estimation of fatigue is straight forward if a frequency domain solution exists. For a wide banded process, an estimate based on the narrow band approximation is too conservative [11].

Proposed methods to overcome this use empirical formulas, based on frequency domain solutions, with correction for bandwidth parameter (Dirlik [28] and Benasciutti and Tovo [11]) or combining damage from high-frequency and low-frequency parts of a bimodal process (Jiao and Moan [46]). The latter was also investigated for application to trimodal processes by Gao and Moan [33]. Benasciutti and Tovo have also investigated methods for wide banded, non-Gaussian processes [10].

Fatigue damage from frequency domain methods are fast to compute, however, the methods do not provide a realistic alternative to time domain simulation and Rainflow counting unless a frequency domain solution for the stress is available. This is the reason that frequency domain methods for estimating fatigue damage were not used in any of the case studies. Nevertheless, they can be valuable in a frequency domain response analysis, e.g. in the study in Paper 4.

3.5.3 Stress calculation

Based on the element forces from the FE solver, nominal axial stress and shear stress was calculated according to Eq. 3.13 [41]. The expression for shear stress assumes St. Venant torsion for a circular member. Figure 3.9 shows the definitions of directions and axis for the tower base.

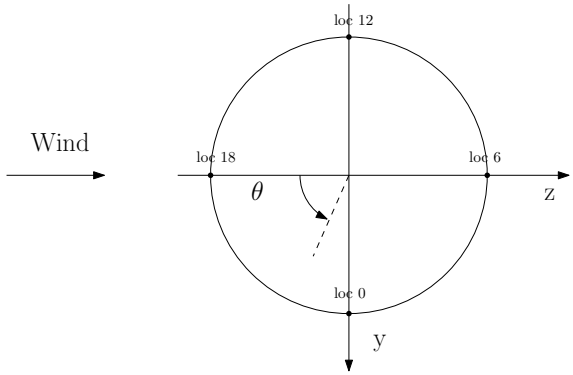

Figure 3.9: Top view of tower base cross section.

$$\begin{aligned}\sigma &= \frac{N_x}{A} + \frac{M_y}{I_y} r_1 \cos\theta - \frac{M_z}{I_z} r_1 \sin\theta \\ \tau &= \frac{M_x}{I_p} R_1 - \frac{2V_y}{A} \cos\theta - \frac{2V_z}{A} \sin\theta\end{aligned} \tag{3.13}$$

Chapter 4

Case studies

This chapter presents the main results from the investigations in the thesis. Detailed descriptions of the background and methodology of the investigations can be found in the appended papers. The investigations seek to answer the research questions proposed in Chap. 1:

- RQ1: How should loads and structural response be modelled in order to properly predict the fatigue life of a floating wind turbine?
- RQ2: Can simplifications in the analysis be made in order to make the FLS analysis more efficient?

4.1 Semi-submersible used in the case study

All the case studies were performed for a three-column single semi-submersible wind turbine with the NREL 5MW on the OC3 Hywind tower [42] placed on one of the columns, a concept inspired by WindFloat [93]. Paper 3 investigates the effect of misaligned wind and waves on four different FWT concepts, but since the author's contribution was analysis for one of the semi-submersibles, this semi-submersible model is the only one described in this chapter.

Two different variations of the SSWT were applied in the investigations, they are, however, quite similar. Paper 1 used a SSWT very similar to the generic WindFloat [93], whereas more details than what was available were required for the study in Paper 2. Papers 2-4 use a model that was developed to have similar characteristics as the generic WindFloat: The outer dimensions and geometry were kept as in [93], but wall thicknesses of the members, location of the ballast tanks and other material and geometric properties were chosen to give a mass distribution close to the generic WindFloat. Also, to achieve more of a catenary effect from the mooring lines than what the mooring system specified in [93] provides, the lines were lengthened and the anchor positions were changed. The

mooring stiffness for small displacements of the platform was, however, found to be the same as specified in [93]. The resulting specifications for the modified platform in Papers 2-4 can be found in Appendix C.

Paper 1 used a modelling method where the submerged part of the platform of the SSWT is modelled as one rigid body and the mooring lines and wind turbine tower and blades were represented by flexible beam elements. The investigations in Paper 2, also focused the forces in the braces of the platform. Thus, a multibody model, where the three columns were modelled as individual rigid bodies connected by FE flexible beam elements, was developed. The use of multibody modelling was verified against a single body model in Appendix C. The effect of hydrodynamic interaction between the columns was taken into account by including the full effect of the *presence* of the other bodies, whereas the effect of *motion* of the other bodies was only partly accounted for. This is more thoroughly described in Paper 2, and an assessment of the effect of hydrodynamic interaction is described in Appendix C.

Paper 1 did not include WindFloat's active ballast system, as simulations with an operating turbine were limited. It was, however, observed, that the mean tilt that was experienced with no ballast system, gave less rotor loads compared to an upright position. By a simple evaluation of the overturning moment from the maximum thrust force of the 5MW turbine (~730 kN) and the pitch restoring stiffness, which results a mean pitch angle of around 13 degrees, it is clear that such an angle will change the loads compared to an upright position. Thus the ballast system was modelled in the subsequent investigations. It was modelled by redistributing the mass between the columns to balance the thrust force and rotor torque.

4.2 Hydrodynamic modelling in fully coupled simulations (Paper 1 [57])

The paper describes a comparative study of responses to wave forces calculated by Morison's equation or by potential theory with additional Morison drag. It is also the first publication verifying and applying Simo-Riflex-AeroDyn, therefore some analyses with combined wind and waves were performed to study the effect of Morison versus potential theory on turbine power production.

The shortcoming of the Morison model is that it can not describe diffraction effects, hydrodynamic interaction between platform members or frequency dependent added mass and damping. On the other hand, potential theory does not include wave kinematics above the MWL. Nevertheless, for a SDOF system in regular waves with one amplitude, it is possible to achieve identical responses with the two formulations.

The Morison model can be implemented with and without forces above the MWL and with and without considering the wave particle velocities and accelerations at updated

member positions. Regular wave analyses were performed to investigate the different implementations of Morison's formula in Simo. The added mass coefficients in the Morison inertia forces were calculated from the potential theory solution with frequency dependent added mass.

As described in Chapter 3, pure Morison forces on surface piercing members lack the force from the unbalanced dynamic pressure on horizontal surfaces. It was found during the study, that including the dynamic pressure was not possible using traditional input to Simo. Thus, an analytical force transfer function for the SSWT was derived and applied together with the Morison forces (modified Morison). The derivation of the transfer functions is shown in Appendix D.

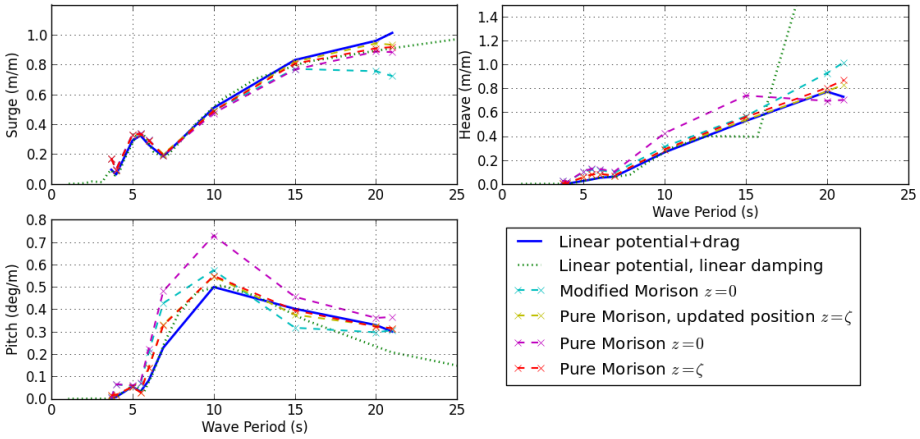

Figure 4.1: Platform RAOs for surge, heave and pitch motion for variants of Morison and for potential and drag force. Inertial coefficients are calculated from potential theory added mass.

Figure 4.1 shows response amplitude operators (RAOs) for surge, heave and pitch motions using potential theory and four approaches to Morison's equation. Results shown in Fig. 4.1 are based on time domain analysis with regular waves, and the response amplitudes are normalised with the input wave amplitude. The response outside the wave frequency was filtered out. The linear potential theory solution without quadratic drag is also shown. Pure Morison with forces calculated up to MWL overestimated heave and pitch motion compared to the potential theory and drag model, but good agreement was obtained by including forces up to wave elevation. Correcting for dynamic pressure under the columns (modified Morison) also gave a better fit, but this method can also be improved further by including forces up to wave elevation. Calculating the forces at the instantaneous position did not have a significant effect for these cases. Diffraction effects seemed to be important in heave response for periods lower than 6.9 s.

Sensitivity analysis of horizontal (subscript h) and vertical (subscript v) inertial coefficients was performed. Figure 4.2 shows that for each wave period, the response in the

potential theory model can be matched by choosing the correct coefficient. When comparing Figure 4.2 to the inertial coefficients calculated from potential theory added mass (listed in Paper 1), it can be observed that the correct coefficients can not always be derived from the potential theory solution.

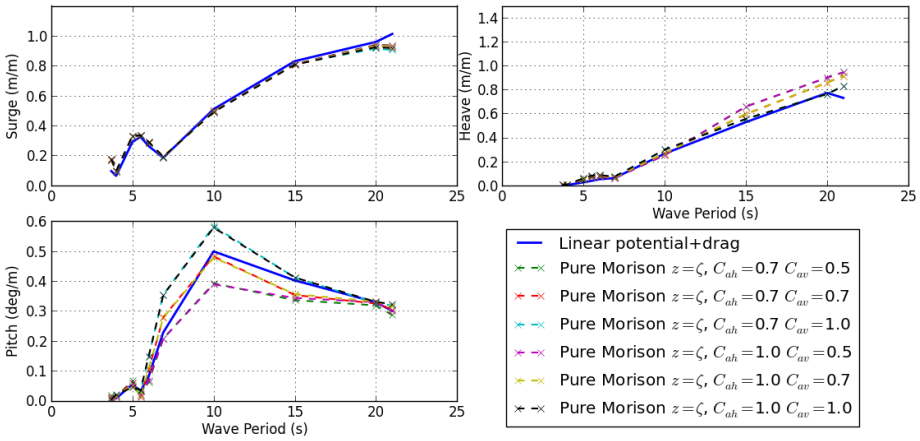

Figure 4.2: Platform RAOs for surge, heave and pitch motion for pure Morison and for potential and drag force for different inertia coefficients

Applying the same added mass coefficients as in the regular wave analyses in Figure 4.1, irregular wave analysis was performed. Irregular waves contain more than one frequency, but the Morison inertial coefficients were determined based on the wave peak period. The mean values of the motions in the irregular wave analysis (shown in Paper 1), were higher for almost all the load cases for the Morison force analyses than for the simulations with potential forces, but only negligible differences were found for the standard deviation. Morison type forces will normally give a third order drift component [30, chap. 5], but this effect comes from the drag term, which is the same for both analyses. However, the Morison model includes inertia force terms above the mean waver line, and the structure is asymmetric about the normal to the wave propagation axis, which due to different phasing of the forces, causes a mean force.

Table 4.1: Mean value and standard deviation of electrical power output in kW for coupled simulations for one wind dominated and one wave dominated environmental condition. Results are shown for a land based and a floating turbine.

	LWT		FWT - Potential + Drag		FWY - Morison	
	μ	σ	μ	σ	μ	σ
Wind dominated	4798	339	4767	384	4734	424.6
Wave dominated	1896	732	1774	619	1774	617

Comparing one wind dominated and one wave dominated load case in coupled wind and

wave analyses (Table 4.1), showed that the hydrodynamic model can have an important effect on the electrical power output of the wind turbine. For the wave dominated case, the mean power output was lower, and the standard deviation of electrical power was higher for the Morison model compared to the potential theory force model. Compared to an onshore turbine, the mean power output was lower for the SSWT. This is partly due to the mean pitch angle of the turbine (no ballast system was applied in these analyses) and due to the motions of the platform that affect the relative velocity seen by the blades.

4.3 Time domain analysis procedures for fatigue assessment of tower and braces (Paper 2 [59])

Long term fatigue analysis for nominal stress in the tower and platform members of a three-column semi-submersible was performed by fully coupled time domain analyses in Simo-Riflex-AeroDyn. The aim of the study was to investigate the necessary simulation duration, number of random realisations (seeds) and bin sizes for the discretisation of the joint wind and wave distribution.

A total of 2316 3-hour time domain simulations were carried out:

- 3-hour realisations of 155 different environmental conditions with aligned wind and waves (10 seeds)
- 10 3-hour realisations of 42 environmental conditions with misaligned wind and waves (10 seeds)
- Additional 3-hour realisation of 346 different environmental conditions (1 seed)

The environmental conditions and their respective probabilities of occurrence were selected from a joint wind- and wave distribution generated from hindcast data from the Buoy Cabo Silleiro, off the coast of Portugal [68].

The 20 year fatigue damage was calculated by Rainflow counting of nominal stress histories in the tower base, pontoon, main beam and brace based on 10 min to 3-hour samples, averaged over 10 seeds. As can be seen in Figure 4.3, estimating the total 20 year fatigue based on 10x1-hour simulations of each load case underestimated damage by less than 4% compared to 3-hour simulations. Using 10x10-minute simulations gave up to 10% smaller damage. Fatigue damage for the tower appeared to be less affected by simulation length than the platform members, pontoon, main beam and brace.

A full evaluation of the required number of seeds in a statistical sense would require a large sample of 3-hour simulations. A sample of 10, which was used in this study, is not statistically significant. The focus was kept on including as many different environmental conditions as possible within the time frame of this work, and thus the number of samples could not be increased. Therefore, a method introduced by Langley [64] to estimate the root mean square (RMS) error of a limited number of program runs was applied.

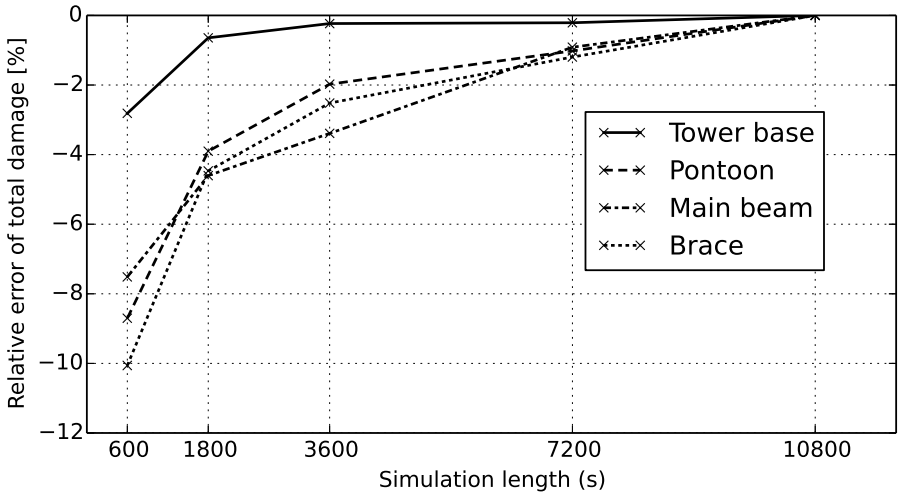

Figure 4.3: Relative difference to 3-hour simulations in 20 year total damage for axial stress fatigue. All results are calculated as the mean value based on 10 seeds.

The resulting RMS error is shown in Figure 4.4. Similar conclusions to what has been described above can be drawn from the RMS estimate; errors are small in general, but larger for 10-minute simulations, and the tower base was less sensitive to the number of seeds than the platform members.

Figure 4.4 also illustrates an important point; that the statistic content is the same in six 10-minute samples as in one 1-hour sample, and thus the expected error is the same.

Based on the results in Figs. 4.3 and 4.4, bin size investigations were performed with 1x3-hour simulations for 501 environmental conditions. The total fatigue was calculated for increasing bin sizes. Table 4.2 shows that by increasing the bin size from 1 to 2 m/s, the total fatigue damage for the tower was reduced by 9%. However, a bin size of 2 m/s, starting at cut-in wind speed (i.e. load cases include 3, 5, 7,.. m/s), means that the most important resonance case at 8 m/s is left out. If a bin size of 2 m/s was used, and the 8 m/s cases were included, the deviation in the total damages would be 0.3% for the tower, 3.2% for the pontoon, 1% for the main beam and 3.1% for the brace. This indicates that a bin size of 2 m/s will give an acceptable damage estimate if 3P resonance cases are included.

The reduction of fatigue damage with increasing wave period was fairly linear, which can explain that the increase of wave period bin size does not cause significant changes in the damage estimates in Table 4.2. Choosing a bin size of 2 s gave an acceptable result in this case, but keep in mind that this conclusion depends on the response characteristics of the platform.

Assuming that the stresses increase linearly with pitch angle, the fatigue damage increase

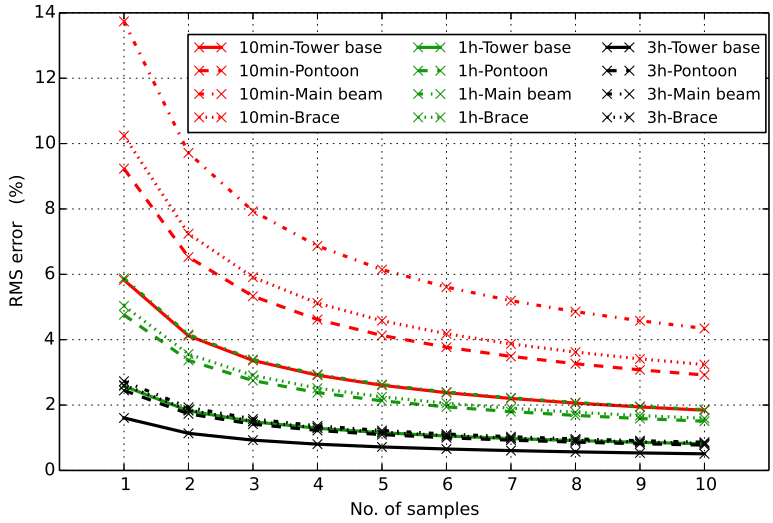

Figure 4.4: Estimated RMS error for 20 year damage, as a function of number of samples.

Table 4.2: 20 year fatigue damage for varying bin size, relative to the smallest bin size. The bin size variation in one parameter was combined with bin sizes of 1 m/s for wind speed, 0.5 m for wave height and 0.5 s for wave period. Please note that the selection of cases representing H_s bin sizes below 1.5 m is limited.

Bin size	Tower base	Pontoon	Main beam	Brace
U_{hub}	D_{rel} (%)	D_{rel} (%)	D_{rel} (%)	D_{rel} (%)
1.0 m/s	100	100	100	100
2.0 m/s	91	90	89	88
3.0 m/s	88	85	79	85
4.0 m/s	85	83	83	81
H_s				
0.5 m	100	100	100	100
1.0 m	101	101	100	99
1.5 m	96	94	96	94
2.0 m	41	38	44	38
T_p				
0.5 s	100	100	100	100
1.0 s	100	100	101	100
1.5 s	104	103	101	103
2.0 s	103	105	104	104

will be in the order of the m-parameter in the S-N curve (which is 3 and 5 in this study, see [25]). This non-linear relationship between motions and damage may be the reason why damage is more sensitive to the increase of bin size for wave heights than for wave periods. However, more cases with variation in wave height should be included to make a firm conclusion about sensitivity to wave height bin size.

An issue that emerged during the long term fatigue analysis, was the uncertainty in the model for calculation of aerodynamic loads. For wind speeds of 7-9 m/s, the blade passing frequency excited the first fore-aft bending mode of the turbine. At resonance, damping is important, and the different options for calculation of loads in AeroDyn: BEM and GDW, gave significantly different levels of aerodynamic damping. This emphasises the importance of assessing aerodynamic models for lower wind speeds, and also the need for a different tower design.

4.4 Effect of misaligned wind and wave directions on tower fatigue (Paper 3 [8])

Four concepts for FWTs were subjected to a selection of environmental conditions with misaligned wind- and waves, to investigate the effect on tower loads and motions compared to aligned wind- and wave conditions: A spar platform, a TLP, one semi-submersible with the tower on a central column (semi 2) and the semi-submersible described in the beginning of this chapter (semi 1). All of them support the NREL 5MW turbine [49] on an OC3 tower [42], and the control system gains were adapted to the individual concepts.

10 1-hour samples of 6 representative environmental conditions were run in Simo-Riflex-AeroDyn with 0° wind direction combined with 0°, 30°, 60° and 90° wave directions (see Figure 4.5), i.e. 24 different conditions. Due to the asymmetry of the semi-submersible described in this thesis, additional cases with 90° wind and 0°-90° waves were run for this concept. Fatigue damage was calculated for both nominal axial stress and shear stress by Rainflow counting of the stress timeseries for various cross section locations and with S-N curves based on DNV recommendations [25]. Nominal axial stress was found to cause significantly more fatigue damage than nominal shear stress.

Figure 4.6 shows a typical pattern for how the expected (average of 10 seeds) fatigue damage for semi 1 varied around the circumference of the tower base for different wave directions when the wind direction was kept constant. The peaks of fatigue damage occurred approximately in line with the wind direction for wave directions 0°, 30° and 90°. 60° waves is an unfavourable direction for this semi-submersible, since it causes large wave excitation, and thus the location of the largest fatigue damage was shifted. The same pattern was observed for semi 2. The spar and the TLP showed patterns where the location of maximum fatigue damage followed the wave direction (see Paper 3).

The aligned wind and wave case gave the highest fatigue damage in Figure 4.6. This was observed to be the case also for the other environmental conditions and for the other

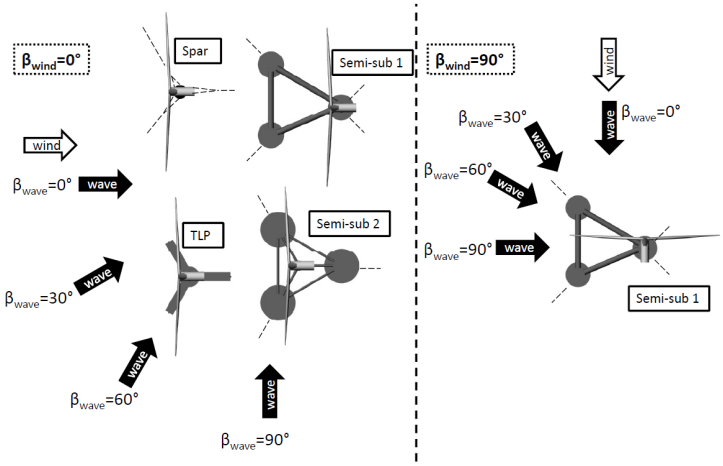

Figure 4.5: Wind and wave directions applied in the analyses.

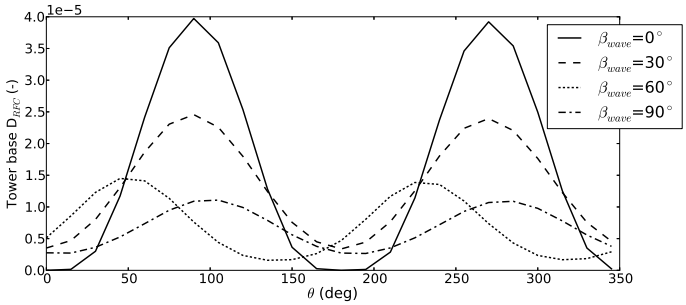

Figure 4.6: Tower base expected fatigue damage due to axial stress as a function of cross section location (90° and 270° are on the wind propagation axis) for semi 1 for H_s=5 m, T_p=14 s and U_w=10 m/s. The wind direction is 0° and the wave direction is β_{wave}.

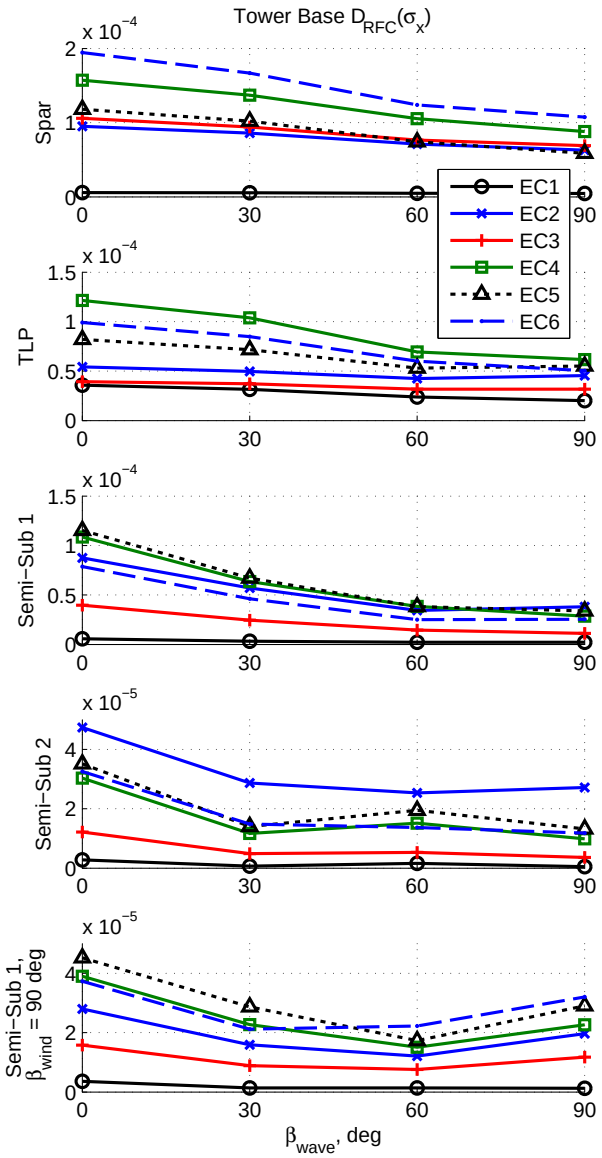

Figure 4.7: Tower base fatigue damage due to axial stress (caused by tower bending). Note that the vertical scale varies among different platforms. EC1-EC6 denote the environmental conditions that are listed in Paper 3.

three concepts. Figure 4.7 compares the expected maximum short term fatigue damage due to nominal axial stress as a function of the wave direction. The maximum value that occurred around the circumference was selected for each load case. Figure 4.7 also shows that wind coming from 90° gave lower fatigue damage than the base case 0°. However, another case that could be critical, based on the observations in this study, is the case were both wind and waves come from 60° .

Similarly to what was seen in the work with Paper 2 and Paper 4, blade passing frequency resonance occurred and gave significant fatigue damage also for the TLP and semi 2. This explains why the benign environmental conditions EC1 (for the TLP) and EC2 (for the semi-submersibles) show high damage in Figure 4.7. The wind speed at which the 3P resonance effect occurred varied slightly between the concepts, as a consequence of different eigenfrequencies for the first flexible mode of the system.

An important result reported in this study was the observed low-frequency damping of wind response due to wave motions - most likely a second order effect. This effect caused increased surge motions in misaligned waves for the spar and the semi-submersibles in the intermediate load cases.

4.5 Frequency versus time domain for fatigue analysis (Paper 4 [60])

Time domain analyses of FWT systems are very time consuming, but necessary to be able to capture non-linear effects and coupled response to wind, waves and control system. Linearised frequency domain analyses have, however, given reasonable results for response analyses for offshore bottom fixed and floating wind turbines in earlier studies, as described in Chap. 2.

A frequency domain (FD) method for calculating tower base bending moments due to wind- and wave loads was developed and compared with time-domain (TD) analyses. A model based on a rigid structure was considered. In addition, an approximate representation, based on the generalised degree of freedom method, of excitation of the first fore-aft bending mode of the tower was investigated for the FD solution. Timeseries of bending moment were found by inverse Fourier transform of the FD variance spectra for 10 seeds, and the standard deviations of the tower base bending moment were compared to those of the TD solutions. Nominal stress in the tower base was calculated from the bending moment histories, and fatigue damage was calculated by an S-N approach.

First, wind and wave analyses were performed separately, then the timeseries of bending moment from the FD analyses were superimposed and compared to the coupled TD analyses.

Table 4.3 shows an overview of the different analyses performed. For a more thorough explanation, including equations for the different models, see Paper 4. The three variations

of the frequency domain method can be characterised as follows:

- FD1 assumes a rigid structure.
- FD2 includes excitation of the first fore-aft bending mode of the turbine (tower and blades) due to the direct wind force and moment, *and* due to platform motion.
- FD3 includes excitation of the first fore-aft bending mode of the turbine due to the direct wind force only.

Table 4.3: Analysis method overview.

	Time/ freq.	Lin./ non-lin.	3D/ 2D	Flexible turbine model
TD	time	non-lin.	3D	full
FD1	freq.	lin.	2D	none
FD2	freq.	lin.	2D	excited by the direct wind force (for cases including wind) and wave induced motion
FD3	freq.	lin.	2D	excited by direct wind force

Figure 4.8 shows a comparison of the results for the wave-only frequency domain analysis where two frequency domain methods are considered (FD1 and FD2). The differences in standard deviation between the FD and TD estimates of tower base bending moment (My), short term fatigue damage (D_{rfc}), platform pitch motions (Y_5) and surge and pitch accelerations($\ddot{Y}_1$, $\ddot{Y}_5$) are shown. The prediction of platform motions and accelerations gave below 14% deviation compared to the TD simulation. It is inherent in the method that platform motions and accelerations are the same for all the FD methods.

The assumption that the turbine is rigid (FD1) seemed to give lower tower base bending moment amplitudes in the wave-frequency range than observed for TD simulations, even if the frequency domain prediction of motions and accelerations were good. Figure 4.8 shows that including the effect of excitation of the first bending mode of the turbine (FD2) gave higher bending moment estimates, and thus came closer to the TD results.

In the evaluation of D_{RFC} (the damage calculated by Rainflow counting of stress histories and S-N curves) for FD1-FD2 compared to TD simulations, FD2 provided the best result for all the wave-only cases (Figure 4.8).

The variance spectra for tower base bending moments from the FD wave-only analysis were compared to spectra from TD simulations (see Paper 4). When applying the flexible dynamic amplification correction (FD2), the solution improved. This indicates that part of the reason why the bending moment was underestimated by the rigid turbine assumption, is dynamic amplification of the lowest fore-aft bending mode of the turbine. The spectra also showed that the flexible model captures some of the the excitation of the first eigen-mode of the turbine (at 2.73 rad/s), however, with too low amplitudes for wave periods 9-10 s. The 3ω for these periods are 1.9-2.1 rad/s, i.e. there will be non-linear excitation

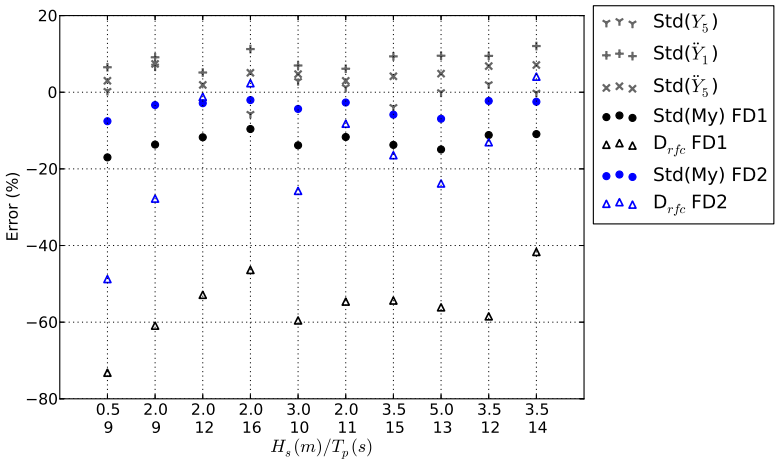

Figure 4.8: Wave-only cases. Errors in FD estimate compared to TD simulations (mean value over 10 samples). Results are shown for two frequency domain methods: FD1 and FD2.

in the region of the first eigenmode of the turbine, which cannot be captured by a linear FD model.

Figure 4.9 shows how the wind-only FD analyses compared to the TD analyses. The standard deviations of accelerations were not predicted very well, but the standard deviations of bending moment were still close to the TD results. This could mean that the bending moments directly from the rotor force contribute significantly more to the tower base bending moments than the wind induced platform motions. Figure 4.9 clearly shows how including the wind force excitation of the lowest eigenmode of the turbine improves the solution (FD3). FD2, which contains the same assumptions as FD3, and in addition includes excitation of the flexible turbine mode due wind induced motion, gave slightly less accurate estimates than FD3. This may be because FD2 includes motion induced dynamics, and as seen in Figure 4.9, wind induced motions were not very well predicted.

The low-frequency wind induced accelerations were underestimated by the FD model for all wind speeds, which can explain the poor estimate of wind induced platform acceleration in Figure 4.9. The low frequency response proved to be very sensitive to both the level of linearised hydrodynamic damping and the level of aerodynamic damping (which was derived for a fixed turbine), but the main cause of poor representation of the low frequency content is presumably non-linear effects being lost in the linearisation of the thrust force.

By looking at the relative error for the FD estimates compared to the TD fatigue damage, the errors range between 24-59% for wind-only, 1-49% for wave-only, and 8-50% for the combined wind- and wave cases, even if bending moment prediction errors were much

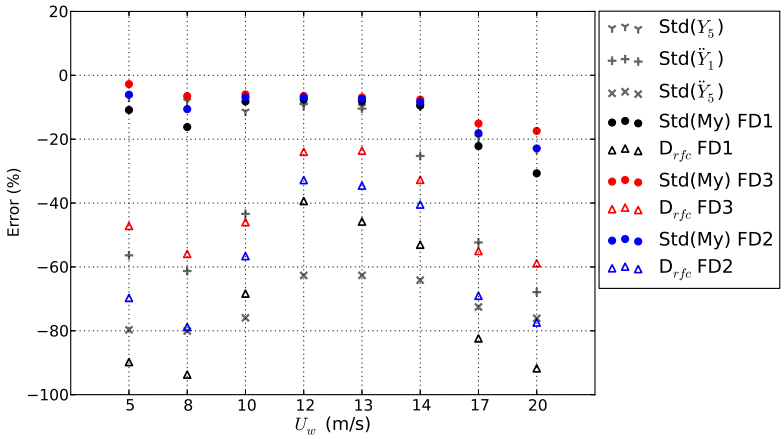

Figure 4.9: Wind-only cases. Errors in FD estimate compared to simulations (mean value over 10 samples). Results for three frequency domain methods: FD1-FD3.

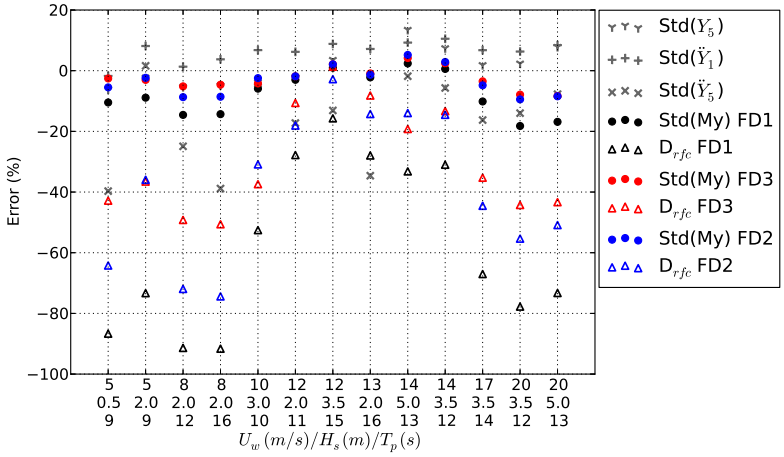

Figure 4.10: Combined wind and waves. Errors in superimposed FD estimates compared to TD simulations (mean value over 10 samples). Results are shown for FD1-FD3.

lower. This is an expected effect since using an S-N approach expresses the damage as proportional to the stress amplitude to the power of m, which in this case was 3 or 5.

For combined wind and waves, Figure 4.10 shows that the errors were in the same range as for the wind- and wave-only simulations, and the trends were similar, i.e. no obvious coupling effects were observed in these results, except for the aerodynamic damping of the wave induced motions, caused by an operating rotor, which was included in the combined FD analysis.

An important coupling effect is the low-frequency aerodynamic damping due to wave motion. However, the low-frequency motions were already "damped" in the FD analysis, since the low-frequency content of wind-induced response was lost in the linearisation of the thrust force. This caused the FD predictions of the combined wind and wave response to be fairly close to the coupled TD response, even though it was not derived from physics assuming wave motions.

Chapter 5

Conclusions and recommendations for further work

The current chapter summarises the contributions to the community of FWT researchers that resulted from the investigations performed during the course of the PhD period. Suggestions for further work, based on issues that were highlighted during the investigations, are described in this chapter.

5.1 Conclusions

This thesis primarily deals with development of numerical methods and their application to fatigue design in an efficient manner, using a semi-submersible as a case study. The emphasis has been on global response analysis for use in fatigue design, thus determination of stress concentrations were kept out of the scope. Coupling existing structural (Riflex) and aerodynamic (AeroDyn) codes, to enable fully coupled simulation of the semi-submersible, was also part of the work with this thesis.

Comparing wave force models based on a simplified model based on Morison forces derived by a potential theory panel model (Paper 1) showed that by tuning the Morison inertia coefficients, the same response could be achieved. However, these inertia coefficients could not be directly derived from potential theory, and neither could they be set to a constant for all wave periods. Diffraction effects were found to be important for wave periods below 7 s. The study also highlighted the importance of including the force due to hydrodynamic pressure under surface piercing columns in the Morison model. The analyses of an operating wind turbine with the two different theories showed that pitch motion has large influence on the mean and the variation of power production, thus it is important to model pitch motion correctly.

The successive studies concerned with simulation procedures and selection of environmental conditions for predicting fatigue damage, with the objective of possibly reducing

the computation time without significantly compromising the accuracy. Sensitivity analysis of simulation length showed that calculating fatigue damage from 1-hour simulations gave less than 4% error in the total fatigue life compared to 3-hour simulations. 10-minute simulations, which are normal for LWTs, gave larger errors for the platform components, but gave less than 3% error for the tower base. This means that 10-minute simulations were not sufficient for fatigue analysis of components with stresses mainly induced by wave loads, but that 10-minute simulations may give a reasonable result for components that are more influenced by wind loads. However, the Kaimal wind spectrum, that was applied here, does not contain the long period variations which could cause response that is more sensitive to simulation length.

The RMS error compared to the average of 10 3-hour realisations was less than 1% for 7 seeds of 3-hour simulations and less than 2% for 9 seeds of 1-hour simulations. Fatigue damage in the platform members was more sensitive to the number of realisations and simulations duration than the damage in the tower base.

While some standards for offshore wind turbines (e.g. DNV-OS-J101) recommends bin sizes to be 1 m/s for U, 0.5 m for H_s and 0.5 s for T_p, when selecting environmental conditions for running a complete fatigue life assessment, the findings in Paper 2 suggest that increasing the bin size for U to 2 m/s will give an acceptable fatigue damage estimate if the wind speed representative of each bin is selected with care. It was found that the fatigue life was fairly insensitive to the T_p bin size, but careful selection of the representative T_p, such that resonance frequencies are included, is also important here. The study did not include enough cases for the smallest bin size of H_s to make a firm conclusion on the proper bin size, but since damage does not vary linearly with wave height, choosing the midpoint of the H_s bin is not expected to be a conservative approach. If the wave bin size is to be increased from the recommended value, a different method of choosing the bin representative H_s should be considered.

In the studies of misaligned wind and wave conditions, it was found that motions perpendicular to the wind increased compared to the co-directional case when waves came from the side. This effect was expected since the rotor damping was no longer present in the misaligned case. However, since the forces contributing to fatigue damage act around different axes, the stresses get a more favourable distribution around the circumference of the tower cross section, and thus aligned wind and waves gave the highest fatigue damage. This conclusion was drawn for all the four different concepts studied in Paper 3: A spar, a TLP and two semi-submersibles. The direction of the co-directional wind and waves is nevertheless important; applying the direction that gives the highest wave induced motions is expected to be a conservative approach.

As for all the other case studies, nominal stress in a net cross section of the tower base was assumed in the investigations of misaligned wind and wave conditions. But in reality there will be hot spots at different locations around the tower base circumference. This has to be taken into account when adopting the conclusions from Paper 3.

A new frequency domain method to estimate the variance spectrum of tower base bend-

ing moment due to wind and wave loading was established in Paper 4. In addition to establishing a general frequency domain model by assuming the structure to be rigid, a generalised coordinates model was developed to include the flexural response of the first fore-aft bending mode of the turbine tower and blades. In the moderate sea states studied, the bending moment calculated by the frequency domain method compared fairly well to non-linear time domain simulations. Low-frequency motions induced by the wind were not very well represented by the frequency domain model, which seemed to be caused by the linearisation of the thrust force. But since the bending moments seemed to be dominated by the moment directly from the thrust force, the inaccurate motion estimates did not have a large impact in this study.

When it comes to calculating fatigue damage by the frequency domain method, larger errors were observed, which is an expected effect due to the exponential relationship between fatigue damage and stress range. Still, the method gave good predictions for some environmental conditions, and can provide a rough estimate of fatigue damage in early design phases.

A coupling effect that was observed in the studies in Papers 3 and 4 is the change in the wind-frequency content of the thrust force when waves are present. This effect was confirmed by isolating the thrust force (see Paper 3) from an analysis without waves and re-applying it in an analysis with waves. The physical cause of this effect was not identified, but is expected to be either a result of non-linear terms in the thrust force formulation or an effect inherent in the method for calculating aerodynamic loads (BEM).

5.2 Recommendations for further work

The following suggestions for further work followed from the investigations in Papers 1-4:

- The conclusions listed above are only proven for a particular semi-submersible wind turbine (and a spar, a TLP and a different SSWT in Paper 3). Further investigations regarding the application of the methods outlined in the papers to other concepts should be made.
- Uncertainties relating to the level of aerodynamic damping at low to intermediate wind speeds emerged in the studies in Paper 2. BEM and GDW gave very different results in 3P resonance of the tower first fore-aft bending mode. Wake dynamics could be important at these wind speeds, but the GDW method is unstable for highly loaded rotors. These uncertainties should be assessed to enable proper modelling at low to intermediate wind speeds.
- 3P resonance was observed in Papers 2-4, also for another semi-submersible concept and for a TLP. The tower should be carefully adapted to each platform type, such that the eigenfrequencies are outside of the 3P range.

- Long term variations in the wind can cause responses in compliant FWTs like the semi-submersible. Most wind spectra applied for wind turbines today do not contain energy at low frequencies. These low frequency variations are not important for bottom fixed structures. For FWTs, however, long term wind variations could have an effect, and thus this should be investigated, using wind spectra from offshore measurements.
- The frequency domain analysis in Paper 4 applied a linearised thrust force by taking the variance spectra of the timeseries of thrust force for a floating wind turbine. This method gave less low-frequent response than the non-linear model, but a better linearisation method could improve frequency domain analysis for floating wind turbines.

References

[1] American Bureau of Shipping. *Floating Offshore Wind Turbine Installations*, 2013.

[2] O. J. Andersen and J. Løvseth. The Frøya database and maritime boundary layer wind description. *Marine structures*, 19(2):173–192, 2006.

[3] A. Arapogianni and et. al. Deep water - the next stop for offshore wind energy. Technical report, EWEA, 2013.

[4] Glosten Associates. Technology summary: Pelastar for offshore wind. `http://www.pelastarwind.com/`. Accessed Dec 11, 2013.

[5] A. Aubault, C. Cermelli, and D. Roddier. Windfloat: A floating foundation for offshore wind turbines part III: Structural analysis. In *Proceedings of the ASME 28th International Conference on Ocean, Offshore and Arctic Engineering*, pages 213–220, Honolulu, USA, 2009. Paper no. OMAE2009-79232.

[6] E. E. Bachynski. *Design and dynamic analysis of tension leg platform wind turbines*. PhD thesis, Norwegian University of Science and Technology, 2014. Thesis no. 4-2014.

[7] E. E. Bachynski, M. Etemaddar, M. I. Kvittem, C. Luan, and T. Moan. Dynamic analysis of floating wind turbines during pitch actuator fault, grid loss, and shutdown. *Energy Procedia*, 35:210–222, 2013.

[8] E. E. Bachynski, M. I. Kvittem, C. Luan, and T. Moan. Wind-wave misalignment effects on floating wind turbines: Motions and tower load effects. *Journal of Offshore Mechanics and Arctic Engineering*, 136(4):041902, 2014.

[9] E. E. Bachynski and T. Moan. Linear and nonlinear analysis of tension leg platform wind turbines. In *Proceedings of the 22nd International Ocean and Polar Engineering Conference*, Rhodes, Greece, 2012.

[10] D. Benasciutti and R. Tovo. Cycle distribution and fatigue damage assessment in broad-band non-gaussian random processes. *Probabilistic engineering mechanics*, 20(2):115–127, 2005.

[11] D. Benasciutti and R. Tovo. Spectral methods for lifetime prediction under wide-band stationary random processes. *International Journal of fatigue*, 27(8):867–877, 2005.

[12] J. S. Bendat and A. G. Piersol. *Random data: analysis and measurement procedures*. John Wiley & Sons, 2011.

[13] M. M. Bernitsas. Viscous forces on circular cylinders in separated flows. case study: Cable strumming. Lecture Notes for NA 621, 1982.

[14] B. H. Bulder, M. Th. van Hees, A. Henderson, R. H. M. Huijsmans, J. T. G. Pierik, E. J. B. Snijders, G. H. Wijnants, and M. J. Wolf. Study to feasibility of and boundary conditions for floating offshore wind turbines. Technical report, ECN, MARIN, Lagerway the Windmaster, TNO, TUD, 2002.

[15] T. Burton, N. Jenkins, D. Sharpe, and E. Bossanyi. *Wind energy handbook*. John Wiley & Sons, 2011.

[16] N. Clauss, E. Lehmann, and C. Ostergaard. *Offshore Structures - Conceptual design and Hydromechanics*, volume I. Springer-Verlag, 1988.

[17] R. D. Cook, D. S. Malkus, M. E. Plesha, and R. J. Witt. *Concepts and applications of finite element analysis*. Wiley, 2002.

[18] A. Cordle and et al. Project UpWind: State-of-the-art in design tools for floating offshore wind turbines. Technical report, UpWind, 2010.

[19] A. J. Coulling, A. J Goupee, A. N. Robertson, J. M. Jonkman, and H. J. Dagher. Validation of a fast semi-submersible floating wind turbine numerical model with deepcwind test data. *Journal of Renewable and Sustainable Energy*, 5:023116, 2013.

[20] L. Cradden, D. Ingram, and T. Davey. Marine renewable integrated application platform - site assessment. Technical Report Deliverable D2.1, University of Edinburgh, UK, 2010.

[21] DCNS. DCNS home page. `http://en.dcnsgroup.com/`. Accessed: Feb 23, 2014.

[22] Det Norske Veritas. *DNV-RP-C205, Environmental Conditions and Environmental Loads*, 2007.

[23] Det Norske Veritas. *SESAM User Manual Wadam*, 2008.

[24] Det Norske Veritas. *DNV-RP-C103, Column-stabilised units*, 2010.

[25] Det Norske Veritas. *DNV-RP-C203, Fatigue Design of Offshore Steel Structures*, 2010.

[26] Det Norske Veritas. *DNV-OS-C103, Column-stabilised units*, 2012.

[27] Det Norske Veritas. *DNV-RP-J103, Design of Floating Wind Turbine Structures*, 2013.

[28] T. Dirlik. *Application of computers in fatigue analysis*. PhD thesis, University of Warwick, 1985.

[29] W. Dong, T. Moan, and Z. Gao. Long-term fatigue analysis of multi-planar tubular joints for jacket-type offshore wind turbine in time domain. *Engineering Structures*, 33(6):2002–2014, 2011.

[30] O. M. Faltinsen. *Sea Loads on Ships and Ocean Structures*. Cambridge University Press, 1990.

[31] Ø. Fredheim. Fatigue analysis of column-brace connection in a semi-submersible wind turbine. Master's thesis, Norwegian University of Science and Technology, 2012.

[32] I. Fylling, K. Mo, K. Merz, and N. Luxcey. Floating wind turbine-response analysis with rigid-body model. In *Proceedings of the European Offshore Wind Conference and Exhibition, September*, pages 14–16, 2009.

[33] Z. Gao and T. Moan. Frequency-domain fatigue analysis of wide-band stationary gaussian processes using a trimodal spectral formulation. *International Journal of Fatigue*, 30(10-11):1944–1955, October-November 2008.

[34] A. Goupee, B. Koo, K. Lambrakos, and R. Kimball. Model tests for three floating wind turbine concepts. In *Offshore Technology Conference*, 2012.

[35] L. Haid, G. Stewart, J. Jonkman, A. Robertson, M. Lackner, and D. Matha. Simulation-length requirements in the loads analysis of offshore floating wind turbines. In *Proceedings of the 32nd International Conference on Ocean, Offshore and Arctic Engineering*, Nantes, France, 2013. Paper no. OMAE2013-11397.

[36] S. Hauptmann, S. Mulski, M. Kühn, and L. Mauer. Advanced drive train modeling in a virtual wind turbine using the multibody simulation code simpack. In *European Wind Energy Conference (EWEC). Milan, Italy: European Wind Energy Association*, 2007.

[37] T. Holmås. *USFOS User's Manual, version 8-1. 2004*.

[38] T. Holmås and J. Amdahl. Design of floating wind turbines. In *Computational methods in marine engineering III, Trondheim, Norway*, 2009.

[39] International Electrotechnical Commission. *IEC61400-1, Wind turbines - Part 1: Wind turbines, design requirements*, 2005.

[40] International Electrotechnical Commission. *IEC61400-3, Wind turbines - Part 3: Design requirements for offshore wind turbines*, 2009.

[41] F. Irgens. *Mechanics of Materials (in Norwegian)*. Tapir, 2006.

[42] J. J. Jonkman. Definition of the floating system for phase IV of OC3. Technical report, National Renewable Energy Laboratory, 2010.

[43] M. L. Buhl Jr. J. Jonkman. *FAST user's guide*, 2005.

[44] Z. Jiang, M. Karimirad, and T. Moan. Dynamic response analysis of wind turbines under blade pitch system fault, grid loss, and shutdown events. *Wind Energy*, 2013.

[45] Z. Jiang, T. Moan, and Z. Gao. A comparative study of shutdown procedures on the dynamic responses of wind turbines. 2014. Under review.

[46] G. Jiao and T. Moan. Probabilistic analysis of fatigue due to gaussian load processes. *Probabilistic Engineering Mechanics*, 5(2):76–83, June 1990.

[47] K. Johannessen, T. S. Meling, and S. Haver. Joint distribution for wind and waves in the northern north sea. *International Journal of Offshore and Polar Engineering*, 12(1), 2002.

[48] B. J. Jonkman. *TurbSim user's guide*, 2009.

[49] J. Jonkman, S. Butterfield, W. Musial, and G. Scott. Definition of a 5-MW reference wind turbine for offshore system development. Technical report, NREL, 2009. NREL/TP-500-38060.

[50] J. Jonkman and W. Musial. Offshore code comparison collaboration (OC3) for IEA Wind Task 23 offshore wind technology and deployment. Technical Report NREL/TP-5000-48191, National Renewable Energy Laboratory, 2010.

[51] J. M. Jonkman. *Dynamics modeling and loads analysis of an offshore floating wind turbine*. PhD thesis, NREL, 2007.

[52] J. M. Jonkman. Dynamics of offshore floating wind turbines - model development and verification. *Wind Energy*, 12(5):459–492, 2009.

[53] M. Karimirad, Q. Meissonnier, Z. Gao, and T. Moan. Hydroelastic code-to-code comparison for a tension leg spar-type floating wind turbine. *Marine Structures*, 24(4):412–435, 2011.

[54] M. Karimirad and T. Moan. Wave-and wind-induced dynamic response of a spar-type offshore wind turbine. *Journal of waterway, port, coastal, and ocean engineering*, 138(1):9–20, 2011.

[55] M. J. Kühn. *Dynamics and design optimisation of offshore wind energy conversion systems*. PhD thesis, Technisce Universiteit Delft, 2001.

[56] M. I. Kvittem. Comparison of rotor forces from Riflex-AeroDyn and RiflexBEM for a semi-submersible wind turbine. Unpublished report, July 2013.

[57] M. I. Kvittem, E. E. Bachynski, and T. Moan. Effects of hydrodynamic modelling in fully coupled simulations of a semi-submersible wind turbine. *Energy Procedia*, 24:351–362, 2012.

[58] M. I. Kvittem and T. Moan. Effect of mooring line modelling on motions and structural fatigue damage for a semisubmersible wind turbine. In *The Twenty-second International Offshore and Polar Engineering Conference*. International Society of Offshore and Polar Engineers, 2012.

[59] M. I. Kvittem and T. Moan. Time domain analysis procedures for fatigue assessment of a semi-submersible wind turbine. *Marine Structures*, 2014.

[60] M. I. Kvittem and T. Moan. Frequency versus time domain fatigue analysis of a semi-submersible wind turbine tower. *Journal of Offshore Mechanics and Arctic Engineering*, 137(1):011901, 2015.

[61] M. I. Kvittem, T. Moan, Z. Gao, and C. Luan. Short-term fatigue analysis of semi-submersible wind turbine tower. In *Proceedings of the ASME 30th International Conference on Ocean, Offshore and Arctic Engineering*, pages 751–759. American Society of Mechanical Engineers, 2011.

[62] D. Laino and A. C. Hansen. *Aerodyn user's guide*, 2002.

[63] D. Laino and A. C. Hansen. *User's Guide to the Computer Software Routines AeroDyn Interface for ADAMS*, 2002.

[64] R. S. Langley. On the time domain simulation of second order wave forces and induced responses. *Applied ocean research*, 8(3):134–143, 1986.

[65] P. K. Larsen. *Design of steel structures (in Norwegian)*. Tapir, 1997.

[66] T. J. Larsen. *How 2 HAWC2, the user's manual*, 2009.

[67] K. H. Lee. *Responses of floating wind turbines to wind and wave excitation*. PhD thesis, Massachusetts Institute of Technology, 2005.

[68] L. Li, Z. Gao, and T. Moan. Joint environmental data at five european offshore sites for design of combined wind and wave energy devices. In *Proceedings of ASME 32th International Conference on Ocean Offshore and Arctic Engineering*, Nantes, France, 2013. Paper no. OMAE2013-10156.

[69] Maine International Consulting LLC. Floating offshore wind foundations: Industry consortia and projects in the united states, europe and japan. Technical report, 2013.

[70] N. Luxcey, H. Ormberg, and E. Passano. Global analysis of a floating wind turbine using and aero-hydro-elastic numerical model. Part 2: Benchmark study. In *Proceedings of 30th International Conference on Ocean Offshore and Arctic Engineering*, Rotterdam, The Netherlands, 2011. Paper no. OMAE2011-50088.

[71] J. F. Manwell, J. G. McGowan, and A. L. Rogers. *Wind Energy Explained*. Wiley, 2009.

[72] MARINTEK. *SIMO Theory Manual*, 2012.

[73] MARINTEK. *RIFLEX Theory Manual*, 2013.

[74] MARINTEK and Det Norske Veritas. *Sesam User Manual, DeepC Theory*.

[75] D. Matha. Model development and loads analysis of an offshore wind turbine on a tension leg platform with a comparison to other floating turbine concepts: April 2009. Master's thesis, University of Colorado, 2010.

[76] M. Matsuishi and T. Endo. Fatigue of metals subjected to varying stress. *Japan Society of Mechanical Engineers, Fukuoka, Japan*, pages 37–40, 1968.

[77] T. Moan, Z. Gao, M. Karimirad, E. E. Bachynski, Etemaddar M., Z. Jiang, M. I. Kvittem, M. Muliawan, and Y. Xing. Recent developments of the design and analysis of floating wind turbines. In *ISCOT: Developments in fixed & floating offshore structures, Busan, South Korea, The Royal Institution of Naval Architects*, 2012.

[78] P. J. Moriarty and A. C. Hansen. *AeroDyn theory manual*, 2005.

[79] W. Musial, S. Butterfield, and B. Ram. Energy from offshore wind. In *Offshore Technology Conference*, pages 1888–1898, 2006.

[80] A. Naess and T. Moan. *Stochastic dynamics of marine structures*. Cambridge University Press, 2012.

[81] F. G. Nielsen, T. D. Hanson, B. Skaare, et al. Integrated dynamic analysis of floating offshore wind turbines. In *Proceedings of the ASME 25th International Conference on Offshore Mechanics and Arctic Engineering*, Hamburg, Germany, 2006. Paper no. OMAE2006-92291.

[82] NORSOK. *N-003, Action and action effects*, 2007.

[83] Windpower Offshore. Floating turbines - japan enters the stage. `http://www.windpoweroffshore.com/article/1211680/floating-turbines---japan-enters-stage`. Accessed: Oct 16, 2013.

[84] H. Ormberg and E. E. Bachynski. Global analysis of floating wind turbines: Code development, model sensitivity and benchmark study. In *Proceedings of the 22nd International Ocean and Polar Engineering Conference*, Rhodes, Greece, 2012.

[85] H. Ormberg, E. Passano, and N. Luxcey. Global analysis of a floating wind turbine using an aero-hydro-elastic model: Part 1: Code development and case study. In *Proceedings of 30th International Conference on Ocean Offshore and Arctic Engineering*, Rotterdam, The Netherlands, 2011. Paper no. OMAE2011-50088.

[86] M. Philippe, A. Babarit, and P. Ferrant. Comparison of time and frequency domain simulations of an offshore floating wind turbine. In *Proceedings of the ASME 30th International Conference on Ocean, Offshore, and Arctic Engineering*, Rotterdam, the Netherlands, 2011. Paper no. OMAE2011-49722.

[87] Marina Platform. Marina platform web page. `http://www.marina-platform.info/`, 2014. Accessed September 19, 2014.

[88] The HiPRWind Project. Hiprwind web page. http://www.hyperwind.eu/, 2013. Accessed May 23, 2013.

[89] A. Robertson. OC4 phase II - 7th full committee meeting. Presentation, June 2013.

[90] A. Robertson and J. Jonkman. Loads analysis of several offshore floating wind turbine concepts. In *21st International Offshore and Polar Engineering conference*, 2011. Rep. no. NREL/CP-5000-50539.

[91] A. Robertson, J. Jonkman, Musial W., F. Vorpahl, and W. Popko. Offshore code comparison collaboration, continuation: Phase II results of a floating semisubmersible wind system. Technical report, National Renewable Energy Laboratory, 2013.

[92] D. Roddier, C. Cermelli, A. Aubault, and A. Weinstein. Windfloat: A floating foundation for offshore wind turbines. *Journal of Renewable and Sustainable Energy*, 2:033104, 2010.

[93] D. Roddier, A. Peiffer, A. Aubault, and J. Weinstein. A generic 5MW WindFloat for numerical tool validation and comparison against a generic spar. In *Proceedings of ASME 30th International Conference on Ocean Offshore and Arctic Engineering*, Rotterdam, The Netherlands, 2011. Paper no. OMAE2011-50278.

[94] I. Rychlik. A new definition of the rainflow cycle counting method. *International journal of fatigue*, 9(2):119–121, 1987.

[95] B. Skaare, T. D. Hanson, F. G. Nielsen, R. Yttervik, A. M. Hansen, K. Thomsen, and T. J. Larsen. Integrated dynamic analysis of floating offshore wind turbines. In *European Wind Energy Conference and Exhibition (EWEA)*, 2007.

[96] Statoil. Hywind. http://www.statoil.com/. Accessed: Jan 2, 2014.

[97] G. Stewart, M. Lackner, A. Robertson, J. Jonkman, and A. J. Goupee. Calibration and validation of a fast floating wind turbine model of the deepcwind scaled tension-leg platform. In *22nd International Offshore and Polar Engineering conference*, 2012. Rep. no. NREL/CP-5000-54822.

[98] E. N. Strømmen. *Theory of bridge aerodynamics*. Springer, 2010.

[99] J. Twidell and G. Gaudiosi. *Offshore Wind Power*. Multi Science Publishing, 2009.

[100] J. Van Der Tempel. *Design of support structures for offshore wind turbines*. PhD thesis, Technisce Universiteit Delft, 2006.

[101] W. J. M. Vijfhuizen. Design of a wind and wave power barge. Master's thesis, MS Dissertation, Department of Naval Architecture and Mechanical Engineering, Universities of Glasgow and Strathclyde, Scotland, 2006.

[102] E. N. Wayman, P. D. Sclavounos, S. Butterfield, J. Jonkman, and W. Musial. Coupled dynamic modeling of floating wind turbine systems. In *Offshore Technology Conference*, volume 139. Houston, 2006.

[103] J. Weinzettel, M. Reenaas, C. Solli, and E. G. Hertwich. Life cycle assessment of a floating offshore wind turbine. *Renewable Energy*, 34(3):742–747, 2009.

[104] J. E. Withee. *Fully coupled dynamic analysis of a floating wind turbine system*. PhD thesis, Massachusetts Institute of Technology, 2004.

[105] Y. Xing, M. Karimirad, and T. Moan. Modelling and analysis of floating spar-type wind turbine drivetrain. *Wind Energy*, 2013.

Appendix A

Appended papers

Paper 1

Effects of hydrodynamic modelling in fully coupled simulations of a semi-submersible wind turbine

By Marit I. Kvittem, Erin E. Bachynski and Torgeir Moan

In Elsevier Energy Procedia, vol 24, p.351-362, 2012

Available online at www.sciencedirect.com
ScienceDirect
Energy Procedia 24 (2013) 351–362
Energy Procedia
www.elsevier.com/locate/procedia

DeepWind, 19-20 January 2012, Trondheim, Norway

Effects of hydrodynamic modelling in fully coupled simulations of a semi-submersible wind turbine

Marit I. Kvittem[a,b], Erin E. Bachynski[b], Torgeir Moan[b]

[a]*NOWITECH, NTNU, NO-7491 Trondheim, Norway*
[b]*Centre for Ships and Ocean Structures, NTNU, NO-7491 Trondheim, Norway*

Abstract

This work examines the dynamic response of a single semi-submersible wind turbine (SSWT) based on different hydrodynamic theories. Comparisons of platform motions and structural responses in the wind turbine are shown for simulations for a model with linear potential flow solution and quadratic drag and simulations with only Morison-type forces. The SSWT modelled in this study is based on WindFloat and carries the NREL 5MW wind turbine and should be considered a large volume structure. This implies that diffraction effects should be considered by using potential flow theory and viscous effects by Morison's equation.

A new coupled simulation code was developed by linking the SIMO and RIFLEX hydrodynamic, structural, and control system computational tools, from MARINTEK, with the aerodynamic forces and wind field generation capabilities of AeroDyn and TurbSim, from NREL. In contrast to other available simulation codes, this combination enabled the implementation of these two different hydrodynamic theories and offered the possibility of finite element mooring line models. Wave-only simulations were considered first, in order to tune and compare potential theory versus the inertia term in Morison's equation. Some limited coupled wave-wind simulations give an indication of the extent to which hydrodynamic modelling affects the global response.

The SSWT case study showed that the Morison model with forces integrated up to wave elevation gave a good representation of the motions compared to the potential flow model with quadratic drag forces. It also showed that motions are sensitive to choice of added mass coefficients, stretching and dynamic pressure under the columns. Combined wind and wave simulations, using a non-optimized control approach, showed that pitch motions influence the power production and blade bending moments.

Keywords:
offshore wind energy, semi-submersible, integrated analysis, hydrodynamics

1. Introduction

The majority of commercial and academic software for analyzing floating wind turbines (FWTs) have been developed from analysis tools for onshore wind turbines. This often means that the software includes advanced aerodynamics and limited hydrodynamics. In many cases, the only hydrodynamics model is slender element theory with Morison-type forces on the submerged part of the structure. A few analysis programs for FWTs come from the offshore industry, often with advanced hydrodynamics but simplified aerodynamics. Certain concepts, such as the spar buoy FWT, are slender enough to justify the use of

Morison's equation [1] together with a simplified treatment of pressure that causes heave motion. For large volume structures such as barges or semi-submersibles, however, diffraction effects may be significant. On the other hand, applying Morison's equation makes it possible to account for non-linear effects that come from calculating the wave forces in the instantaneous position of the platform. These effects may also be important. The consequences of applying different hydrodynamic theories have not yet been studied due to limitations in analysis tools.

The Morison equation has been used as the hydrodynamic model for for semi-submersible wind turbine (SSWT) analysis before, by for instance Phuc and Ishihara [2]. They conclude that the Morison model compares well with model tests for a SSWT with slender elements in regular waves. This result cannot be assumed to hold for WindFloat and most other semi-submersibles with large-diameter elements, and must also be examined critically for irregular wave conditions. A code-to-code comparison for calculating motions of a 1/64 scale drill rig semi-submersible was conducted by the ITTC Ocean Engineering Committee [3]. Their conclusion was that both potential forces and viscous forces should be included in the analysis, and that the effect of wave height was large in heave.

In this work the effect of hydrodynamic load modelling for a single SSWT is investigated. The SSWT design under consideration is very similar to the WindFloat concept [4]. Since a proper description of hydrodynamic loads requires both potential theory and viscous drag, quadratic drag elements are included in both models presented here. For simplicity, the drag coefficients are the same for both the potential and the Morison model. Added mass coefficients were calculated based on the frequency dependent added mass from the potential theory solution. After coefficients were found, regular and irregular wave analyses were performed for both the Morison model and the potential theory model, and response characteristics were investigated and compared. Limited analyses with an operating turbine and turbulent wind load were run to study the effect of hydrodynamic modelling on power production.

2. Methodology

2.1. Potential Theory and Morison's Equation

Two practical options for hydrodynamic load calculation in a global analysis are potential flow theory and Morison's equation. The first order potential flow theory applied here considers the solution of a linearized boundary value problem for inviscid, incompressible flow about a rigid body. This approach, using a panel method solution, accounts for Froude-Krylov forces and diffraction effects for large volume structures. The resulting solution is frequency-dependent and linear with respect to wave amplitude.

Morison's equation is a semi-empirical method for calculating wave loads on slender structures. For a fixed cylindrical pile, Morison's equation is equivalent to the potential flow solution when the wavelength to diameter (λ/D) ratio is large and viscous effects are negligible [5]. Morison's equation does not, however, account for diffraction effects, which, as a rule of thumb for fixed cylinders, are important for wavelengths shorter than five times the diameter [6]. Furthermore, the Morison formulation is extended to non-slender members, including, for example, the heave plates of the semi-submersible in this study. Due to the quadratic drag force and the formulation in terms of relative velocities and accelerations, Morison's equation is solved in the time domain with frequency-independent coefficients.

Although we are interested in a coupled multiple degree-of-freedom (DOF) system, let us consider the time-domain equation of motion for a floating single DOF system in order to compare these hydrodynamic models. According to pure potential flow theory, the single DOF system takes the form of Eq. 1 [7]:

$$(M + A_\infty)\ddot{x}(t) + \int_{-\infty}^{\infty} \kappa(t-\tau)\dot{x}(\tau)d\tau + Cx(t) + K\left(x(t)\right) = F^{FK} + F^{D} \tag{1}$$

where M is the dry mass, A_∞ is the added mass for high frequencies, $x(t)$ is the system displacement, $\kappa(t-\tau)$ is retardation function accounting for frequency-dependent added mass and damping, C is the hydrostatic restoring force, F^{FK} is the Froude-Krylov force and F^{D} is diffraction force. The first and second time derivatives are expressed by $\dot{x}$ and $\ddot{x}$. In practice, we also include a quadratic damping term (C_q) to approximate viscous effects, as well as non-linear restoring forces ($K(x(t))$) from the mooring system. The

quadratic damping term depends on the difference between the water particle velocity (u) and the body velocity. The resulting equation of motion for potential flow including viscous drag is then:

$$(M + A_\infty)\,\ddot{x}(t) + \int_{-\infty}^{\infty} \kappa(t-\tau)\dot{x}(\tau)d\tau + Cx(t) + K\,(x(t)) = F^{FK} + F^{D} + C_q|u - \dot{x}|\,(u - \dot{x}) \tag{2}$$

The same system, including nonlinear restoring forces, according to Morison-type wave loading is expressed by Eq. 3, where we have the same quadratic damping and no retardation function [7].

$$M\ddot{x}(t) + Cx(t) + K\,(x(t)) = (\rho_w V + m_a)a - m_a\ddot{x} + C_q|u - \dot{x}|\,(u - \dot{x}) \tag{3}$$

In Eq. 3, we have introduced the density of water (ρ_w), the volume of displaced water (V), a constant added mass (m_a), and the water particle acceleration (a).

Examining these two formulations, we can see that it is possible to tune the Morison equation coefficients to obtain identical responses for a single DOF system in regular waves of constant amplitude. The Morison model cannot, however, necessarily capture the equivalent hydrodynamic coupling effects for a multiple DOF system as in the potential flow formulation. Furthermore, the frequency-dependence and linear damping contributions are lost. On the other hand, the potential flow formulation does not consider wave particle accelerations above the waterline, and requires solving the Cummins equation, which introduces some computational cost. The applicability of these theories to the considered platform, which is described in the following section, is considered in greater detail in Section 2.3.

2.2. Single Semi-submersible Wind Turbine

The model investigated in this study is a semi-submersible substructure very similar to WindFloat [4], with the NREL 5MW turbine [8] (see Fig. 2.2) and OC3 tower [9]. The SSWT is modeled in SIMO/RIFLEX, a tool for coupled analysis of moored floating structures. Mooring lines, tower and blades are modeled by flexible RIFLEX elements, while the floating body is modeled as rigid in SIMO, with linear hydrostatic stiffness and coupled frequency-dependent added mass and linear damping. The force and motion transfer functions and retardation functions are calculated with Wadam [10] potential theory software. SIMO has the option to attach elements with Morison force model to the body, which was done here to add quadratic drag. In the Morison model, the added mass, damping and force transfer functions are set to zero, while both acceleration terms (added mass) and quadratic damping terms from Morison's equation are included.

In both models, the non-dimensional vertical drag coefficient, $C_D = 2C_q/\rho A^{proj}$, for the heave plate is given in [4] as 7.5 and we assume a horizontal drag coefficient of 1.0 for the columns based on DNV-RP-C205 [11]. As a first comparison of the models, Table 1 lists the natural periods of the system found by decay analyses for potential theory and for Morison equation with $C_a = 1.0$ for both columns and heave plates.

Fig. 1: WindFloat (courtesy of Principle Power)

Mode	Panel T (s)	Morison T (s)
Surge	99.8	97.3
Heave	19.9	21.4
Pitch	39.9	40.7

Table 1: Damped natural periods, assuming $C_a = 1.0$ for both horizontal and vertical Morison forces. $C_D = 7.5$ for heave plates and $C_D = 1.0$ for columns.

Four different variations of the Morison model were studied: pure Morison forces as in Eq. 3, with forces integrated up to mean water level (1) or up to wave elevation (2), pure Morison including the effect of calculating forces at instantaneous position (3), and Morison with a correction for dynamic pressure under the columns (4). Due to the surface piercing elements, this dynamic pressure correction gives a better representation of the forces in the vertical plane. This correction in Morison model (4) is implemented via an analytically derived force transfer function applied to the platform in SIMO.

2.3. Added Mass Coefficients

The dimensional added mass (m_a) for the Morison model is computed as in Eq. 4 for horizontal forces on the columns and Eq. 5 for vertical forces on the heave plates. In Eqs. 4- 5, R is the radius of the column or plate and L is the length of the column. Similar equations are found in [12] and [13] for cylinders and caissons, respectively. The values of the coefficients C_a must be tuned for different wave frequencies.

$$m_a^{hor} = \rho_w C_a^{hor} \pi R_{col}^2 L_{col} \tag{4}$$

$$m_a^{ver} = \rho_w C_a^{ver} \frac{2\pi}{3} R_{plate}^3 \tag{5}$$

Table 2 shows the range of wave cases considered. The wave heading is normal to the rotor plane (that is, in the x direction) as displayed in Fig. 2.2, hence only surge, heave and pitch motions are studied. These cases are applied in both regular and irregular waves, where for irregular waves the periods are peak periods and heights are significant heights. Morison added mass coefficients are calculated based on frequency dependent added mass from potential theory. Two of the cases are also run with wind loads for an operating turbine (see Tab. 3).

Table 2: Load cases

Wave period (s)	3.7	4.0	5.0	5.5	6.0	6.9	10.0	15.0	20.0	21.0
Wave height (m)	1.0	1.0	1.0	1.0	1.5	2.0	3.0	6.0	9.0	9.0

These load cases represent a range of different conditions, where different hydrodynamic effects may be of importance. The wave heights are selected to be appropriate for the given period. Figure 2 shows where the load cases in Tab. 2 are located in a theory validity diagram based on the cylinder diameter. The diagram is valid for a cylinder fixed to the ground [14], so it only gives an indication of which effects may be important for the freely floating body with multiple components. The conclusions drawn from Fig. 2 are that for wave periods 3.7 s to 6.0 s, diffraction may be important, while for periods 20 s and 21 s viscous drag may be important. Both Morison and diffraction theory may be applied to the intermediate cases, where inertial effects dominate.

2.4. Fully Coupled Analyses

In order to understand the impact of the different hydrodynamic theories on wind turbine simulation results, it is also important to consider the full floating system. Table 3 summarizes the two chosen wind-wave conditions: Condition 1, representing below-rated wind and gentle seas, and Condition 2, representing a typical operational condition. The wind fields, generated in TurbSim, correspond to the normal turbulence model (NTM) for class B of the IEC 61400-3 standard, with the power law applied for the shear profile [15]. At lower wind speed, the characteristic turbulence intensity is somewhat higher. The wave conditions were chosen to approximately correspond with the wind field characteristics according to typical North Sea conditions given by Faltinsen, 1990 [5].

Simulations for identical wind and wave time series were carried out for a land-based wind turbine (disregarding all wave input) and for two different hydrodynamic models: the potential flow theory with

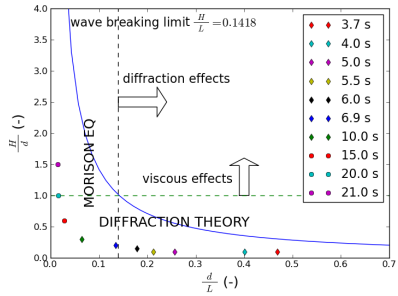

Fig. 2: Regions of validity of potential flow theory and Morison's equation (assuming fixed bodies) [14]

Table 3: Combined wind-wave simulation conditions

	Condition 1	Condition 2
Mean Wind Speed (90 m)	8 m/s	16 m/s
Power Law Exponent [15]	0.14	0.14
Characteristic Turbulence Intensity (90 m)	19.16 %	16.30 %
Significant Wave Height	1.5 m	6.0 m
Peak Wave Period	6.0 s	15.0 s
Simulation Length (excluding transient)	1800 s	1800 s

additional quadratic drag, and the pure Morison formula with integration up to the free surface (Morison model (2)), with coefficients as in Tab. 4. Wind and waves were applied in the x direction, i.e. normal to the rotor plane as displayed in Fig. 2.2.

The same generator torque and blade pitch control system were applied to all of the models, with the gains described in [8]. Floating systems generally require modifications to the control system in order to avoid negative feedback in over-rated wind conditions [16, 17], when the thrust force at the nacelle decreases for increasing relative wind speed. The horizontal velocity due to pitch at WindFloat's nacelle in these conditions is sufficiently low such that the destabilizing effect is small compared to the hydrodynamic damping, but an improved control system will be included in future work. It is also important to note that the aerodynamic model employed in these simulations does not account for dynamic wake effects, which may have important consequences for floating wind turbines due to the sheared inflow, which is exacerbated by the mean platform pitch. The dynamic wake option is available in the AeroDyn code for sufficiently high wind speed, but the BEM option with dynamic stall was applied here for consistency at different wind speeds.

3. Coupled Wind-Wave Simulation Tool

A new coupled simulation code (S-R-A) was developed by linking the SIMO [18] and RIFLEX [19] hydrodynamic, structural, and control system computational tools, from MARINTEK, with the aerodynamic forces and wind field generation capabilities of AeroDyn and TurbSim, from NREL [20]. The simulation tool employs the finite element solver available in the combined SIMO/RIFLEX tool, passing position and velocity information to the aerodynamic code via DLL at the first iteration of each time step. The DLL

returns lumped forces along the wind turbine blades. An external control system applies the generator torque according to a look-up table and blade pitch commands via PI control as in the NREL 5MW definition [8].

3.1. Finite Element Model

In the finite element model, the wind turbine tower is modeled with axisymmetric beam elements, while the blades consist of doubly symmetric cross sections. In contrast to the FAST model, the model includes the torsional degree of freedom of the blades. The control system, which is also coupled to the finite element program, applies appropriate torque directly to the low speed shaft and sets the angle of the rigid connection between the hub and blade root. Additional details regarding the wind turbine module of SIMO/RIFLEX (without AeroDyn and TurbSim) can be found in [21, 22].

3.2. Aerodynamic Model

The AeroDyn program provides both blade element momentum (BEM) and generalized dynamic wake (GDW) models for the aerodynamic force calculation [23]. The results shown in this paper employ the BEM method with the Beddoes dynamic stall model, but no dynamic wake effects.

3.3. Verification of Land-Based Wind Turbine Performance

Prior to using the S-R-A code for simulation of a floating offshore wind turbine, the global performance of a land-based wind turbine was compared against available tools such as FAST and HAWC2 [24]. Simulations of the NREL 5 MW wind turbine show good agreement regarding power production, rotor rotation, blade loads and deflections and tower loads. Fig. 3, as an example, compares several performance indicators for the FAST and S-R-A codes. The S-R-A results are shown for a fully flexible model and for a model with exaggerated torsional stiffness for the blades. As shown, the control pitch required at higher wind speeds decreases when the blades are flexible in torsion, in agreement with published results [25].

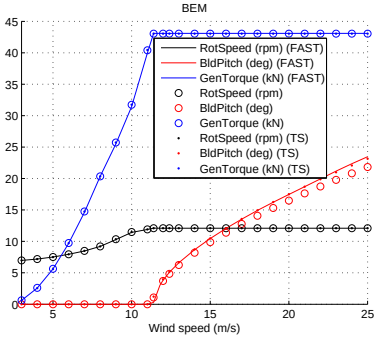

Fig. 3: Global performance indicators for the land-based NREL 5MW wind turbine. Rotor speed, blade pitch, and generator torque are compared for FAST, fully flexible RIFLEX-AeroDyn, and RIFLEX-AeroDyn with exaggerated torsional blade stiffness (indicated TS).

4. Results

4.1. Regular Wave Condition

First, added mass coefficients were calculated based on added mass from the potential theory solution, see Tab. 4. These coefficients were used for the Morison inertia forces in further analyses, if not stated otherwise. Figure 4 shows response amplitude operators (RAOs) using potential theory and four approaches

to Morison equation. Results shown in Fig. 4 are based on time domain analysis with regular waves, normalized with the input wave amplitude. The response outside the wave frequency was filtered out, so only linear wave excitation is included. The linear potential theory solution without quadratic drag is also shown. The wave heights used for these analyses are listed in Table 2. When quadratic drag is included, there is a quadratic relation between wave height and response, and this effect was not considered in this paper since the quadratic drag coefficients were the same for the two models.

Table 4: Coefficients calculated from Eq. 5 based on $A(\omega)$ from potential theory solution.

T_P (s)	3.7	4.0	5.0	5.5	6.0	6.9	10.0	15.0	20.0	21.0
C_a^{hor} (-)	0.51	0.76	0.65	1.05	1.35	1.18	1.07	1.06	1.03	1.03
C_a^{ver} (-)	0.88	0.88	0.88	0.88	0.89	0.89	0.90	0.91	0.91	0.91

From Fig. 4 it is clear that pure Morison with forces calculated up to mean water level overestimated heave and pitch motion compared to the potential theory and drag model, but by including forces up to wave elevation we got a good agreement. Correcting for dynamic pressure under the columns also gave a better fit, but this method can be improved by including forces up to wave elevation. For wave periods 20 and 21 seconds, surge motions for the modified Morison case were lower than the rest. This may be due to surge-pitch coupling effects. Calculating the forces at the instantaneous position did not have a significant effect for these cases.

Diffraction effects seemed to be important in heave response for periods lower than 6.9 s, which is in agreement with the theory validity diagram in 2.

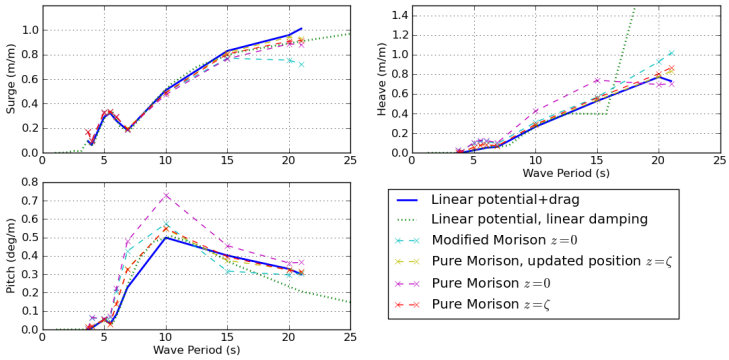

Fig. 4: Platform RAOs for surge, heave and pitch motion for variants of Morison and for potential and drag force. Inertial coefficients as in Table 4.

In addition, regular wave analyses with different horizontal (subscript h) and vertical (subscript v) inertial coefficients and integration of forces up to wave elevation were performed. The results are shown in Fig. 5, and it is clear that for each wave period the response in the potential theory model can be matched by choosing the correct coefficient. And the correct coefficients are not necessarily derived from the potential theory solution.

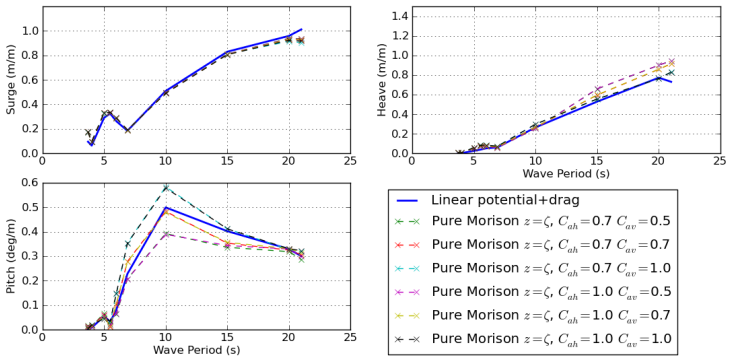

Fig. 5: Platform RAOs for surge, heave and pitch motion for pure Morison and for potential and drag force for different inertia coefficients

4.2. Irregular Wave Condition

After determining the coefficients in Tab. 4, the potential theory model and the pure Morison model with forces up to wave elevation were exposed to irregular wave conditions. Figure 6 shows the statistical properties of the irregular wave response for both the Morison model and the potential and drag model. Linear potential damping was equal to zero since it was significantly smaller than the drag damping. The wave time series was the same for both models in each load case. These results were based on one single time series per load case, where the simulation time is 30 minutes. This is not a sufficient statistical basis, but gives an indication of trends because the purpose is to compare between the Morison model and the potential plus drag model, and the wave time series are identical.

There was little difference in standard deviations in all degrees of freedom. The mean value of surge motion was higher for the Morison model than for the potential model for long wave periods. This may be due to the extra drift force caused by the inertia forces above mean water level acting on an asymmetric structure.

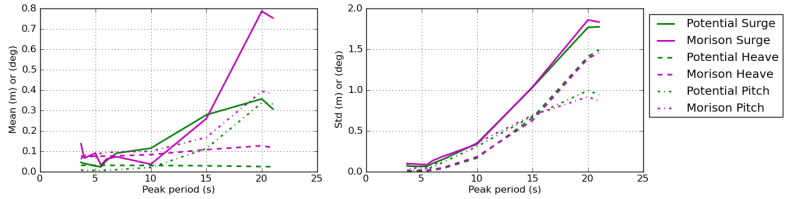

Fig. 6: Statistical properties for response to irregular waves with no wind

4.3. Turbulent Wind and Irregular Waves

A brief investigation of responses in turbulent wind and irregular wave conditions is presented here. One should note that these results correspond to limited stochastic analyses and that future work to reduce statistical uncertainties is planned.

Statistical results for the Condition 1 and 2 simulations are shown in Tables 5 and 6, respectively. In Condition 1, the wind forces were dominant, and the wind turbulence dominated the variability of all of the performance parameters. As shown in Table 5, there was very little statistical difference in the power production, turbine performance, blade loads, and floater motions when comparing simulations with the potential and Morison theory hydrodynamics models. The power production of the floating platform was, however, somewhat lower than that of the land-based tower. The reduction in power production of the floating platform compared to the land-based tower was in part due to the mean platform pitch, which decreases the efficiency of the energy harvesting, and also due to the pitch motion of the turbine, which followed the wind and reduced the relative velocity seen by the blades. The reduced mean power led to a corresponding decrease in power variability. The effect of the motions on the blade loads was also evident: there was a clear increase in the out-of-plane bending moment due to gravity effects. In-plane loads, which are dominated by gravity effects as the blades rotate, were not significantly affected by the floating platform motions.

Table 5: Wind-wave Condition 1 simulation statistics

	Land-Based		WF - Potential + Drag		WF - Morison	
	μ	σ	μ	σ	μ	σ
Electrical Power (kW)	1896	732	1774	619	1774	617
Generator Torque (kNm)	20.47	5.73	19.59	5.06	19.59	5.04
Blade Pitch (deg)	0	0	0	0	0	0
Rotor Speed (rpm)	9.39	0.96	9.24	0.83	9.23	0.83
Blade Root Out-Of-Plane Bending Moment (kNm)	5812	1450	5967	1550	5970	1571
Blade Root In-Plane Bending Moment (kNm)	596	2564	561	2513	561	2510
Surge (m)	n/a	n/a	11.59	2.85	11.94	3.09
Heave (m)	n/a	n/a	-0.01	0.03	0.04	0.03
Pitch (deg)	n/a	n/a	6.42	1.67	6.53	1.66

In Condition 2 (Table 6), the effects of the wave forces were more evident. As in Condition 1, the electrical power output from the floating turbines decreased compared to the land-based turbine. In contrast to Condition 1, however, the variability of the electrical power and generator torque increased for the floating platform. The power and generator torque varied slightly more for the Morison model than for the potential theory model, which can be attributed to the small increase in platform pitch motions.

Table 6: Wind-wave Condition 2 simulation statistics

	Land-Based		WF - Potential + Drag		WF - Morison	
	μ	σ	μ	σ	μ	σ
Electrical Power (kW)	4798	339	4767	384	4734	424.6
Generator Torque (kNm)	41.33	2.46	41.08	2.81	40.78	3.10
Blade Pitch (deg)	11.15	2.92	10.46	3.54	10.47	3.56
Rotor Speed (rpm)	12.10	0.25	12.09	0.27	12.09	0.30
Blade Root Out-Of-Plane Bending Moment (kNm)	5205	1645	5847	1850	5837	1900
Blade Root In-Plane Bending Moment (kNm)	1180	2621	1155	2524	1116	2510
Surge (m)	n/a	n/a	12.72	2.19	13.57	2.33
Heave (m)	n/a	n/a	-0.01	0.61	0.06	0.64
Pitch (deg)	n/a	n/a	7.18	1.87	7.37	1.96

To further demonstrate the differences between the hydrodynamic models when applied to coupled sim-

ulations, power spectra results from Condition 2 are shown in Fig. 7. The top left panel shows the wind in the global x direction measured at the hub for all three models as well as the wave elevation at the origin. The platform pitch for the two hydrodynamic models is shown in the second panel. As shown, the Morison model gave larger variation in platform pitch at both the wind and wave frequencies.

The low-speed shaft rotation speed (ω, shown in the third panel) is a complex result of the incoming wind, generator torque and blade pitch control actions, inertial effects, and platform motions. The controller is able to regulate the wind-driven variations (slower than 0.6 rad/s), but does not correct for variations in the wave frequency range. Thus, the differences in platform wave-induced motion can be seen in the rotation speed spectrum.

The blade 1 out-of-plane (OOP) bending moment is similarly difficult to dissect. The bending moment showed strong variation related to the blade pitch angle (not shown, but consistent between all three models) with large 1p variations. The platform pitch motion increased the amplitude of the 1p cycles, largely due to gravitational loading.

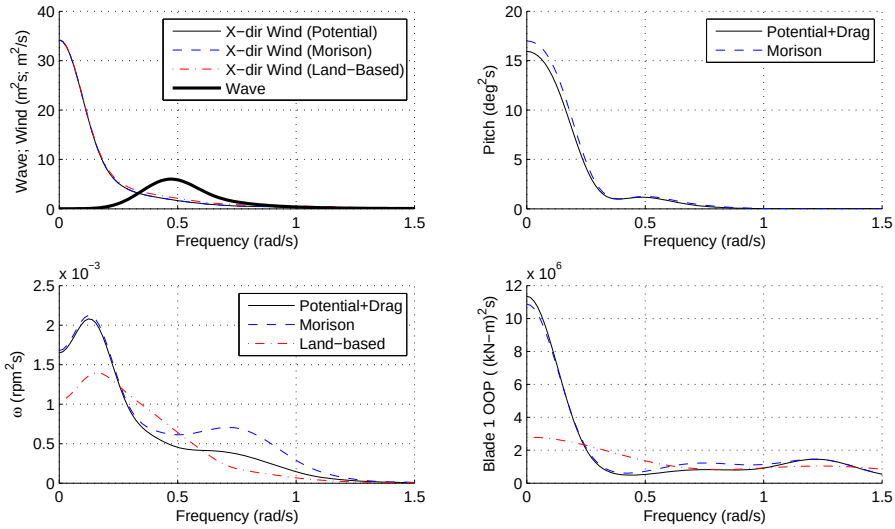

Fig. 7: Selected variance spectra: combined wind-wave Condition 2

5. Conclusions

A comparison of wave-induced response of a semi-submersible wind turbine using Morison equation and potential theory with Morison drag was performed by means of the analysis software SIMO/RIFLEX coupled to AeroDyn. First, added mass coefficients for the Morison equation were calculated based on the potential theory added mass. Then variations of models with wave forces from Morison's equation were run in regular and irregular wave analyses and compared to the potential theory solution. A sensitivity study on inertia coefficients was also performed. To study the effect of Morison versus potential theory on power production, fully coupled analyses with wind and waves were performed.

The results from these studies showed that it is possible to obtain the same response amplitudes in regular waves for periods above 7 seconds by choosing proper coefficients. For wave periods below 7 seconds, diffraction effects became important for heave motions. Surge motions were fairly insensitive to the choice of added mass coefficients. Results also showed that inertia coefficients directly calculated from the potential theory solution do not necessarily give the best agreement between Morison's equation and potential theory.

Pure Morison forces overestimated heave and pitch motion compared to the potential theory solution, but by including forces above mean water level good agreement was achieved. Also, adjusting pure Morison with dynamic pressure under the columns improved the results, though the method for including the dynamic pressure has potential for improvement. Calculating the forces at the updated position of the platform did not have a significant effect.

In the irregular wave analysis there were no significant differences between the two theories in the standard deviation of the motions. Differences in the mean surge motion were observed, which may be caused by inertial forces above the mean water level acting on an asymmetric structure.

Pitch motions decreased the relative wind velocity seen by the turbine blades and led to a decrease in power efficiency compared to a land-based turbine. As a consequence of larger pitch motions predicted with the Morison model than with the potential flow model, the predicted power production was more variable than in the potential theory model.

Having analysis software capable of describing advanced hydrodynamics is important when studying large volume structures, but for this particular semi-submersible the findings showed that slender body theory by Morison is sufficient for the wave periods between 7 and 21 seconds. The coupled simulation tool made it possible to study the impact of pitch motions on power production and blade bending moments, which showed to be significant. A better control strategy is required to improve the power performance and reduce the pitch motions of the platform. Large pitch motions influence extreme loads, fatigue life and power production of the system, so having a good prediction of responses to wind and waves is crucial.

References

[1] M. Karimirad, Z. Gao, T. Moan, Dynamic motion analysis of catenary moored spar wind turbine in extreme environmental condition, in: Proceedings of the European Offshore Wind Conference, Sweden, 2009.
[2] P. V. Phuc, T. Ishihara, A study on the dynamic response of a semi-submersible floating offshore wind system part 2: Numerical simulation, in: Proceedings of the International Conferences of Wind Engineering 12, Cairns, Australia, 2007.
[3] M. Takagi, A comparison of methods for calculating the motion of a semi-submersible, Ocean Engineering 12 (1) (1985) 45–97.
[4] D. Roddier, A. Peiffer, A. Aubault, J. Weinstein, A generic 5MW WindFloat for numerical tool validation and comparison against a generic spar, in: Proceedings OMAE 2011, 2011, paper no. OMAE2011-50278.
[5] O. M. Faltinsen, Sea Loads on Ships and Ocean Structures, Cambridge University Press, 1990.
[6] N. Barltrop, Floating Structures: A Guide for Design and Analysis, 1998.
[7] MARINTEK, SIMO Theory Manual (2009).
[8] J. Jonkman, S. Butterfield, W. Musial, G. Scott, Definition of a 5-MW reference wind turbine for offshore system development, Tech. rep., NREL, NREL/TP-500-38060 (2009).
[9] J. Jonkman, Definition of the Floating System for Phase IV of OC3, Tech. rep., National Renewable Energy Laboratory (2010).
[10] Det Norske Veritas, SESAM User Manual Wadam (2008).
[11] Det Norske Veritas, Environmental conditions and environmental loads, Tech. Rep. DNV-RP-C205 (2007).
[12] N. Clauss, E. Lehmann, C. Ostergaard, Offshore Structures - Conceptual design and Hydromechanics, 1988.
[13] S. Chakrabarti, Added mass and damping of a TLP column model, in: Proceedings of the Offshore Technology Conference, Houston, Texas, 1990, pp. 559–571.
[14] M. M. Bernitsas, Viscous forces on circular cylinders in separated flows. case study: Cable strumming., lecture Notes for NA 621 (1982).
[15] International Electrotechnical Commission, Wind turbines - Part 3: Design requirements for offshore wind turbines, Tech. Rep. IEC61400-3 (2009).
[16] T. J. Larsen, T. D. Hanson, A method to avoid negative damped low frequent tower vibrations for a floating, pitch controlled wind turbine, Journal of Physics: Conference Series, The Second Conference on The Science of Making Torque from Wind 75.
[17] J. M. Jonkman, Influence of control on the pitch damping of a floating wind turbine, in: Proceedings of the 2008 ASME Wind Energy Symposium, no. NREL/CP-500-42589, 2008.
[18] MARINTEK, SIMO User's Manual (2007).
[19] MARINTEK, RIFLEX User's Manual (2009).
[20] National Renewable Energy Laboratory - National Wind Technology Center, NWTC design codes (nov 2011). URL `http://wind.nrel.gov/designcodes/`

[21] H. Ormberg, E. Passano, N. Luxcey, Global analysis of a floating wind turbine using an aero-hydro-elastic model: Part 1: Code development and case study, in: Proceedings of the 30th International Conference on Ocean, Offshore, and Arctic Engineering, Rotterdam, the Netherlands, no. OMAE2011-50114, 2011.
[22] N. Luxcey, H. Ormberg, E. Passano, Global analysis of a floating wind turbine using and aero-hydro-elastic numerical model. Part 2: Benchmark study, in: Proceedings of the 30th International Conference on Ocean, Offshore, and Arctic Engineering, Rotterdam, the Netherlands, no. OMAE2011-50088, 2011.
[23] P. J. Moriarty, A. C. Hansen, AeroDyn theory manual, Tech. Rep. NREL/TP-500-36881 (2005).
[24] T. J. Larsen, How 2 HAWC2, the user's manual, Tech. Rep. Risø-R-1597(ver. 3-9) (2009).
[25] J. Jonkman, W. Musial, Offshore code comparison collaboration (OC3) for IEA Wind Task 23 offshore wind technology and deployment, Tech. Rep. NREL/TP-5000-48191, National Renewable Energy Laboratory (2010).

Paper 2

Time domain analysis procedures for fatigue assessment of a semi-submersible wind turbine

By Marit I. Kvittem and Torgeir Moan

Accepted for publication in Journal of Marine Structures, 2014

Time domain analysis procedures for fatigue assessment of a semi-submersible wind turbine

Marit I. Kvittem*[1,2] and Torgeir Moan[2]

[1] *NOWITECH, Norwegian University of Science and Technology, Trondheim, Norway*
[2] *CeSOS, Norwegian University of Science and Technology, Trondheim, Norway*

September 21, 2014

Abstract

Long term time domain analysis of the nominal stress for fatigue assessment of the tower and platform members of a three-column semi-submersible was performed by fully coupled time domain analyses in Simo-Riflex-AeroDyn. By combining the nominal stress ranges with stress concentration factors, hot spot stresses for fatigue damage calculation can be obtained. The aim of the study was to investigate the necessary simulation duration, number of random realisations and bin sizes for the discretisation of the joint wind and wave distribution. A total of 2316 3-hour time domain simulations, were performed.

In mild sea states with wind speeds between 7 and 9 m/s, the tower and pontoon experienced high fatigue damage due to resonance in the first bending frequency of the tower from the tower wake blade passing frequency (3P).

Important fatigue effects seemed to be captured by 1 hour simulations, and the sensitivity to number of random realisations was low when running simulations of more than one hour. Fatigue damage for the tower base converged faster with simulation duration and number of random realisations than it did for the platform members.

Bin sizes of 2 m/s for wind, 1 s for wave periods and 1 m for wave heights seemed to give acceptable estimates of total fatigue damage. It is, however, important that wind speeds that give coinciding 3P and tower resonance are included and that wave periods that give the largest pitch motion are included in the analysis.

Keywords: offshore wind, semi-submersible, integrated analysis, fatigue

1 Introduction

Fatigue damage is known to be a problem for bottom fixed offshore wind turbine substructures, and is also expected to be significant to floating wind turbines (FWTs). Adequate fatigue strength should be ensured by design. Wind parks consist of units with similar designs, and are thus vulnerable to "common cause"

*marit.irene.kvittem@ntnu.no

failures, which means that the economic consequences of poor fatigue design are serious. It is important, therefore, to make good fatigue estimates early in the design process.

Whereas for a wave only case, environmental conditions are taken from a scatter *table* (two variables: wave height and period), environmental conditions for a combined wind and wave case have to be taken from a scatter *block* (three variables: wind speed, wave height and period). This increases the number of combinations of wind and sea states that needs to be included in the fatigue damage assessment significantly compared to an onshore turbine or a traditional offshore structure. Wind- and wave directions and current are additional parameters that further increase the number of load cases.

The equations of motion for a wind turbine on a compliant sub-structure has many non-linear contributions: Catenary mooring line forces, viscous and aerodynamic forces and large displacements that require the loads to be calculated at the updated position. Due to these non-linearities the wind and wave loads on the structure cannot be treated separately, which means that all combinations of wind and wave loads must be analysed individually. Analysis of a non-linear system must also be performed in the time-domain, which is much more computationally time consuming than in the frequency domain.

Another issue is the discrepancy between guidelines for onshore wind turbines and for floating platforms when it comes to simulation length requirements. Due to the long natural periods of a compliant floating platform, it is often necessary to simulate from 3 to 6 hours to capture slowly varying response to wave and wind loads. This is emphasized in the new offshore standard for floating wind turbines from DNV [1]. Fixed wind turbines have higher natural frequencies, and the slowly varying response will be static, thus the normal simulation time for wind turbines is ten minutes. It is also common practice to assume ten minute stationary wind in wind statistics, whereas it is 1 to 6 hours for waves. Karimirad and Moan [2] found that a minimum of 3 hour simulations were needed to capture extreme bending moments for a 5 MW spar turbine, unless proper extrapolation was used. However, extreme values relate to the ultimate limit state, and do not normally contribute to fatigue due to the high return period.

In summary, all of these factors lead to a large number of environmental conditions that need to be simulated in the time domain for one to 6 hours. Also, to account for statistical uncertainty, a number of different realisations of the wind and wave histories must be included in the fatigue assessment. This requires unrealistic amounts of computing capacity and time in the design phase, and is the motivation for studying the parameters that make the execution time so long.

A recent paper by Haid et al. [3] studied the effect of simulation length on fatigue and ultimate loads for the OC3 spar buoy wind turbine, and concluded that the fatigue damage in the tower, blades and mooring system was more sensitive to the treatment of residuals in rainflow cycle counting than to simulation length. This work was done using the non-linear aero-hydro-servo-elastic tool FAST.

Earlier work by the authors [4], analyses applying the simplified aerodynamics model TDHmill in combination with Simo-Riflex indicated that 6-7 realisations of 1-hour wind and wave histories will give a fatigue estimate close to the damage based on the average of 10 3-hour realisations. This was, however,

based on a limited number of environmental conditions.

The current study aims at assessing simulation requirements for fatigue damage estimation, and the key questions are:

- How many realisations are needed to capture the effect of statistical uncertainty?
- What simulation duration is necessary to capture the important effects of slowly varying loads?
- What is the maximum bin size for the discretisation of the joint wind and wave distribution?

Fatigue for a a three column, catenary moored semi-submersible with the NREL 5MW [5] supported by the OC3 tower [6] (see Fig. 1) was examined. The single semi-submersible wind turbine (SSWT) was inspired by WindFloat [7]. The simulation tool used was Simo-Riflex-AeroDyn from Marintek and CeSOS. 10 realisations of 197 3-hour environmental conditions were simulated, with a CPU time approximately twice real time. The environmental conditions were strategically chosen from a joint wind and wave distribution to identify special expected and unexpected load effects.

These simulations serve as basis for comparisons of the fatigue damage for varying simulation lengths (from 10 minutes to 3 hours) and for varying number of realisations (1 to 10) of the same environmental conditions. The results were also used to identify load cases and effects that contribute significantly to fatigue, and to examine the effect of increasing the bin sizes for load case selection. The effect of misaligned wind and waves was also examined.

2 Modelling of the semi-submersible wind turbine and loads

2.1 Platform description

The WindFloat concept was chosen as inspiration for the floating platform in this study, and the platform geometry given in [7] was kept, but since more detailed specifications than what is available was necessary, a different design with similar global characteristics was developed (Tab. 1). The new platform was developed to have a mass distribution similar to WindFloat, but no extensive design check was performed on the assumed wall thicknesses. Compared to the OC4 DeepCWind concept, which is also a semi-submersible wind turbine concept, the column plate thicknesses for this design are smaller, while the braces and pontoons have thicker plates. The brace dimensions for the DeepCWind platform were found sufficient in an initial design check [17] for the central North Sea. Specifications for the turbine, the NREL 5MW reference turbine, can be found in [5], and in [6] for the tower.

The control system constants from the OC3 Hywind spar study were applied [6], with a constant torque strategy above rated wind speed. This controller is tuned to avoid negative damping above rated wind speed due to the pitch motion of the OC3 Hywind platform. This was done by setting the control system natural frequency to 0.2 rad/s, which is outside of the wave frequency

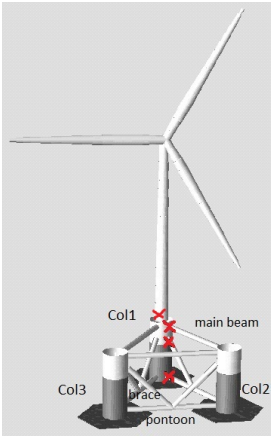

(a) Structural model. Locations for which fatigue results are presented in Sec. 6 are marked with 'x'.

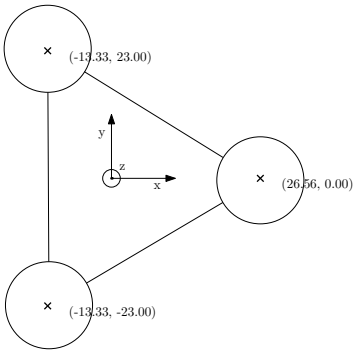

(b) Top view. The coordinate system z = 0 is in the mean water line.

Figure 1: Semi-submersible wind turbine.

range and below the natural pitch frequency of the spar platform. 0.2 rad/s is above the natural pitch frequency of the SSWT (0.17 rad/s) in this study, but setting control constants to get below this will give too much variation in the power production. Even though the controller natural pitch frequency could not be set below this limit, applying the OC3 Hywind constants gave less pitch motion than the land based controller. The negative damping instability was not observed for this platform, probably due to the heave plates, which provide viscous damping for pitch motion.

Table 1: Mass, damping and restoring data. All values are given for the platform without the turbine (rotor-nacelle-assembly and tower), unless otherwise noted, and are valid for zero thrust force ballast condition.

Displacement with WT	4810e6 kg
Mass with WT	4619e6 kg
Centre of gravity with WT	(-0.331 m, 0.0 m, 1.489 m)
Mass	4019e6 kg
Centre of gravity	(-4.300 m, 0.0 m, -7.857 m)
Radius of gyration Rxx	22.29 m
Radius of gyration Ryy	19.62 m
Radius of gyration Rzz	26.06 m
Radius of gyration Ryz	4.69 m
Hydrostatic stiffness Heave	2445 kN
Hydrostatic stiffness Roll	749815 kNm
Hydrostatic stiffness Pitch	7548571 kNm

2.1.1 Mooring

The platform is positioned by four mooring lines, two lines attached to column 1 and one line attached to each of the two other columns. In order to get natural periods for surge, sway and yaw close to what is specified for the generic WindFloat, a new mooring system was designed. A simple Riflex mooring line model was used, together with the mooring line equations in Ref. [18], to achieve the desired stiffness. The lines have 60 m of chain on top, 30 tonnes, 3.8 m^3 clump weight between chain and polyester rope, 769.8 m of polyester rope in the middle and 232.58 m of chain at the bottom.

2.1.2 Ballast system

The WindFloat platform has an active ballast system to keep the turbine upright and thus maximise power output as the wind direction and intensity change. This is done by pumping water ballast between the columns with a reaction time of 20 minutes [7] to significant changes in the mean wind speed and direction. The function of the ballast system is illustrated in Fig. 2 .

The initial ballast in the SSWT in these analyses was distributed to account for the asymmetric loading of the platform, i.e. the weight of the turbine and mooring system. During operation, the mean thrust force, tower drag and rotor torque give the platform a constant tilt. To get an upright configuration of the

Table 2: Fairlead and anchor line positions.

	x	y	z
Fairlead 1	31.56	0	-17
Fairlead 2	-15.78	-27.33	-17
Fairlead 3	-15.78	27.33	-17
Fairlead 4	31.56	0	-17
Anch 1	738.07	-706.51	-320
Anch 2	-721.76	-733.31	-320
Anch 3	-721.76	733.31	-320
Anch 4	738.07	706.51	-320

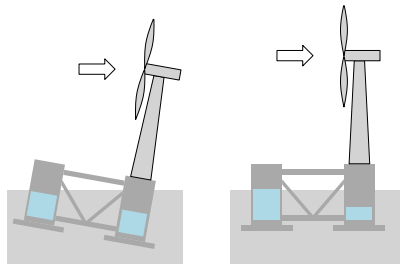

(a) Unballasted platform with turbine in operation.

(b) Ballasted platform with turbine in operation.

Figure 2: Illustration of ballast system.

platform in operation, a ballast system was modelled. Since the reaction time of the ballast system is long compared to other the dynamic loads on the system, it was modelled as constant ballast, and a new ballast distribution was calculated for every mean wind speed. Thus, mass distribution and restoring was updated for each environmental condition. The ballast distribution between column 1 and columns 2 and 3 (see numbering in Fig. 1a) was calculated from the thrust force and tower drag for constant wind velocity with a power law wind shear. The ballast distribution between column 2 and column 3 was calculated based on the rotor torque.

Table 3: Mass distribution for different wind speeds. Mass and vertical position of the centre of gravity (z_G) are given for the column, including heave plates and ballast.

U_{hub}	Column 1		Column 2		Column 3	
(m/s)	Mass (kg)	z_G (m)	Mass (kg)	z_G (m)	Mass (kg)	z_G (m)
0.0	749,418	-10.358	1400,128	-7.918	1400,128	-7.918
8.0	658,582	-10.439	1441,151	-7.715	1449,940	-7.671
11.2	579,217	-10.384	1476,078	-7.539	1494,378	-7.446
25.0	659,277	-10.439	1435,887	-7.741	1454,509	-7.648
49.0	652,823	-10.440	1448,425	-7.678	1448,425	-7.678

Samples of masses and centre of gravity for different wind speeds are presented in Tab. 3. In the cases with wind coming in from the side, where the rotor was rotated to be perpendicular to the wind, the same methodology to balance the thrust force and torque was used.

2.1.3 Eigenperiods

Some important eigenperiods (damped), found by decay analyses of the no thrust force ballast condition, are listed in Tab. 4. The tower first fore-aft bending frequency is higher than the fixed NREL 5 MW tower frequencies, and in this case that means that it will be within the range of the blade passing frequencies for lower wind speeds. This would normally call for a redesign of the tower. However, the analyses performed for this paper were also used in a comparison study of fatigue for different FWT concepts, where the same turbine and tower were used on different floating platforms [19]. In Ref. [19], the resonance effect was seen also for a TLP and the semi-submersible used in the OC4 study [20]. Thus, instead of optimising the design, it seems relevant to keep this standard design and highlight the issue.

2.2 Coupled analysis code

The coupled analysis tool Simo-Riflex-AeroDyn was applied in this study. Simo-Riflex from Marintek ([8], [9]) is suitable for time domain simulations of floating rigid bodies (Simo) coupled to flexible beam elements (Riflex).

The structural model of the turbine tower, blades and shaft was made up by beam elements. The rotor speed and the power output were controlled by a generator torque controller a blade pitch controller, respectively. Aerodynamic forces on the blades were calculated by AeroDyn [10], which reads a turbulent

Table 4: Damped natural periods for the platform ballasted for a zero wind condition.

Mode	T (s)
Surge	107.0
Sway	124.8
Heave	19.9
Roll	35.6
Pitch	37.4
Yaw	68.5
Tower 1st	2.3

wind field and applies the aerodynamic nodal loads to the blade elements. This method was verified by Ormberg and Bachynski [11].

Simo [12] solves the equation of motion in time domain for a single or multiple rigid bodies based on a frequency domain solution of the hydrodynamic loads by a panel method code (e.g. Wadam [13]). In addition, viscous forces can be included by a drag formulation. The traditional modelling method is to assume the complete platform as a rigid body. However, internal member forces of a statistically indeterminate structure can not be extracted from such an analysis. Thus, in order to get forces in the braces, the three columns of the platform were modelled as individual Simo bodies with potential theory forces, and the connecting braces were modelled as Riflex beam elements with Morison type forces.

2.3 Hydrodynamic forces

2.3.1 Potential theory model for columns and heave plates

The dynamic equilibrium equation for the columns (and heave plates) include mass forces, hydrostatic stiffness, gravity, buoyancy, external forces from Riflex, retardation functions accounting for frequency dependent added mass and linear damping, and wave excitation forces.

Wave force transfer functions according to the potential theory and the retardation functions for the columns with heave plates were obtained using multi body analysis in Wadam [13]. The heave plates were modelled by assuming a flat plate at the bottom of the columns in the Wadam analysis.

Hydrodynamic interaction between the columns was taken into account by applying the multi body analysis. However, some limitations on hydrodynamic interaction are inherent in the coupled Simo-Riflex software. This means that for one body, the effect of the presence of the other bodies was included in the force transfer functions and retardation functions, but the effect of motion of the other bodies was only accounted for in the force transfer functions, not in the retardation functions. The wave forces from Wadam include Froude-Krylov ($\mathbf{F}^{FK}$) and diffraction ($\mathbf{F}^{D}$) forces, as shown in Eq. 1.

$$\mathbf{F}^{HYD} = \mathbf{F}^{FK} + \mathbf{F}^{D} \tag{1}$$

In addition to the wave forces according to linear potential theory, viscous drag forces were included for both the columns and the heave plates. The drag

terms were calculated as described in the following section. The total wave forces in 6 degrees of freedom then becomes a sum of Froude-Krylov, diffraction and drag forces.

Difference frequency force transfer functions were not included since these are computationally very expensive to find in a multibody panel model analysis. A single body analysis in Wadam showed that the difference frequency forces for this platform are most predominant in surge and sway. These motions can contribute to fatigue, but in the current study excluding second order wave forcing was a trade-off for being able to calculate fatigue damage in the platform members.

2.3.2 Morison force model for beams, pontoons and braces

The wave forces on the slender beams, braces and mooring lines were calculated by Morison's formula (Eq. 2). The equation shows how the axial, lateral or transversal force, dF acting on a strip of the member, in its local coordinate system, are expressed in the simulations.

$$dF = \rho A\dot{u} + \rho A C_m \left(\dot{u} - \ddot{r}\right) + \frac{\rho}{2} D C_d |u - \dot{r}| \left(u - \dot{r}\right) \tag{2}$$

A is the cross section area, D is the reference area normal to the flow direction, i.e. the outer diameter for a circular cross section and the heave plate area for heave motion of the heave plates, and ρ is the seawater density. u is the wave particle velocity and r is the local member displacement, both in the direction of the force. C_d is the non-dimensional drag term, which is direction specific and C_m is the added mass coefficient, which is assumed to be zero for the longitudinal direction.

Table 5 shows the C_m and C_d coefficients applied in the analysis. For the mooring chains the non dimensional drag coefficients were taken from DNV-OS-E301 [14]. A drag coefficient of 1.0 for the columns was chosen to get a conservative estimate of the excitation forces on the columns. This value is higher than recommended in DNV-RP-C205 [15] for fixed cylinders, and may not give conservative damping values in surge and sway motions. Therefore, a sensitivity analysis comparing fatigue damage in the tower and braces was carried out with a drag coefficient of 0.7 for the columns, at relevant wave periods. This analysis gave less than 1.5% difference in all cases, and provided confidence that the results are not sensitive to the column drag coefficient. In heave, pitch and roll, the heave plates contribute to most of the hydrodynamic damping for this platform.

Vertical Morison drag terms for the heave plates and transversal/lateral drag terms for the columns were calculated by the last term in Eq. 2. The heave plate drag coefficient in Tab. 5 is based on model tests and numerical analysis of the WindFloat concept [16].

2.4 Aerodynamic loads in low wind speeds

At low wind speeds, wake dynamics can be significant. AeroDyn has the option of calculating the aerodynamic loads by simple BEM or by a generalized dynamic wake (GDW) model. The BEM method in AeroDyn does not include a dynamic wake correction, although it exists in other codes using BEM. In addition to

Table 5: Non-dimensional quadratic drag and added mass coefficients. For columns and heave plates added masses are found by potential theory.

Component	Transverse C_d (-)	Longitudinal C_d (-)	C_m (-)
Columns	1.0	0.0	-
Mooring chain	2.4	1.15	1.0
Mooring polyester rope	1.6	0.0	1.0
Main beam and pontoons	1.0	0.0	1.0
Braces	1.0	0.0	1.0
Heave plates	7.5	0.0	-

accounting for wake damping, GDW has the advantage of less computation time than BEM. The validity of the GDW model, however, is limited to higher wind speeds (unstable behaviour is reported for axial induction factors above 1/3, observed at 8 m/s and below for certain fixed turbines [10]). A floating wind turbine will pitch and surge, which affects the relative wind speed, and hence it will move in and out of the unstable range of GDW at wind speeds close to the limit (8 m/s).

This lead to unphysical instabilities in the analyses with particular combinations of waves and wind timeseries at 9 m/s. By changing to BEM, this effect was avoided.

However, between 7 and 9 m/s tower resonance due to the blade passing frequency (3P) load was observed, which led to high fatigue damage for these cases. Damping determines the amplitude of resonant behaviour, and damping may be lost or gained by including the dynamics of a wake. In a comparison between a simulation with BEM and one with GDW, without the unstable behaviour, GDW gave significantly less fatigue for 9 m/s wind. Since this damping is very important for the outcome of this study, and since the authors believe that GDW gives a more physical representation of the aerodynamic loads at this wind speed, GDW was used for the 9 m/s case. The few unstable analyses were rerun with a different wind seed. For the 7 and 8 m/s case the rotor would be too highly loaded, which would result in too many unstable analyses. Instead, tower structural Rayleigh damping was increased from a stiffness proportional coefficient 0.001 to 0.002, values which correspond to damping ratio of 0.3% and 0.6%, respectively, at the tower first fore-aft bending frequency. The original OC3 tower specifies a structural damping ratio of 1.0%, which is constant for all frequencies. Since only Rayleigh damping was available in the structural solver used in this study, damping ratio was initially chosen to be 1.0% between the first and second bending mode of the tower. Doubling the stiffness proportional stiffness gives a damping ratio close to and below what was specified for the OC3 tower, and is thus considered a conservative value.

3 Environmental data

3.1 Joint wind and wave distribution

In a study under the combined wind and wave power unit project, Marina Platform, joint wind and wave distributions for five sites in European waters were established [21], based on hindcast data of 1-hour averaged sea states and wind. The WindFloat prototype is located in the Atlantic Sea, off the coast of Portugal. Thus, the chosen environmental probability distribution of 1-hour sea states applied in this analysis was taken from the Buoy Cabo Silleiro site, off the coast of northern Portugal.

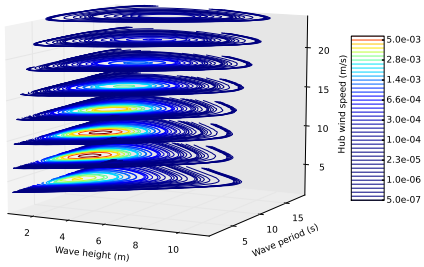

Figure 3: Joint wind and wave distribution.

3.2 Simulation length, wind and wave loads

Each environmental condition was simulated in Simo-Riflex-AeroDyn for 3 hours, plus 350 seconds warm up and transient, with 10 different stochastic samples of wind and wave timeseries. The 350 seconds of warm up and transient response contains 50 seconds controller warm up and 150 seconds of constant wind, and were removed from the results before post processing.

64-bit TurbSim [22] was used to simulate the 3-hour turbulent wind field. Turbulence was generated applying the Kaimal spectrum and the IEC normal turbulence model [23] with a reference turbulence intensity of 0.12. A power law wind shear profile with exponent of 0.14 was used for the mean wind speed component.

Since the power spectrum for wind measured over longer periods has small variations in the 1-hour range [24], it seems to be valid to assume 1 hour stationary wind fields. More recent research suggests that this gap does not exist [25], but the assumption has proven to give satisfactory models in the wind industry [26]. For fatigue analysis the very low-frequency variation from 1-3 hour changes in the wind, will most likely not have any impact compared to the high-frequency variations.

Irregular waves were generated in Simo with a 3-parameter Jonswap spectrum with a peak factor of 3.3, using Airy linear wave theory [12]. Long crested

waves were assumed. The misaligned wind and wave cases are described in Sec. 5.

4 Fatigue damage calculation

Axial stress σ in net cross sections of the different structural members was calculated for 24 points around the circumference of the pipe cross sections. The base metal cross sections of the members were used in the stress calculation and it was assumed that hot spot stress amplitudes are proportional to the nominal member stresses. Since it was the effects of simulation parameters that were under investigation in this study, an SCF of 1.0 was applied (the actual hot spot stress is proportional to this value). For a more detailed study with for multi axial stress conditions, possible different SCFs for different stress components need to be considered.

Nominal axial stress was calculated according to Eq. 4 [27]. Figure 4 shows the definitions of directions and axis for the tower base.

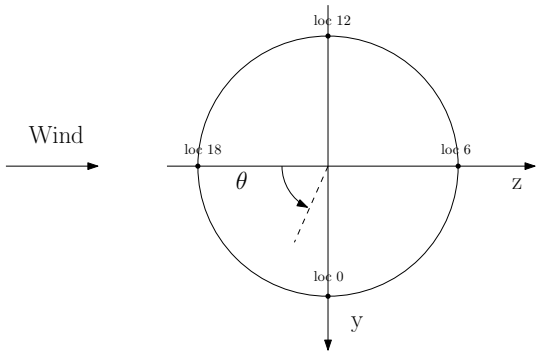

Figure 4: Top view of tower base cross section.

$$\sigma = \frac{N_x}{A} + \frac{M_y}{I_y} r_1 \cos\theta - \frac{M_z}{I_z} r_1 \sin\theta \tag{3}$$

N_x is the axial force, A is the nominal cross sectional area, M_y and M_z are bending moments and I_y and I_z are the sectional moments of area.

Rainflow counting was performed for the stress timeseries and fatigue was calculated by S-N-curves from DNV [28] and Miner's sum. Residual half cycles from the Rainflow counting were counted as half amplitudes.

Since fatigue damage occurs in welds rather than in the base material, S-N curves for girth welds were used. Based on the joint geometry, S-N curve D for σ was chosen, with categories "air" for tower and "cathodic protection" for the other members. The offshore wind turbine standard DNV-OS-J101 [29] states that the "in seawater with cathodic protection" curve can be used for members in the splash zone and water, assuming no repair and a guaranteed coating life of 15 years. In this study the service life is 20 years, but since the aim of the

study was not to perform fatigue design, the 15 year coating lifetime rule is disregarded.

To find the total damage over a service life of 20 years, damage estimates were multiplied by the respective probability and a scaling factor to adjust for the fact that the probability distribution yields for 1-hour sea states (T^{distr}) (see Eq. 4).

In traditional summations of fatigue damage, the probability is multiplied by the bin volume to achieve a total probability of 1. When the environmental conditions are not equally spaced, which was the fact in this study, it is not possible to find a bin volume, thus the scaling factor $p^{tot}/\sum_{i=1}^{N^{lc}} p_i$ was introduced instead. For the study of simulation length requirements and the number of stochastic samples, this factor cancels out, since damage for the same environmental conditions are compared, thus the factor will be a constant.

$$D_{total} = N^{20yr} \frac{p^{tot}}{\sum_{i=1}^{N^{lc}} p_i} \frac{T^{distr}}{T^{sim}} \frac{1}{N^{seeds}} \sum_{i=1}^{N^{lc}} \sum_{j=1}^{N^{seeds}} D_{ij} p_i \tag{4}$$

In Eq. 4, D_{total} is the accumulated damage over 20 years for the included environmental conditions, p^{tot} is the total probability of all load cases within the operation range of the turbine and with a probability above 10^{-4}, p_i is the point probability of environmental condition i, N^{20yr} is the number of 1-hour sea states in 20 years, N^{seeds} is the number of realisations of wind and waves, N^{lc} is the number of environmental conditions in the analysis, D_{ij} is the damage for a simulation for realisation number j of environmental condition i, with duration T^{sim}. T^{distr} is the averaging period for the applied joint wind and wave distribution, i.e. 1 hour.

Since this study focused on a turbine in operation, it was assumed that it will be in operation the whole time during wind conditions between cut-in and cut-out wind speeds. This is, of course, not a realistic assumption, but an operation time factor will not affect the results in this study. For a full lifetime fatigue assessment, downtime, along with survival, fault and installation, must also be included in separate analyses.

5 Load case selection

The IEC standard for design requirements for offshore wind turbines [30] recommends the following bin size for joint wind and wave assessment:

- Mean wind speed: 2 m/s
- Significant wave height: 0.5 m
- Peak wave period: 0.5 s

The DNV standard for column stabilised units [31] specifies that fatigue limit state analysis should cover events down to a probability level of 10^{-4}.

If the recommended bin sizes are used the total number of environmental conditions that have a marginal probability higher than 10^{-4} is 1539, not accounting for the directionality of wind or waves. Each load case must be simulated for at least 3-hours and with a certain number of different seeds for

random phase angles to capture worst representative wave loads. This requires excessive simulation time and capacity.

The number of random seeds required by the IEC standard [30] is 6. But since the structural response of a FWT to environmental loads is very different from a fixed structure, more variability in the response statistics is a possible outcome of these analysis. Thus, with the intention of being able to see convergence in the results, the number of seeds was increased to 10.

In this study, simulations were carried out in three phases: The first covered the necessary simulation length and number of seeds, the second covered wind-wave misalignment. After analysing the results from the first phase, additional environmental conditions were added for the study of environmental condition bin size in the third phase. A total of 2316 simulations were carried out:

- 3-hour realisations of 155 different environmental conditions with aligned wind and waves (10 seeds)
- 3-hour realisations of 42 environmental conditions with misaligned wind and waves (10 seeds)
- Additional 3-hour realisation of 346 different environmental conditions (1 seed, only used for studying the effect of bin size)

5.1 Phase 1 - Environmental conditions for simulation lengths and number of seeds

The present analysis was based on the recommended bin sizes for waves from the IEC standard, and the lower an upper turbine operation wind speed limits, together with 1 m/s bins for mean wind speed. Applying the 10^{-4} probability threshold together with turbine operation range limits, leaves 2201 load cases that have a total accumulated probability of 81%. From these, 155 environmental conditions (see Fig. 5) were selected to reflect different load case groups:

1. Base case with large bin sizes
2. 5% most probable load cases
3. Special cases with critical frequencies
4. Variation in wave height
5. Variation in wave period
6. Variation in wind/wave misalignment

As a first step, a few load cases are selected as base cases, shown as "Base case" in Fig. 5. The basic assumption in selecting these cases is that fatigue damage increases with wave height (given wave period) and that important dynamic effects are captured. A coarse grid of mean wind speeds and wave periods was selected from the 2201 load cases with probability above 10^{-4}.

The 11 most probable environmental conditions were also chosen. The reason for not including more is that one obtains many cases with low wind speed and small waves and not much variation between the cases.

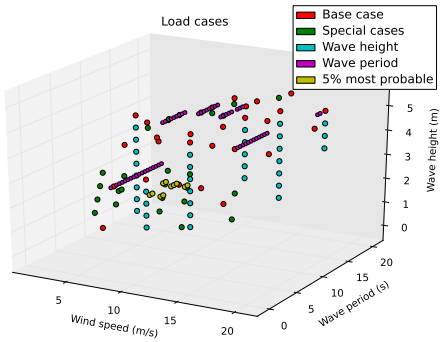

Figure 5: The 155 environmental conditions analysed in this study. Wind speed refers to hub wind.

To find how fatigue damage varies with wave height, some of the base cases were run with varying wave height. The load cases were chosen such that different wind speeds and peak periods were represented in the selection.

There are certain dynamic effects, which depend on wave period and wind speed, that can cause large fatigue damage. To make sure that these were included in the analyses, loads that might increase fatigue loading were identified:

- Wave length corresponding to when wave forces have 180 degree phase difference on columns, in this case 7.2 s and 7.7 s
- Heave resonance at 19.9 s
- Tower wake 3P loads close to tower first mode fore-aft and side-to-side bending at 2.3 s, which corresponds to mean wind speeds around 7 m/s
- Higher harmonics of drag forces (mainly 3ω) close to structural flexible modes. Most relevant wave periods give 3ω in a range between rigid body modes and the tower first bending mode, and other flexible natural frequencies are expected to be higher, so only the shortest periods are relevant to capture this phenomenon.
- Higher turbulence intensity at lower wind speeds
- Rated wind speed for maximum thrust force on rotor

Based on these criteria, combinations of wave peak periods 2.5, 6.5, 7.0, 7.5, 8., 16., 20 s and mean wind speeds 3., 5., 9., 11., 15., 23 m/s were chosen from the 1539 load cases mentioned above. From these, combinations with the largest wave height were chosen as the first step to screen load cases.

5.2 Phase 2 - Environmental conditions for wind-wave misalignment

When wind and waves come from different directions, tower bending moments can increase from the aligned case since the rotor no longer provides damping

for wave excitation. This has been documented through analyses for offshore turbines with monopile foundations [32], and is also expected to be a problem for floating wind turbines [33]. In the current study, some of the base cases were run with misaligned wind and waves (0-90°), both with head wind and wind from the side with the rotor yawed 90° (see Fig. 6). Since a joint wind and wave distribution with directional distribution did not exist for this site, and since including directions will drastically increase the number of load cases, the misaligned wind and wave cases were only performed to check the validity of assuming unidirectional wind and long crested waves.

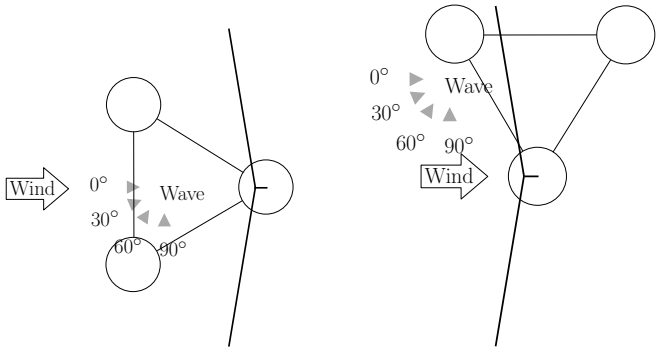

Figure 6: Top view illustration of wind and wave directions for the misaligned cases.

The turbine has a yaw mechanism to make the rotor plane normal to the wind, and since the mass and restoring properties of the platform are not symmetric, wind coming from a different direction than the one assumed in this study, causes different load responses. To get an impression of the effect of wind direction, the misalignment cases were also run for wind from the side (incoming wind angle of 90°). When wind comes from the side, it will cause the platform to yaw. Riflex can not yet model the yaw mechanism, but the rotor should be kept normal to the wind, thus the platform was given an initial yawed position, calculated based on the thrust force for a fixed turbine. This was not done for yaw due to waves, since this yaw moment was observed to be significantly lower than the yaw due to an eccentric thrust force.

5.3 Phase 3 - Environmental conditions for bin size evaluation

Since the results from the load cases listed above showed that determining fatigue damage from only 1 realisation of a 3-hour environmental condition gave reasonable estimates, one 3-hour realisation of evenly spread load cases were performed to be able to say something about the discretisation of the environmental conditions when calculating the total fatigue damage.

346 additional load cases were run, using a bin size of 1 m/s for wind speed, 1.5 m for wave height and 1 s for wave period. These load cases were only used

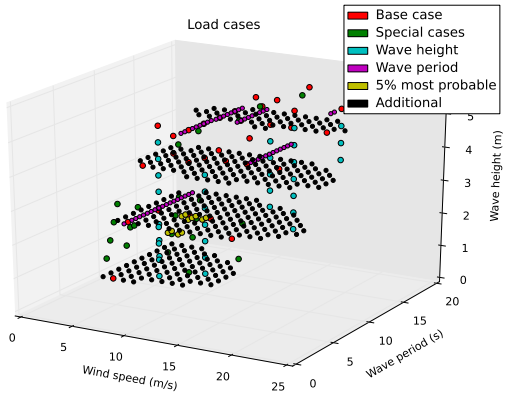

Figure 7: 346 additional environmental conditions, used for studying the effect of bin size. Only one 3-hour realisation of the additional environmental conditions was run.

to study how load case selection and bin sizes affect the total fatigue damage estimate. The additional load cases, together with the original load cases, are shown in Fig. 7.

6 Simulation results

Fatigue damage was calculated for both axial and shear stress components, but shear stress fatigue damage was significantly lower than for axial stress. Thus, the shear stress fatigue was excluded from the paper.

All results presented in this section refer to the cross section location with the maximum 10-seed average damage. The points where fatigue was calculated for the different members are shown in Fig. 1.

6.1 Load conditions that cause large fatigue damage

Wind speeds 7 m/s and 9 m/s caused high short term fatigue damage (Fig. 8) compared to what one would expect for mild wind conditions. For the higher wind speed cases (17 m/s and 20 m/s) fatigue damage is also high, but for these cases wave height is higher, thus higher damage was expected.

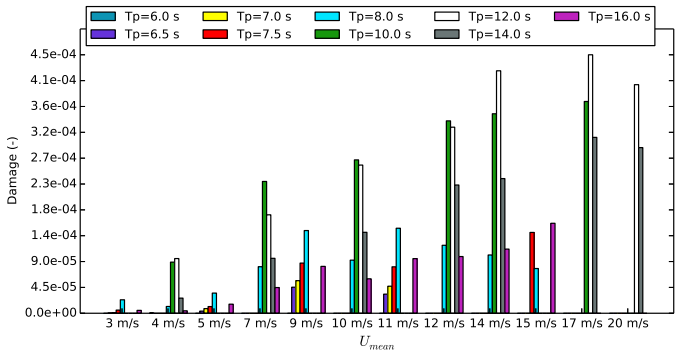

Figure 8: 3-hour fatigue damage in tower bottom for base case and special cases, arranged by wind speed and wave period. Wave heights vary between 0.5-4.5 m for below rated wind and 2.5-5.5 m for above rated wind.

Tower wake 3P loads at low wind speeds (approximately 2.67 rad/s for 7 m/s and 3.26 rad/s for 9 m/s) are close to the tower first bending mode (2.73 rad/s). This results in resonance in the tower at low wind speeds, which causes high fatigue damage. The contribution from these load cases is large in the long term fatigue analysis since this range of wind speeds occurs frequently.

This is normally not a problem for fixed foundations since the tower natural frequency is lower. The natural frequency is lower both because there are no rigid body modes and because towers are normally longer than for floating platforms. For a floating platform, there is a risk that the first bending frequency of the tower is within the three times rotational speed of the rotor in the below rated operating state.

6.2 Simulation length and number of random realisations

The total 20 year fatigue damage was calculated by Eq. 4 for the environmental conditions in Fig. 5. The number of samples varied from 1 to 10 and simulation lengths were varied from 10 minutes to 3 hours. The 10 min to 2 hour simulations were obtained by sampling stress histories from the steady state 3-hour timeseries. The fatigue damages calculated based on 10 min to 2 hour durations were scaled up for comparison with 3 hour damages.

Estimating the total 20 year fatigue based on 10x1-hour simulations of each load case underestimated damage by less than 4% compared to 10x3-hour simulations (Fig. 9). Using 10x10-minute simulations underestimated the damage by 10%. Fatigue damage for the tower appeared to be less affected by simulation length than the platform members, pontoon, main beam and brace.

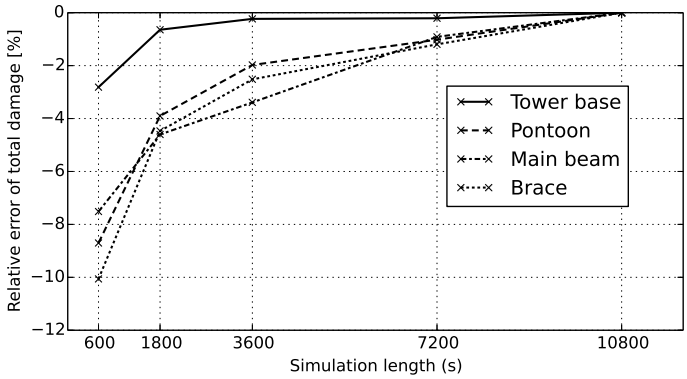

Figure 9: Relative difference to 3-hour simulations in 20 year total damage (Eq. 4) for axial stress fatigue. The average damage from 10 samples was used for all the simulation lengths shown.

In essence, a 3-hour simulation contains the same statistical content as 3x1-hour or 6x30-min simulations. I.e., using longer simulations reduces the number of seeds required. It was found that the long term fatigue damage calculated based on 10-minute simulations varied more with seed number, and gave larger errors compared to the 10 seed average than for the longer simulation lengths (Fig. 10). Another important observation is that the error for fatigue in the tower base was very small.

A full evaluation of the required number of seeds in a statistical sense would require a large sample of 3-hour simulations. A sample of 10, which was used in this study, is not statistically significant. Moreover, the fact that the order of the samples is random, contributes to the non-converging behaviour of the data in Fig. 10. The focus was kept on including as many different environmental conditions as possible within the time frame of this work, and thus the number of samples could not be increased. Therefore, a method introduced by Langley [34] to estimate the root mean square (RMS) error of a limited number of program runs (Eq. 5) was applied.

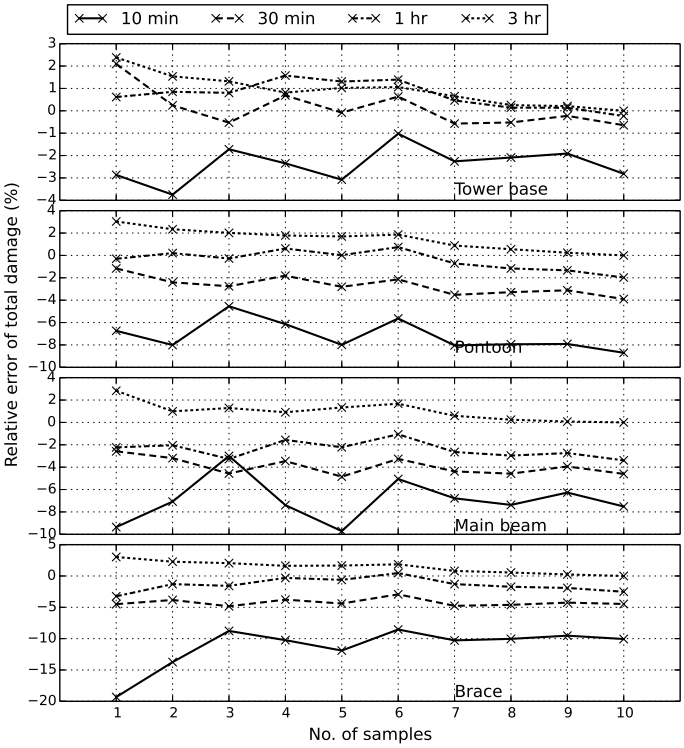

Figure 10: 20 year damage as a function of the number of samples, calculated as the cumulative average of N^{seeds}, where N^{seeds} varied from 1 to 10. The error refers to the damage calculated from 10x3-hour simulations.

$$\delta = \frac{1}{\sqrt{N^{seeds}}} \frac{\sigma_D}{\mu_D} \tag{5}$$

μ_D and σ_D in this context are the mean value and the standard deviation, respectively, of the 20 year fatigue damage.

The resulting RMS error is shown in Fig. 11. Similar conclusions to what has been described earlier in this section can be drawn from the RMS estimate; errors are small in general, but larger for 10-minute simulations, and the tower base was less sensitive to the number of seeds than the platform members.

Figure 11 also illustrates an important point; that the statistic content is the same in six 10-minute samples as in one 1-hour sample, and thus the expected error is the same.

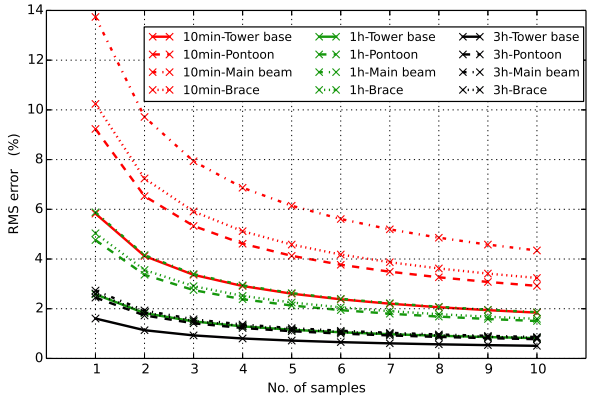

Figure 11: Estimated RMS error for 20 year damage, as a function of number of samples.

6.3 Bin size and load case selection

The discretisation of long term environmental conditions (determining bin size) must ensure that all important load effects are captured such that a realistic and conservative estimate of the fatigue damage can be determined. Moreover, a course grid of environmental conditions also means fewer simulations and thus fewer random samples.

In this section, the influence of bin size on the 20 year fatigue damage is investigated based on 1 realisation of the load cases labelled "additional" in Fig. 7, as well as 10 seed average damage from the load cases in Fig. 5.

6.3.1 Bin size for wind speeds

The total fatigue was calculated for increasing bin sizes. Table 6 shows that by increasing the bin size from 1 to 2 m/s, the total fatigue damage for the

tower was reduced by 9%. However, a bin size of 2 m/s, starting at cut-in wind speed (i.e. load cases include 3, 5, 7,.. m/s), means that the most important resonance case at 8 m/s is left out. If a bin size of 2 m/s was used, and the 8 m/s cases were included, the deviation in the total damages would be 0.3% for the tower, 3.2% for the pontoon, 1% for the main beam and 3.1% for the brace. This indicates that a bin size of 2 m/s will give an acceptable damage estimate if 3P resonance cases are included.

Table 6: Variation of 20 year fatigue damage in tower base for varying bin size, relative to the smallest bin size. The bin size is 1 m/s for wind speed, 0.5 m for wave height and 0.5 s for wave period, unless otherwise specified. The damage is calculated according to Eq. 6. Please note that the selection of H_s representing bin sizes below 1.5 m is limited.

Bin size U_{hub}	Tower base D_{rel} (%)	Pontoon D_{rel} (%)	Main beam D_{rel} (%)	Brace D_{rel} (%)	No. of env. cond.
1.0 m/s	100	100	100	100	478
2.0 m/s	91	90	89	88	219
3.0 m/s	88	85	79	85	152
4.0 m/s	85	83	83	81	120
H_s					
0.5 m	100	100	100	100	478
1.0 m	101	101	100	99	234
1.5 m	96	94	96	94	410
2.0 m	41	38	44	38	101
T_p					
0.5 s	100	100	100	100	478
1.0 s	100	100	101	100	442
1.5 s	104	103	101	103	161
2.0 s	103	105	104	104	245

The number of environmental conditions included in the calculation of the total fatigue damage for different bin sizes is shown in the rightmost column of Tab. 6. What can be observed, is that the total fatigue damage changes more from 478 to around 200 environmental conditions when changing the wind speed bin size, than when changing the wave height or wave period bin size. The relatively low sensitivity to the number of seeds, which was described in Sec. 6.2, is consistent with this. Thus, it seems that the total fatigue damage was more sensitive to the bin size parameter than the number of environmental conditions.

In the H_s section of Tab. 6, the number of environmental conditions is smaller for bin size 1.0 m than for 1.5 m. The same can be observed for T_p. This has to do with the distribution and the selection of simulated environmental conditions (as shown in Fig. 7).

6.3.2 Bin size for wave periods

To be able to evaluate if the most important wave periods are included in the total fatigue damage assessment, comparisons of damage for load cases with

varying wave period were carried out ("wave period" in Fig. 5). These comparisons indicated that pitch motion has a significant contribution to fatigue damage in all members. Figures 12 and 13 show the highest damages for 10-12 s waves, which coincides with a peak in the pitch response amplitude operator. The reduction of fatigue damage with increasing wave period in Figs. 12 and 13 is fairly linear, which can explain that the increase of wave period bin size do not cause significant changes in the damage estimates in Tab. 6. Choosing a bin size of 2 s gave an acceptable result in this case, but keep in mind that this conclusion depends on the response characteristics of the platform.

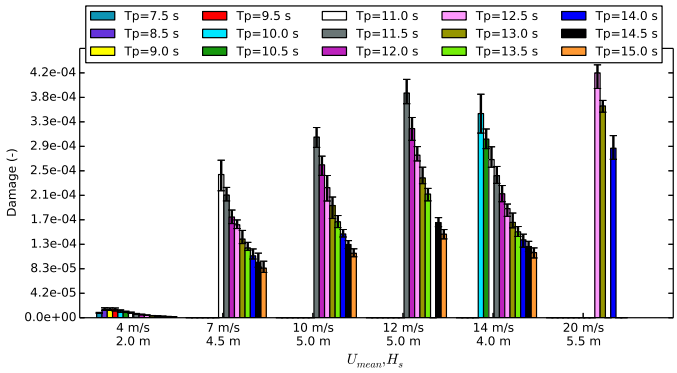

Figure 12: 3-hour short term fatigue damage due to axial stress in the tower base for varying wave period, averaged over 10 seeds. Maximum/minimum observed damage in all realisations is shown with errorbars.

The selection of load cases called "additional" in Fig. 7 has a bin size of 1 s for wave periods, which means that the damage for bin size 0.5 s in Tab. 6 does not include all possible load cases with 0.5 s bin size. However, comparing damage weighted with probability for the cases labelled "wave period" in Fig. 7 with a bin size of 1.0 s only gives 0.4-3.9% difference compared to a bin size of 0.5 s.

6.3.3 Bin size for wave heights

Table 6 indicates that 1.0 m bin size for wave heights will give acceptable results. The bin size for wave heights in the "additional" load cases (Fig. 7) is 1.5 m. Calculating fatigue for the load cases that have a bin size of 0.5 m, 1.5 m bin size gives 1.0-9.4% difference (17-32% for 4 m/s wind and 12 s waves).

One possible explanation for damage being more sensitive to the increase of bin size for wave heights can be found in the wave induced pitch motion of the platform. Assuming that only forces on the tower caused by pitch motion causes tower fatigue, and that the stresses increase linearly with pitch angle, the fatigue damage increase will be non-linear (in the order of the m-parameter in the fatigue curve, which is 3 and 5 in this study, see [28]). Nonetheless, as can be seen in Fig. 7, more cases with variation in wave height should be included

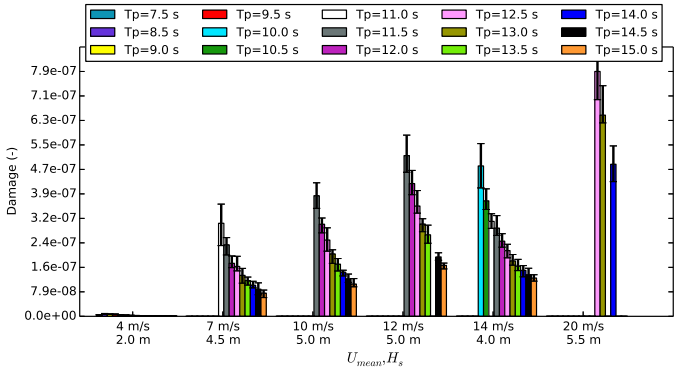

Figure 13: 3-hour short term fatigue damage due to axial stress in the brace for different wind speeds, wave heights and periods, averaged over 10 seeds. Maximum/minimum observed damage in all realisations is shown with errorbars.

to make a firm conclusion about sensitivity to wave height bin size.

6.4 Total fatigue damage for other sites

Although this study was not an attempt to do full fatigue damage assessment, and no explicit values for long term fatigue damage is presented, it should be mentioned that the calculated damages indicate an unacceptably low fatigue life, since installation, survival conditions, faults and parked condition also require parts of the allowable fatigue damage, and since weld geometries most likely will give stress concentration factors higher than 1.

In order to give an impression of how much the long term fatigue damage can be reduced by applying environmental data from other sites, sensitivity was performed by using the probability distributions from the other sites addressed in [21]. The relative total 20-year fatigue damage (Eq. 4) compared to the Portugal location was:

- 69-82% for site no. 1 (Atlantic, France)
- 89-94% for site no. 5 (Atlantic, Great Britain)
- 121-130% for site no. 14 (North Sea - Norway)
- 64-78% for site no. 15 (North Sea - Denmark)

The water depth in site no. 1, 5 and 15 is lower than assumed in this study, and thus they are not relevant sites for this particular SSWT, considering that the mooring design would have to be redesigned. The numbers do, however, give an idea of the sensitivity of fatigue damage to wind- and wave distribution at different sites.

6.5 Misaligned wind and wave conditions

Uni-directional wind and waves, with long crested waves, were assumed in the above sections. Fatigue damage calculated based on misaligned wind and waves indicated that this was a conservative assumption (Fig. 14). The reason for the different conclusion in [33] and [32] will be further discussed in another paper with misalignment as the main focus [19]. In short, the bending moments from wind and waves act around different axes, and thus the contribution to fatigue damage comes in different cross section locations. This is clearly seen for the tower. Bottom fixed turbines get fatigue damage due to flexible modes, which do not have very high hydrodynamic damping. For the SSWT large contributions to fatigue damage come from the rigid body motions of the platform (roll and pitch), and these motions have high drag damping from the heave plates. Wind from other angles than 0° and 90° have not been simulated, and fatigue damage may be higher with aligned wind and waves from other angles.

Figure 14a shows an incoming wind angle of 0°, and Fig. 14b shows the 90° case, both with the rotor facing the wind (see Fig. 6 for a definition of the directions). In general, the 0° case displayed significantly higher short term damage than the 90° case, which is most likely due to the wave excitation being smaller when coming from the side. And even when the wave excitation come from the front, the wind comes from the side, and the forces act around different axes, causing less fatigue damage.

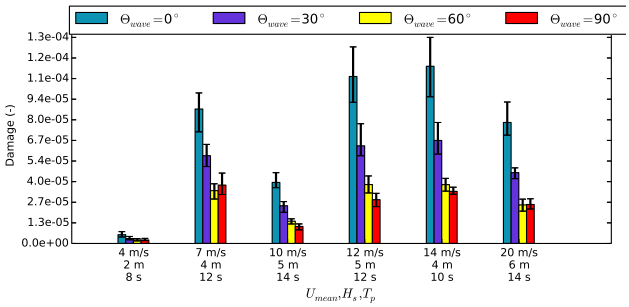

(a) Incoming wind angle 0°.

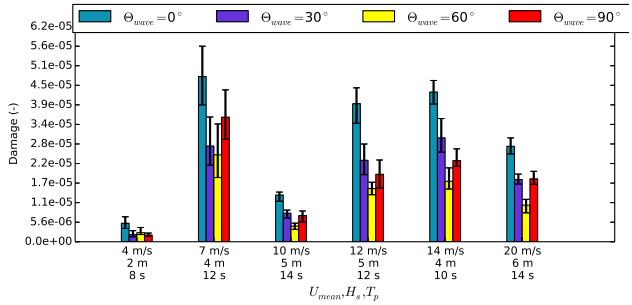

(b) Incoming wind angle 90°.

Figure 14: 1-hour fatigue damage based on axial stress in tower base for misaligned wind and waves, averaged over 10 seeds. Maximum/minimum observed damage in all realisations is shown with errorbars. A definition of directions can be seen in Fig. 6.

7 Conclusions

This study deals with fatigue analysis for a wide range of environmental conditions for a semi-submersible wind turbine with the purpose of studying the effect of simulation length, the number of necessary realisations of wind and wave loads, bin size and wind-wave misalignment.

The study showed that blade passing frequency resonance in the tower and pitch motion of the platform were the most significant contributors to fatigue damage in the tower and pontoon. Capturing resonant responses is important when choosing load cases for fatigue analysis. Choosing load cases that do not give high fatigue damage is also important, to get a realistic fatigue estimate for the service life.

Based on 10x3-hour simulations of 155 environmental conditions, the sensitivity to simulation length and number of realisations was investigated. By calculating fatigue based on 10-minute samples, fatigue damage was underestimated by up to 10%. For 1-hour durations, the estimate was 4% below the 3-hour damage. The simulations showed that the overall trend for the fatigue damage estimate decreased with number of random realisations. The RMS error compared to the average of 10 3-hour realisations was less than 1% for 7 seeds of 3-hour simulations and less than 2% for 9 seeds of 1-hour simulations. Fatigue damage in the platform members was more sensitive to the number of realisations and simulations duration than the damage in the tower base.

Based on the conclusions that only 1 3-hour realisation gave a satisfactory fatigue damage estimate, 346 additional environmental conditions were analysed to study the effect of bin size. A bin size of 2 m/s for wind speeds gave acceptable damage estimates, provided that wind speeds for the important resonance frequency at 8 m/s was included. For waves bin sizes of 1 s for T_p gave similar estimates as 0.5 s, but with respect bin size for H_s, fatigue damage was more sensitive to bin size.

Misaligned wind and waves seemed to give less fatigue than unidirectional wind and waves, which means that it is conservative to assume unidirectionality. However, which parts of the platform structure that experience the highest fatigue damage, will depend on the wave direction.

Placing a turbine on a floating platforms alters the natural frequencies of the turbine itself. For the platform in this study, the tower first fore-aft and side-to-side bending frequencies are within the range of the blade passing frequency for wind speeds 7-9 m/s. This lead to resonance in the tower for these wind speeds. At resonance it is important to have a proper representation of the aerodynamic and structural damping. This is however an issue in some state-of-the-art aerodynamic models, since BEM without dynamic wake correction does not include wake damping, and the generalised dynamic wake model in AeroDyn is unstable for wind speeds around 8 m/s and below. This calls for an improvement of aerodynamic codes applied in the analysis of floating wind turbines.

Fatigue damages observed in this study indicate that fatigue damage will be unacceptably high for the tower. Since resonant motion in the first bending frequency of the tower contributes significantly to fatigue below rated wind speed, towers should be designed for each platform type to have resonance frequencies outside of the blade passing frequency range.

8 Acknowledgements

The authors wish to acknowledge the support from NOWITECH and the Norwegian Research Council through Centre for Ships and Ocean Structures at NTNU.

References

[1] Det Norske Veritas. *DNV-RP-J103, Design of Floating Wind Turbine Structures*, 2013.

[2] M. Karimirad and T. Moan. Extreme dynamic structural response analysis of catenary moored spar wind turbine in harsh environmental conditions. *Journal of offshore mechanics and Arctic engineering*, 133(4), 2011.

[3] L. Haid, G. Stewart, J. Jonkman, A. Robertson, M. Lackner, and D. Matha. Simulation-length requirements in the loads analysis of offshore floating wind turbines. In *Proceedings of the 32nd International Conference on Ocean, Offshore and Arctic Engineering*, Nantes, France, 2013.

[4] M. I. Kvittem, T. Moan, Z. Gao, and C. Luan. Short-term fatigue analysis of semi-submersible wind turbine tower. In *Proceedings of 30th International Conference on Ocean Offshore and Arctic Engineering*, Rotterdam, The Netherlands, 2011. Paper no. OMAE2011-50278.

[5] J. Jonkman, S. Butterfield, W. Musial, and G. Scott. Definition of a 5-MW reference wind turbine for offshore system development. Technical report, NREL, 2009. NREL/TP-500-38060.

[6] J. Jonkman. Definition of the floating system for phase IV of OC3. Technical report, National Renewable Energy Laboratory, 2010.

[7] D. Roddier, A. Peiffer, A. Aubault, and J. Weinstein. A generic 5MW WindFloat for numerical tool validation and comparison against a generic spar. In *Proceedings of ASME 30th International Conference on Ocean Offshore and Arctic Engineering*, Rotterdam, The Netherlands, 2011. Paper no. OMAE2011-50278.

[8] MARINTEK. *RIFLEX User's Manual*, 2013.

[9] MARINTEK. *SIMO User's Manual*, 2013.

[10] D. Laino and A. C. Hansen. *AeroDyn users guide*, 2002.

[11] H. Ormberg and E. E. Bachynski. Global analysis of floating wind turbines: Code development, model sensitivity and benchmark study. In *Proceedings of the 22nd International Ocean and Polar Engineering Conference*, Rhodes, Greece, 2012.

[12] MARINTEK. *SIMO Theory Manual*, 2012.

[13] Det Norske Veritas. *SESAM User Manual Wadam*, 2008.

[14] Det Norske Veritas. *DNV-OS-E301, Offshore standard-position mooring*, 2010.

[15] Det Norske Veritas. *DNV-RP-C205, Environmental Conditions and Environmental Loads*, 2007.

[16] Principle Power. Wamit model for WindFloat 5 MW. Technical report, Principle Power, 2010.

[17] C. Luan, Z. Gao, and T. Moan. Modelling and analysis of a semi-submersible wind turbine with a central tower with emphasis on the brace system. In *Proceedings of the 32nd International Conference on Ocean, Offshore and Arctic Engineering*, Nantes, France, 2013.

[18] O. M. Faltinsen. *Sea Loads on Ships and Ocean Structures*. Cambridge University Press, 1990.

[19] E. E. Bachynski, M. I. Kvittem, C. Luan, and T. Moan. Wind-wave misalignment effects on floating wind turbines. To be published, 2014.

[20] A. Robertson, J. Jonkman, Musial W., F. Vorpahl, and W. Popko. Offshore code comparison collaboration, continuation: Phase II results of a floating semisubmersible wind system. Technical report, National Renewable Energy Laboratory, 2013.

[21] L. Li, Z. Gao, and T. Moan. Joint environmental data at five european offshore sites for design of combined wind and wave energy devices. In *Proceedings of ASME 32th International Conference on Ocean Offshore and Arctic Engineering*, Nantes, France, 2013. Paper no. OMAE2013-10156.

[22] B. J. Jonkman. *TurbSim users guide*, 2009.

[23] International Electrotechnical Commission. *IEC61400-1, Wind turbines - Part 1: Wind turbines, design requirements*, 2005.

[24] I. Van der Hoven. Power spectrum of horizontal wind speed in the frequency range from 0.0007 to 900 cycles per hour. *Journal of Meteorology*, 14(2):160–164, 1957.

[25] J. Apt. The spectrum of power from wind turbines. *Journal of Power Sources*, 169(2):369–374, 2007.

[26] T. Burton, N. Jenkins, D. Sharpe, and E. Bossanyi. *Wind energy handbook*. John Wiley & Sons, 2011.

[27] F. Irgens. *Mechanics of Materials (in Norwegian)*. Tapir, 2006.

[28] Det Norske Veritas. *DNV-RP-C203, Fatigue Design of Offshore Steel Structures*, 2010.

[29] Det Norske Veritas. *DNV-RP-J101, Design of Offshore Wind Turbine Structures*, 2010.

[30] International Electrotechnical Commission. *IEC61400-3, Wind turbines - Part 3: Design requirements for offshore wind turbines*, 2009.

[31] Det Norske Veritas. *DNV-RP-C103, Column-stabilised units*, 2010.

[32] T. Fischer, W. Vries, P. Rainey, B. Schmidt, K. Argyriadis, and M. Kühn. Offshore support structure optimization by means of integrated design and controls. *Wind Energy*, 15(1):99–117, 2012.

[33] L. Barj, S. Stewart, G. Stewart, M. Lackner, J. Jonkman, A. Robertson, L. Haid, and D. Matha. Impact of wind/wave misalignment in the loads analysis of a floating wind turbine. In *Poster presentation at AWEA Wind Power*, 2013.

[34] R. S. Langley. On the time domain simulation of second order wave forces and induced responses. *Applied ocean research*, 8(3):134–143, 1986.

Paper 3

Wind-wave misalignment effects on floating wind turbines: motions and tower fatigue load effects

By Erin E. Bachynski, Marit I. Kvittem, Chenyu Luan, Torgeir Moan

Accepted for publication in Journal of Offshore Mechanics and Arctic Engineering in November 2014

Is not included due to copyright

Paper 4

Frequency versus time domain analysis for fatigue of a semi-submersible wind turbine

By Marit I. Kvittem and Torgeir Moan

Accepted for publication in Journal of Offshore Mechanics and Arctic Engineering in February 2015

Is not included due to copyright

Appendix B

Abstracts of additional papers

Short-term fatigue analysis of semi-submersible wind turbine tower

Marit I. Kvittem*[1,2], Torgeir Moan[2], Zhen Gao[2] and Chenyu Luan[3]

[1] *NOWITECH, Norwegian University of Science and Technology, Trondheim, Norway*
[2] *CeSOS, Norwegian University of Science and Technology, Trondheim, Norway*
[3] *NTNU, Norwegian University of Science and Technology, Trondheim, Norway*

Published in Proceedings of 30th International Conference on Ocean, Offshore and Arctic Engineering, 2011.

Abstract

Coupled time domain analyses of a semi-submersible wind turbine are performed with the intention to study motions affecting fatigue damage at the base of the tower. The software applied is SIMO/RIFLEX with the extension TDHmill, which gives the wind thrust force and gyro moment on the wind turbine as point loads in the tower top.

Short term environmental conditions are chosen from a joint wind and wave distribution for a site in the Northern North Sea. Variance spectra, mean value, standard deviation, kurtosis, skewness and Vanmarcke's bandwidth parameter are calculated for stresses at the base of the tower. Damage is calculated for each short term condition by two methods; rainflow counting and narrow band approximation. The accuracy of narrow band approximation estimates for fatigue are examined for the structure in question.

Time domain simulations are carried out for different sea states and fatigue damage is calculated for each case. Simulations show that turbulent wind dominates the response at low wind speeds and the response spectral density function tends to be very wide-banded. For wave dominated response, spectra have lower bandwidth, and narrow banded approximation for fatigue damage gives estimates 20-50% above rainflow counted damage.

*marit.irene.kvittem@ntnu.no

Effect of mooring line modelling on motions and structural fatigue damage for a semi-submersible wind turbine

Marit I. Kvittem*[1,2] and Torgeir Moan[2]

[1] *NOWITECH, Norwegian University of Science and Technology, Trondheim, Norway*
[2] *CeSOS, Norwegian University of Science and Technology, Trondheim, Norway*

Published in Proceedings of the Twenty-second International Offshore and Polar Engineering Conference, 2012.

Abstract

Most current software applied for motion analysis of floating wind turbines employ some kind of linearized mooring line model, ignoring mooring line dynamics. The impact of these assumptions are well known for offshore oil platforms, but for a floating wind turbine the wind-to-wave load ratio is higher, and the experiences from the offshore industry cannot be applied directly. However, these experiences state that linearized models can provide good prediction of fatigue damage applying frequency domain analysis, which can significantly shorten analysis time.

In this paper a single semi-submersible wind turbine (SSWT) was investigated with a linearized mooring line model and compared with an advanced finite element mooring line model for three different mooring line configurations. The parameters investigated were platform motion characteristics and bending moment in the tower. These analyses were carried out by a numerical tool obtained by integrating the hydrodynamic software SIMO/RIFLEX and AeroDyn for aerodynamic loads on the blades of the turbine.

The results from these analyses showed significant differences in the standard deviations for sway and yaw motions and sideways bending moment in the tower between the linearized model and the full mooring line model. The linearized model gave relatively good predictions of surge motions of the platform and fore-aft bending moment in the tower. Wave frequency response, which normally contributes most to fatigue, was not particularly influenced by mooring line modellig. Nevertheless, an improved model should include mooring line damping and coupling effects.

*marit.irene.kvittem@ntnu.no

Dynamic analysis of floating wind turbines during pitch actuator fault, grid loss, and shutdown

Erin E. Bachynski*[2], Mahmoud Etemaddar[2], Marit I. Kvittem[1,2], Chenyu Luan[1,2] and Torgeir Moan[2]

[1] *NOWITECH, Norwegian University of Science and Technology, Trondheim, Norway*
[2] *CeSOS, Norwegian University of Science and Technology, Trondheim, Norway*

Published in Elsevier Energy Procedia, vol 35, p.210-222, 2013.

Abstract

Coupled non-linear aero-hydro-servo-elastic simulations of three types of floating wind turbines (spar, semi- submersible, and tension leg platform) are carried out for several fault cases over a range of environmental conditions based on correlated wind and wave data from the North Sea. Three particular fault scenarios are considered: 1) blade seize, where the pitch actuator of one blade is blocked, 2) blade seize, recognized by the controller and followed by shutdown (grid disconnection and aerodynamic braking), and 3) grid loss followed by shutdown. The platform motions and structural loads caused by fault events are compared to loads encountered during normal operation and during selected extreme weather conditions. Although the global motions and mooring line loads tend to be largest during storm conditions, selected platforms experience large pitch or yaw motions due to blade seize and shutdown. Imbalance loads due to blade seize can lead to particularly large loads on the blades and tower, and the shutdown process can impose relatively large edgewise blade loads.

*erin.bachynski@ntnu.no

Appendix C

Specifications for a semi-submersible wind turbine with active ballast system

Platform specifications

The WindFloat concept was chosen as inspiration for the floating platform described in this section, and the outer dimensions in [93] was kept, but since more detailed specifications than what is available was necessary, a different design with similar global characteristics was developed.

Environment

Depth 320 m. Seawater density 1025 $\frac{kg}{m^3}$.

Platform geometry

Table C.1: Platform geometry.

Number of columns	3
Column diameter	10.0 m
Column center to center	46.0 m
Main beam and pontoon diameter	2.0 m
Braces diameter	1.5 m
Operating draught	17.0 m
Airgap	10.0 m
Heave plate edge length	15.0 m
Turbine tower foundation above MSL	10.0 m
Pontoon vertical position	-15.0 m
Ballast tank bottom lower level	-13.0 m

Steel

Table C.2: Properties for steel components.

Density	7850 $\frac{kg}{m^3}$
Column plate thickness	30 mm
Main beam and pontoon diameter plate thickness	30 mm
Braces plate thickness	25 mm
Heave plate effective thickness	50 mm

Turbine

Table C.3: Turbine data for NREL 5MW with OC3 tower.

Total mass	599,718 kg
Global centre of gravity	(26.27 m,0.00 m, 64.13 m)
Hub height above MSL	90.0 m
Rated wind speed	11.2 $\frac{m}{s}$

Mooring

The lines have 60 m of chain on top, 30 tonnes, 3.8 m^3 clump weight between chain and polyester rope, 769.8 m of polyester rope in the middle and 232.58 m of chain at the bottom.

Table C.4: Fairlead and anchor line positions.

	x	y	z
Fairlead 1	31.56	0	-17
Fairlead 2	-15.78	-27.33	-17
Fairlead 3	-15.78	27.33	-17
Fairlead 4	31.56	0	-17
Anch 1	738.07	-706.51	-320
Anch 2	-721.76	-733.31	-320
Anch 3	-721.76	733.31	-320
Anch 4	738.07	706.51	-320

Ballast system

The WindFloat platform has an active ballast system to keep the turbine upright and thus maximise power output as the wind direction and intensity changes. This is done by pumping water ballast between the columns, and the system reacts in 20 minutes to significant permanent changes in the wind.

The ballast in the SSWT in these analyses was distributed to account for the asymmetric loading of the platform, i.e. the weight of the turbine and mooring system. Other loads that gives the platform a permanent tilt is the rotor thrust force and wind drag on the tower. The rotor torque gives a sideways tilt. Since the reaction time of the ballast system is long compared to other dynamic loads on the system, it was modelled as constant ballast. A new ballast distribution is calculated for every wind speed. The ballast distribution between column 1 and columns 2 and 3 is calculated from the thrust force and tower drag for constant wind velocity with a power law wind shear. The ballast distribution between column 2 and column 3 is calculated based on the rotor torque. Thus, mass distribution and restoring is updated for each environmental condition. Samples of masses and centre of gravity for different wind speed is presented in Table C.5.

Table C.5: Mass distribution for different wind speeds. Mass and centre of gravity is given for the whole column.

	Column 1		Column 2		Column 3	
Wind speed $(\frac{m}{s})$	Mass (kg)	z_{COG} (m)	Mass (kg)	z_{COG} (m)	Mass (kg)	z_{COG} (m)
0.0	749,418	-10.358	1400,128	-7.918	1400,128	-7.918
8.0	658,582	-10.439	1441,151	-7.715	1449,940	-7.671
11.2	579,217	-10.384	1476,078	-7.539	1494,378	-7.446
25.0	659,277	-10.439	1435,887	-7.741	1454,509	-7.648
49.0	652,823	-10.440	1448,425	-7.678	1448,425	-7.678

Mass, damping and restoring

Table C.6: Mass, damping and restoring data. Inertia and restoring are given for platform without turbine, ballasted for zero wind thrust.

Displacement	4810E6 kg
Mass	4619E6 kg
Centre of gravity	(-0.331 m, 0.0 m, 1.489 m)
Mass without turbine and mooring	4019E6 kg
Centre of gravity without turbine and mooring	(-4.300 m, 0.0 m, -7.857 m)
Radius of gyration Rxx	22.29 m
Radius of gyration Ryy	19.62 m
Radius of gyration Rzz	26.06 m
Radius of gyration Ryz	4.69 m
Hydrostatic stiffness Heave	2445E3 N
Hydrostatic stiffness Roll	749815E3 Nm
Hydrostatic stiffness Pitch	7548571E3 Nm

Viscous forces

The viscous forces on the slender elements of the platform are calculated by the Morison formula. The coefficients applied are listed in Table C.7.

Table C.7: Non-dimensional quadratic drag coefficients.

Component	Transverse C_d (-)	Longitudinal C_d (-)	C_m (-)
Columns	1.0	0.0	0.0
Mooring chain	2.4	1.15	1.0
Mooring polyester rope	1.6	0.0	1.0
Main beam and pontoons	1.0	0.0	1.0
Braces	1.0	0.0	1.0
Heave plates	7.5	0.0	0.0

Verification of multibody model

Traditional modelling of floater motion considers the complete platform as a rigid body (Figure C.1a). However, internal member forces of a statistically indeterminate structure can not be extracted from such an analysis. Thus, in order to get forces in the braces, the three columns of the platform were modelled as individual Simo bodies with potential theory forces, and the connecting braces were modelled as Riflex beam elements with Morison type forces (Figure C.1b).

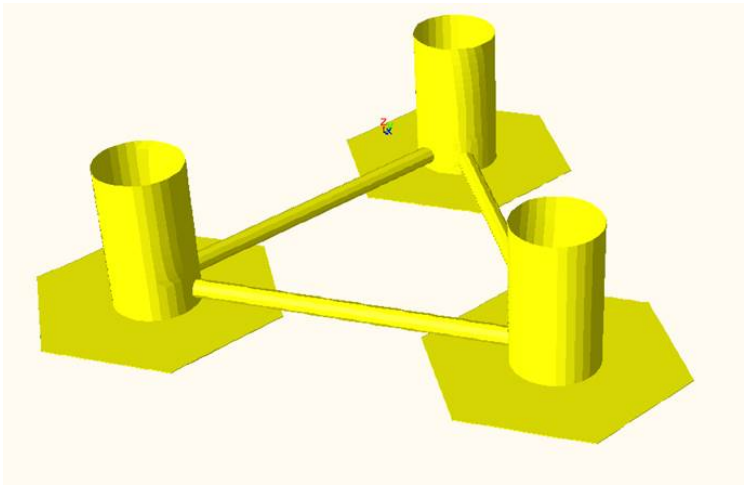

(a) Single body model

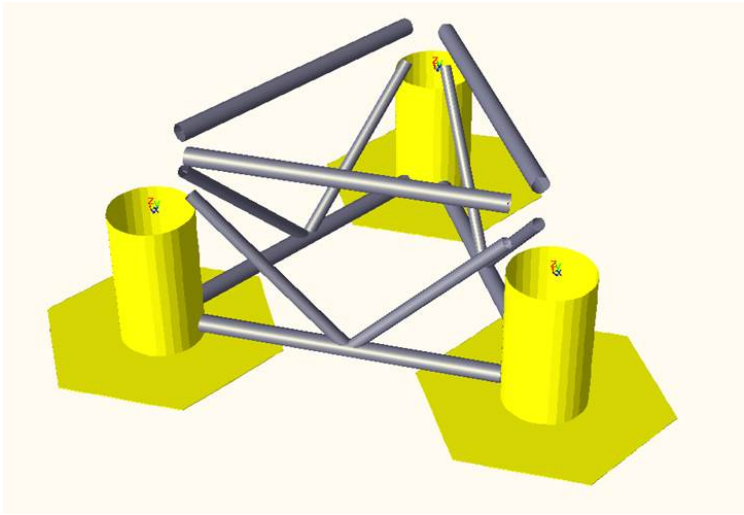

(b) Multi body model

Figure C.1: Illustration of the two different modelling strategies. The yellow parts are modelled as rigid bodies and the grey parts are modelled as flexible beam elements.

Through decay simulations, it was confirmed that both the single body and the multibody model gave the same natural periods for rigid body motion (Table C.8). Comparison was also made for response in regular waves.

Hydrodynamic interaction between the columns can be taken into account by applying a multi body analysis. However, some limitations on hydrodynamic interaction are inherent in the coupled Simo-Riflex software. This means that for one body, the effect of the presence of the other bodies was included in the force transfer functions and retardation functions, but the effect of motion of the other bodies was only accounted for in the force transfer functions, not in the retardation functions. Comparisons of added mass forces for the multibody and the single body models are shown in Figures C.2 and C.3.

Natural periods

Table C.8: Natural periods.

Mode	Single body T (s)	Multibody T (s)
Surge	107.0	107.0
Sway	124.8	124.8
Heave	19.9	19.9
Roll	35.6	35.6
Pitch	37.4	37.4
Yaw	68.5	68.5
Tower 1st	2.3	2.3

Added mass forces

Figures C.2 and C.3 show that the difference in added mass forces for three different modelling strategies are similar for an acceleration of 1 m/s^2. The modelling strategies are:

- One body with full hydrodynamic interaction.
- Three bodies with no interaction.
- Three bodies with interaction in the diagonal sub-matrices of the global added mass matrix.

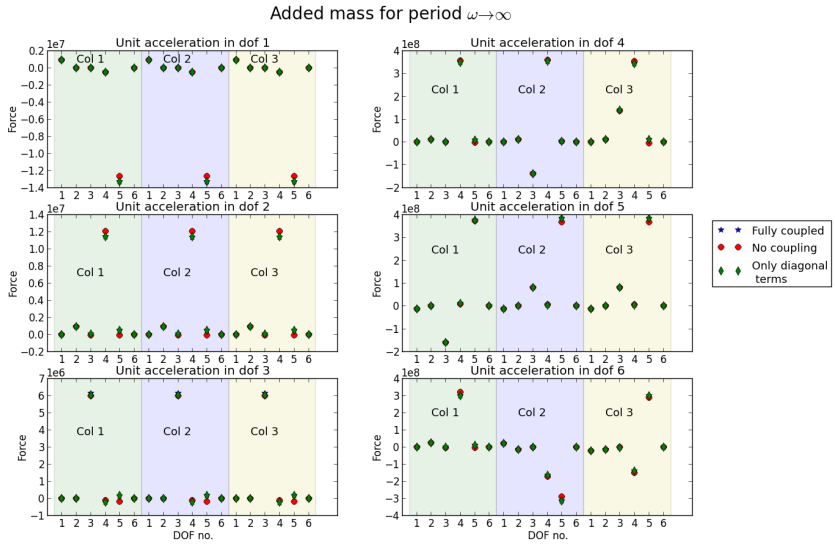

Figure C.2: Added mass forces due to 1 m/s^2 accelerations for small wave periods.

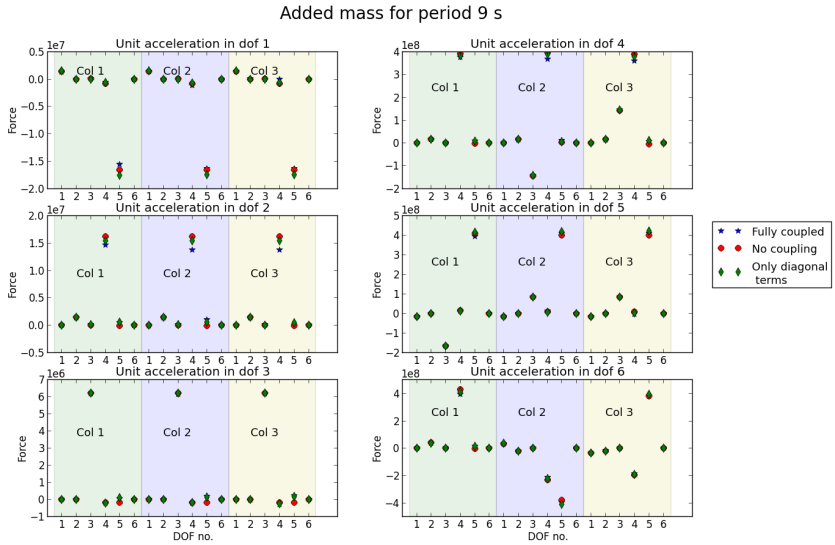

Figure C.3: Added mass forces due to 1 m/s^2 accelerations for wave period 9 s.

Response in regular waves

The response in regular waves was compared for the single body and the multibody model. The braces were not included in the panel model for the single body model, but in the comparison, this was compensated for by adding extra restoring in the single body model and by setting added mass of the braces in the multi body model to zero. Morison coefficients for other parts were as given in Table C.7.

Table C.9: Load cases

Wave period (s)	3.7	4.0	5.0	5.5	6.0	6.9	10.0	15.0	20.0	21.0
Wave height (m)	1.0	1.0	1.0	1.0	1.5	2.0	3.0	6.0	9.0	9.0

Figure C.4 shows response amplitude operators obtained by running regular wave analyses for different wave periods and heights, see Table C.9. The figure shows the mean of the response peaks normalized by the wave height. There is good agreement between the two models. Differences may be due to either interaction effects or that the choice of added mass coefficients for the pontoons do not match the potential solution.

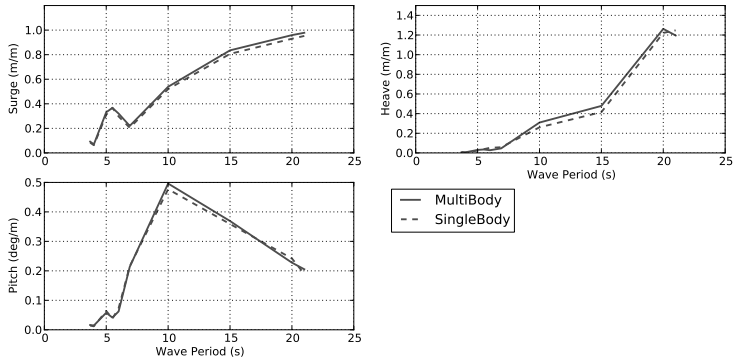

Figure C.4: Response amplitude operators from regular wave analysis of single body model and multi body model with flexible braces.

Appendix D

Analytical Morison force transfer functions

Force transfer functions including vertical dynamic pressure

A pure Morison type wave force model does not take into account the unbalanced vertical component of the dynamic pressure under a surface piercing column. In this note, transfer functions in heave, roll and pitch for Morison forces, including the effeect of dynamic pressure, for a three-column semi-submersible with heave plates are derived. Vertical forces do not contribute to surge, sway an yaw forces, thus they are not treated herein. Reference to the theory behind the derivations can be found in [16], and the x-y plane locations of the columns can be seen in Fig. D.1.

Table D.1: Nomenclature

g	Gravitational acceleration
ω	Wave frequency
t	Time
k	Wave number $k = \omega^2/g$
x,y,z	Position in global coordinate system
β	Wave heading angle
d	Draught, positive
R	Column radius
ρ	Sea water density of mass
C_a	Added mass coefficient
V	Displaced volume of column and heave plate (small)

Velocity potential on complex form with unit wave amplitude:

$$\phi = \frac{g}{\omega} i e^{i(\omega t + \theta)} \tag{D.1}$$

Where phase angle θ is:

$$\theta = -kx\cos\beta - ky\sin\beta \tag{D.2}$$

Particle accelerations in horizontal and vertical direction and dynamic pressure:

$$\begin{aligned} a_1 &= i\omega^2 e^{kz} e^{i(\omega t+\theta)} \\ a_3 &= -\omega^2 e^{kz} e^{i(\omega t+\theta)} \\ p_d &= \rho g e^{kz} e^{i(\omega t+\theta)} \end{aligned} \tag{D.3}$$

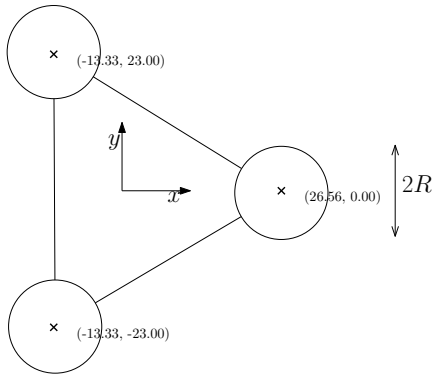

Figure D.1: Top view

Vertical wave forces

For a unit wave in $x = 0$:

$$\zeta(t) = e^{i\omega t} \tag{D.4}$$

Vertical inertial force, when assuming added mass can be calculated from the volume of a half sphere and force due to the acceleration of the platform is ignored:

$$F_3^{inertia} = (\rho V + C_a \rho \frac{2\pi}{3} R^3) a_3(z = -d) \tag{D.5}$$

which gives the following load amplitude:

$$F_3^{inertia^*} = -(\rho V + C_a \rho \frac{2\pi}{3} R^3)\omega^2 e^{-kd} \tag{D.6}$$

For the semi-submersible we have surface piercing columns, and the dynamic pressure acting on the bottom of these columns are not included in the Morison formulation. Hence the vertical force due to dynamic pressure must also be included in the Morison model. Vertical force due to dynamic pressure under columns can be found as follows:

$$F_3^{dynpres} = \pi R^2 p_d \tag{D.7}$$

which gives the following load amplitude:

$$F_3^{dynpres^*} = \rho g \pi R^2 e^{-kd} \tag{D.8}$$

Horizontal wave forces

The horizontal force is found by integrating the inertia term along the length of the column (z direction).

$$F_1^{inertia} = \rho \pi R^2 (1 + C_a) \int_{-d}^{0} a_1(z) dz \tag{D.9}$$

which gives the following load amplitude:

$$F_1^{inertia^*} = i \rho g \pi R^2 (1 + C_a)(1 - e^{-kd}) \tag{D.10}$$

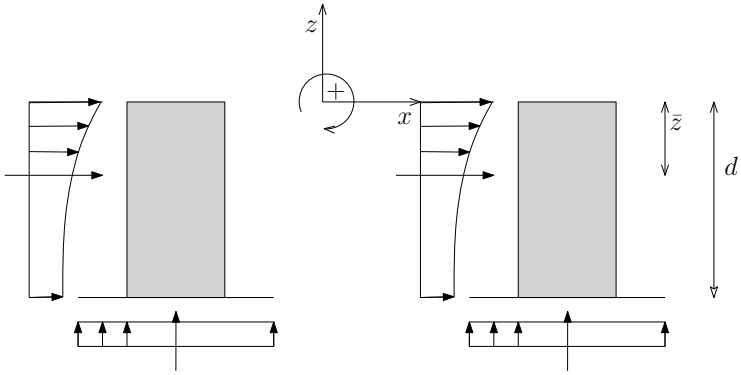

Figure D.2: Wave forces, showing pressure and resulting force.

Heave, roll and pitch forces

Total surge, heave and pitch forces due to wave with heading β is taken as the sum of the forces on each column. θ is a function of β and the position of each column.

$$
\begin{aligned}
F_1^* &= \left[\sum_1^{n=3} F_1^{inertia^*} e^{i\theta_n} \right] e^{i\omega t} \\
F_3^* &= \left[\sum_1^{n=3} (F_3^{inertia^*} + F_3^{dynpres^*}) e^{i\theta_n} \right] e^{i\omega t} \\
F_5^* &= \left[\sum_1^{n=3} F_1^{inertia^*} e^{i\theta_n} \bar{z} - \sum_1^{n=3} (F_3^{inertia^*} + F_3^{dynpres^*}) e^{i\theta_n} x_n \right] e^{i\omega t}
\end{aligned}
\tag{D.11}
$$

And the point of attac for the resultant horizontal force on a column, $\bar{z}$, is found by:

$$\bar{z} = \frac{1}{A}\int_{-d}^{0} e^{kz} z dz = \frac{1}{kA}\left(-\frac{1}{k} + e^{-kd}d + \frac{1}{k}e^{-kd}\right)$$
$$A = \int_{-d}^{0} e^{kz} dz = \frac{1}{k}\left(1 - e^{-kd}\right) \tag{D.12}$$

The forces obtained by Eq. D.11 are compared to a linear panel method solution in Figure D.3. A comparison of the forces from Eq. D.11 without the dynamic pressure term is shown in Fig. D.4. The importance of including the dynamic pressure in a pure Morison force model is obvious, in particular for heave forces.

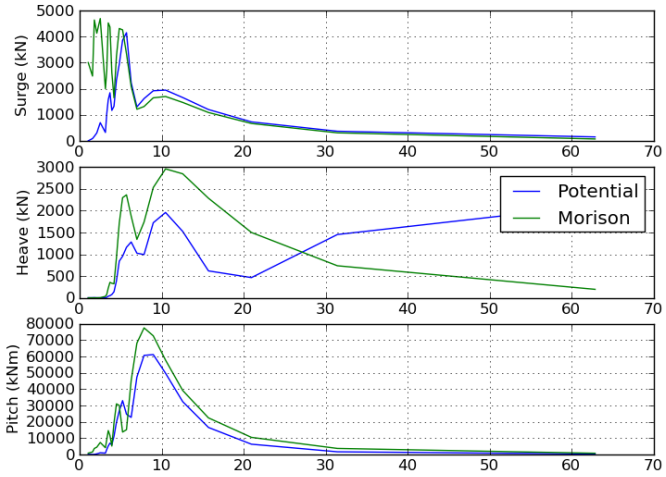

Figure D.3: Analytical Morison and potential theory transfer function excluding dynamic pressure.

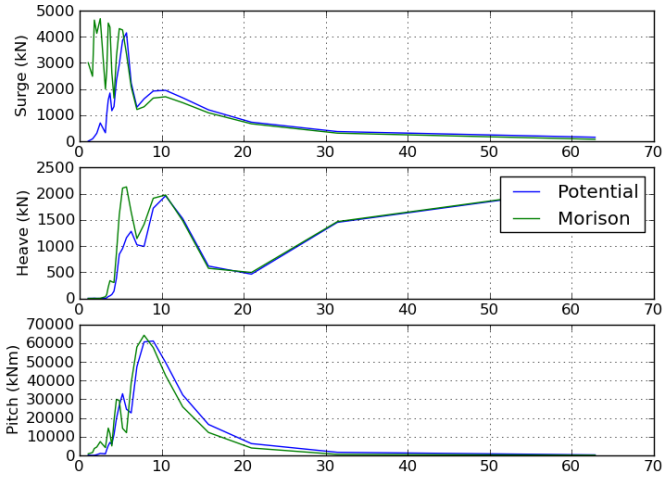

Figure D.4: Analytical Morison and potential theory transfer function including dynamic pressure.

Contribution to excitation force due to dynamic pressure

Since this is not included for slender elements in Simo, a force transfer function is derived analytically and applied to the Simo body to account for these forces. These transfer functions are derived below. Transfer function for roll motion (important for 90 deg wave heading) is also included.

$$
\begin{aligned}
F_3^* &= \sum_{1}^{n=3} F_3^{dynpres^*} e^{i\theta_n} \\
F_4^* &= \sum_{1}^{n=3} F_3^{dynpres^*} e^{i\theta_n} y_n \\
F_5^* &= -\sum_{1}^{n=3} F_3^{dynpres^*} e^{i\theta_n} x_n
\end{aligned}
\tag{D.13}
$$

Appendix E

Standards and guidelines on FLS design

Since no standard or guidelines for FWTs existed at the time the work with this thesis started, a review of existing guidelines that could form a basis for fatigue design of FWTs was performed. Relevant guidelines were considered to be standards and guidelines for floating offshore structures and bottom fixed offshore wind turbines. The current chapter gives an overview of statements about fatigue design from relevant design codes.

IEC 61400-3: Wind turbines - design requirements for offshore wind turbines

- The joint probability distribution shall be extended to include wind and wave directions if necessary
- Minimum bin sizes: 2 m/s for wind speed, 0.5 m for H_s, 0.5 s for T_p and 30° for wind and wave direction
- Design load cases are shown in Table 2.1

DNV-RP-F205: Global performance analysis of deepwater floating structures

- Frequency domain analysis is extensively used for fatigue analyses of floating units
- Coupled analysis (floater, mooring system, risers) needs to be performed to accurately predict system response in fatigue load cases

DNV-OS-C103/DNV-RP-C103: Column stabilised units

- Site specific environmental data shall be undertaken in the analyses
- Local detailed FEM analysis of critical connections should be performed to find appropriate SCFs

- If the semi-submersible classifies as a Y-unit in harsh environment, stochastic fatigue analysis has to be performed, otherwise, simplified fatigue analysis as described in [26] can be performed
- The stochastic analysis procedure is illustrated by Figure E.1
- For the stochastic analysis, a screening analysis using a simplified approach can be performed to identify critical structural details
- The FLS response analysis should cover the range of probability levels from 10^{-1} to 10^{-4}, for exceedance of stress ranges in the platform lifetime
- Short crested waves with a cos^4 spreading function should be applied in fatigue analyses
- Fatigue analyses shall include directional probability of the environmental data
- Where non-linear effects may be considered insignificant, frequency domain analysis are sufficient
- For details not sufficiently covered by DNV-RP-C203 [25], local FE analysis must be performed

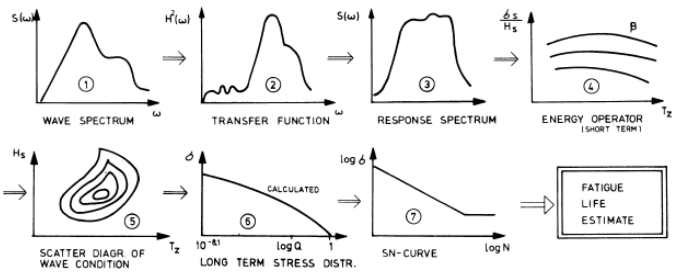

Figure E.1: Stochastic method for frequency domain stress analysis for oil and gas platforms [24].

NORSOK-N-003: Action and Action Effects

- Linear wave theory is relevant for fatigue analysis
- Difference frequency wave forces may be important for global motions
- Time domain methods are normally not required for fatigue analysis
- Simplified approaches to determine fatigue damage may be used if properly validated
- In addition to linear wave loads, sum-frequency wave loads, variable buoyancy, slamming, vortex shedding and mechanical vibration can contribute to fatigue

- Stress ranges for wide-banded or non-Gaussian histories should be determined by an appropriate cycle counting method, e.g. Rainflow counting
- A simplified method for establishing the relation between stress and wave height for fatigue analysis may be used (see [82])

Appendix F

Use of buoyancy compensating force in coupled Simo-Riflex models

This is a note prepared by the author on a modelling method for coupled Simo-Riflex, developed by ph.d. candidate Chenyu Luan and the author.

Table F.1: Nomenclature

$B = \rho g \forall$	Buoyancy force
$C(i,j)$	Restoring matrix term for indices (i,j)
COB	Centre of buoyancy
COG	Centre of gravity for rigid part of the floating body
$G = mg$	Weight of the rigid part of the floating body
g	Gravitational acceleration
m	Mass of the rigid part of the floating body
W	Weight of Riflex elements
x_b,y_b,z_b	Centre of buoyancy location in global coordinate system
x_g,y_g,z_g	Centre of gravity location in global coordinate system
ρ	Sea water mass density
$\forall$	Displaced volume of body

Buoyancy compensating force in Simo

Simo-Riflex is traditionally used for coupled analysis of platforms modelled as a rigid Simo body with flexible Riflex elements for mooring lines. Restoring matrix and force transfer functions are imported to Simo from pressure panel analyses in Wadam or Wamit.

A basic assumption in Simo is that the Simo floating body, without the weight of the Riflex elements, is neutrally buoyant. In reality it is the weight of the floating body *including* the

flexible elements that is neutrally buoyant. In Simo the assumption is that the effects of gravity and buoyancy in the equation of motion is taken into account through the restoring matrix. This is not the case for Riflex, which thought the finite element method includes gravity and buoyancy as nodal forces. This inconsistency is the reason why a so called *buoyancy compensating force*, acting in the centre of buoyancy, must be specified in Simo.

This is a suitable way of modelling when the mooring line weight is applied symmetrically and is much smaller than the platform weight. In the case of floating wind turbines, the platform (the rigid part of the model) is not always symmetrically loaded with the weight of the flexible elements (i.e. when the centre of buoyancy and the centre of gravity of the platform, *without* Riflex elements, do not have the same x or y coordinates). Using the method of the buoyancy compensating force will in this case create unphysical forces on the platform. How Simo interprets the forces acting on the floating body with buoyancy compensating force and asymmetrical load from riflex elements is illustrated in Fig. F.1.

As can be seen by Figure F.1, when modelling the traditional way in Simo, there will be a moment acting on the body, that in reality is cancelled out by the gravity force. This will give an incorrect static configuration and possibly problems with running the analysis. In the dynamic analysis, when the body moves, this additional force will give an unphysical restoring moment.

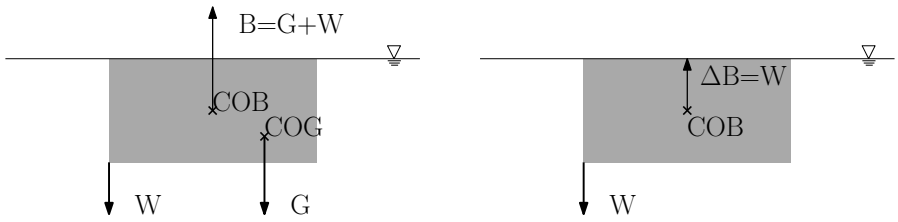

(a) Forces acting on the neutrally buoyant model.

(b) Simo interpretation where B=G.

Figure F.1: Discretisation of physical models with asymmetrical gravitational loads. Forces refer to global directions (not following the body).

Proposed procedure for floating wind turbine models

The following proposed modelling method eliminates the problem of the unphysical Simo body moment. It is also an attempt to have only "real" forces in the model, to make it more intuitive and less prone to modelling errors. In the proposed method, an upward specified force at the buoyancy center of the hull to represent the buoyancy, and a downward specified force to represent the gravity.

These specified forces will give restoring forces since their directions refer to global directions. However, this effect is already included in the restoring matrix that is obtained

from Wadam or Wamit. In order to avoid to count the restoring effect twice, this part of the restoring coefficients must be subtracted from the original restoring matrix, such that the restoring coefficients only include the water line area stiffness.

This method also works for models where the weight of Riflex elements is symmetric about the Simo body origin. Points 1) through 4b) serve as a general approach to modelling of floating wind turbines in coupled Simo-Riflex. There are also other modelling strategies, not mentioned here, that will give the same results.

1. Calculate mass, inertia and mass distribution for the floating wind turbine platform with and without the turbine
2. Do hydrodynamic panel method analysis in Wadam or Wamit with input describing the whole system of platform and turbine
3. Import output from Wadam/Wamit to Simo (Sima, DeepC or Simo inpmod)
4. In Simo sys-*.dat file, change the following to describe the platform *without* the turbine and mooring lines:
   (a) Mass and inertia
   (b) Centre of gravity
   (c) Add a specified force equal to the weight of the body (W) in the centre of gravity OR use the GRAVITY FORCE INCLUDED option in Simo
   (d) Add a specified force equal to the buoyancy (B) of the body in the centre of buoyancy
   (e) Subtract the part of the restoring terms (4,4), (5,5), (4,6) and (5,6) that are caused by G and B, see Eq. F.1. The new restoring coefficients could also be calculated in Wadam or Wamit by specifying the gravity centre and the buoyancy centre at the same point.

$$
\begin{aligned}
C(4,4)^{new} &= C(4,4)^{Wadam} - \rho g \forall z_b + m g z_g \\
C(5,5)^{new} &= C(5,5)^{Wadam} - \rho g \forall z_b + m g z_g \\
C(4,6)^{new} &= C(4,6)^{Wadam} + \rho g \forall x_b - m g x_g \\
C(5,6)^{new} &= C(5,6)^{Wadam} + \rho g \forall y_b - m g y_g
\end{aligned}
\tag{F.1}
$$

Previous PhD theses published at the Departement of Marine Technology (earlier: Faculty of Marine Technology) NORWEGIAN UNIVERSITY OF SCIENCE AND TECHNOLOGY

Report No.	Author	Title
	Kavlie, Dag	Optimization of Plane Elastic Grillages, 1967
	Hansen, Hans R.	Man-Machine Communication and Data-Storage Methods in Ship Structural Design, 1971
	Gisvold, Kaare M.	A Method for non-linear mixed -integer programming and its Application to Design Problems, 1971
	Lund, Sverre	Tanker Frame Optimalization by means of SUMT-Transformation and Behaviour Models, 1971
	Vinje, Tor	On Vibration of Spherical Shells Interacting with Fluid, 1972
	Lorentz, Jan D.	Tank Arrangement for Crude Oil Carriers in Accordance with the new Anti-Pollution Regulations, 1975
	Carlsen, Carl A.	Computer-Aided Design of Tanker Structures, 1975
	Larsen, Carl M.	Static and Dynamic Analysis of Offshore Pipelines during Installation, 1976
UR-79-01	Brigt Hatlestad, MK	The finite element method used in a fatigue evaluation of fixed offshore platforms. (Dr.Ing. Thesis)
UR-79-02	Erik Pettersen, MK	Analysis and design of cellular structures. (Dr.Ing. Thesis)
UR-79-03	Sverre Valsgård, MK	Finite difference and finite element methods applied to nonlinear analysis of plated structures. (Dr.Ing. Thesis)
UR-79-04	Nils T. Nordsve, MK	Finite element collapse analysis of structural members considering imperfections and stresses due to fabrication. (Dr.Ing. Thesis)
UR-79-05	Ivar J. Fylling, MK	Analysis of towline forces in ocean towing systems. (Dr.Ing. Thesis)
UR-80-06	Nils Sandsmark, MM	Analysis of Stationary and Transient Heat Conduction by the Use of the Finite Element Method. (Dr.Ing. Thesis)
UR-80-09	Sverre Haver, MK	Analysis of uncertainties related to the stochastic modeling of ocean waves. (Dr.Ing. Thesis)
UR-81-15	Odland, Jonas	On the Strength of welded Ring stiffened cylindrical Shells primarily subjected to axial Compression
UR-82-17	Engesvik, Knut	Analysis of Uncertainties in the fatigue Capacity of

		Welded Joints
UR-82-18	Rye, Henrik	Ocean wave groups
UR-83-30	Eide, Oddvar Inge	On Cumulative Fatigue Damage in Steel Welded Joints
UR-83-33	Mo, Olav	Stochastic Time Domain Analysis of Slender Offshore Structures
UR-83-34	Amdahl, Jørgen	Energy absorption in Ship-platform impacts
UR-84-37	Mørch, Morten	Motions and mooring forces of semi submersibles as determined by full-scale measurements and theoretical analysis
UR-84-38	Soares, C. Guedes	Probabilistic models for load effects in ship structures
UR-84-39	Aarsnes, Jan V.	Current forces on ships
UR-84-40	Czujko, Jerzy	Collapse Analysis of Plates subjected to Biaxial Compression and Lateral Load
UR-85-46	Alf G. Engseth, MK	Finite element collapse analysis of tubular steel offshore structures. (Dr.Ing. Thesis)
UR-86-47	Dengody Sheshappa, MP	A Computer Design Model for Optimizing Fishing Vessel Designs Based on Techno-Economic Analysis. (Dr.Ing. Thesis)
UR-86-48	Vidar Aanesland, MH	A Theoretical and Numerical Study of Ship Wave Resistance. (Dr.Ing. Thesis)
UR-86-49	Heinz-Joachim Wessel, MK	Fracture Mechanics Analysis of Crack Growth in Plate Girders. (Dr.Ing. Thesis)
UR-86-50	Jon Taby, MK	Ultimate and Post-ultimate Strength of Dented Tubular Members. (Dr.Ing. Thesis)
UR-86-51	Walter Lian, MH	A Numerical Study of Two-Dimensional Separated Flow Past Bluff Bodies at Moderate KC-Numbers. (Dr.Ing. Thesis)
UR-86-52	Bjørn Sortland, MH	Force Measurements in Oscillating Flow on Ship Sections and Circular Cylinders in a U-Tube Water Tank. (Dr.Ing. Thesis)
UR-86-53	Kurt Strand, MM	A System Dynamic Approach to One-dimensional Fluid Flow. (Dr.Ing. Thesis)
UR-86-54	Arne Edvin Løken, MH	Three Dimensional Second Order Hydrodynamic Effects on Ocean Structures in Waves. (Dr.Ing. Thesis)
UR-86-55	Sigurd Falch, MH	A Numerical Study of Slamming of Two-Dimensional Bodies. (Dr.Ing. Thesis)
UR-87-56	Arne Braathen, MH	Application of a Vortex Tracking Method to the Prediction of Roll Damping of a Two-Dimension Floating Body. (Dr.Ing. Thesis)

UR-87-57	Bernt Leira, MK	Gaussian Vector Processes for Reliability Analysis involving Wave-Induced Load Effects. (Dr.Ing. Thesis)
UR-87-58	Magnus Småvik, MM	Thermal Load and Process Characteristics in a Two-Stroke Diesel Engine with Thermal Barriers (in Norwegian). (Dr.Ing. Thesis)
MTA-88-59	Bernt Arild Bremdal, MP	An Investigation of Marine Installation Processes – A Knowledge - Based Planning Approach. (Dr.Ing. Thesis)
MTA-88-60	Xu Jun, MK	Non-linear Dynamic Analysis of Space-framed Offshore Structures. (Dr.Ing. Thesis)
MTA-89-61	Gang Miao, MH	Hydrodynamic Forces and Dynamic Responses of Circular Cylinders in Wave Zones. (Dr.Ing. Thesis)
MTA-89-62	Martin Greenhow, MH	Linear and Non-Linear Studies of Waves and Floating Bodies. Part I and Part II. (Dr.Techn. Thesis)
MTA-89-63	Chang Li, MH	Force Coefficients of Spheres and Cubes in Oscillatory Flow with and without Current. (Dr.Ing. Thesis
MTA-89-64	Hu Ying, MP	A Study of Marketing and Design in Development of Marine Transport Systems. (Dr.Ing. Thesis)
MTA-89-65	Arild Jæger, MH	Seakeeping, Dynamic Stability and Performance of a Wedge Shaped Planing Hull. (Dr.Ing. Thesis)
MTA-89-66	Chan Siu Hung, MM	The dynamic characteristics of tilting-pad bearings
MTA-89-67	Kim Wikstrøm, MP	Analysis av projekteringen for ett offshore projekt. (Licenciat-avhandling)
MTA-89-68	Jiao Guoyang, MK	Reliability Analysis of Crack Growth under Random Loading, considering Model Updating. (Dr.Ing. Thesis)
MTA-89-69	Arnt Olufsen, MK	Uncertainty and Reliability Analysis of Fixed Offshore Structures. (Dr.Ing. Thesis)
MTA-89-70	Wu Yu-Lin, MR	System Reliability Analyses of Offshore Structures using improved Truss and Beam Models. (Dr.Ing. Thesis)
MTA-90-71	Jan Roger Hoff, MH	Three-dimensional Green function of a vessel with forward speed in waves. (Dr.Ing. Thesis)
MTA-90-72	Rong Zhao, MH	Slow-Drift Motions of a Moored Two-Dimensional Body in Irregular Waves. (Dr.Ing. Thesis)
MTA-90-73	Atle Minsaas, MP	Economical Risk Analysis. (Dr.Ing. Thesis)
MTA-90-74	Knut-Aril Farnes, MK	Long-term Statistics of Response in Non-linear Marine Structures. (Dr.Ing. Thesis)
MTA-90-75	Torbjørn Sotberg, MK	Application of Reliability Methods for Safety Assessment of Submarine Pipelines. (Dr.Ing.

		Thesis)
MTA-90-76	Zeuthen, Steffen, MP	SEAMAID. A computational model of the design process in a constraint-based logic programming environment. An example from the offshore domain. (Dr.Ing. Thesis)
MTA-91-77	Haagensen, Sven, MM	Fuel Dependant Cyclic Variability in a Spark Ignition Engine - An Optical Approach. (Dr.Ing. Thesis)
MTA-91-78	Løland, Geir, MH	Current forces on and flow through fish farms. (Dr.Ing. Thesis)
MTA-91-79	Hoen, Christopher, MK	System Identification of Structures Excited by Stochastic Load Processes. (Dr.Ing. Thesis)
MTA-91-80	Haugen, Stein, MK	Probabilistic Evaluation of Frequency of Collision between Ships and Offshore Platforms. (Dr.Ing. Thesis)
MTA-91-81	Sødahl, Nils, MK	Methods for Design and Analysis of Flexible Risers. (Dr.Ing. Thesis)
MTA-91-82	Ormberg, Harald, MK	Non-linear Response Analysis of Floating Fish Farm Systems. (Dr.Ing. Thesis)
MTA-91-83	Marley, Mark J., MK	Time Variant Reliability under Fatigue Degradation. (Dr.Ing. Thesis)
MTA-91-84	Krokstad, Jørgen R., MH	Second-order Loads in Multidirectional Seas. (Dr.Ing. Thesis)
MTA-91-85	Molteberg, Gunnar A., MM	The Application of System Identification Techniques to Performance Monitoring of Four Stroke Turbocharged Diesel Engines. (Dr.Ing. Thesis)
MTA-92-86	Mørch, Hans Jørgen Bjelke, MH	Aspects of Hydrofoil Design: with Emphasis on Hydrofoil Interaction in Calm Water. (Dr.Ing. Thesis)
MTA-92-87	Chan Siu Hung, MM	Nonlinear Analysis of Rotordynamic Instabilities in Highspeed Turbomachinery. (Dr.Ing. Thesis)
MTA-92-88	Bessason, Bjarni, MK	Assessment of Earthquake Loading and Response of Seismically Isolated Bridges. (Dr.Ing. Thesis)
MTA-92-89	Langli, Geir, MP	Improving Operational Safety through exploitation of Design Knowledge - an investigation of offshore platform safety. (Dr.Ing. Thesis)
MTA-92-90	Sævik, Svein, MK	On Stresses and Fatigue in Flexible Pipes. (Dr.Ing. Thesis)
MTA-92-91	Ask, Tor Ø., MM	Ignition and Flame Growth in Lean Gas-Air Mixtures. An Experimental Study with a Schlieren System. (Dr.Ing. Thesis)
MTA-86-92	Hessen, Gunnar, MK	Fracture Mechanics Analysis of Stiffened Tubular Members. (Dr.Ing. Thesis)

MTA-93-93	Steinebach, Christian, MM	Knowledge Based Systems for Diagnosis of Rotating Machinery. (Dr.Ing. Thesis)
MTA-93-94	Dalane, Jan Inge, MK	System Reliability in Design and Maintenance of Fixed Offshore Structures. (Dr.Ing. Thesis)
MTA-93-95	Steen, Sverre, MH	Cobblestone Effect on SES. (Dr.Ing. Thesis)
MTA-93-96	Karunakaran, Daniel, MK	Nonlinear Dynamic Response and Reliability Analysis of Drag-dominated Offshore Platforms. (Dr.Ing. Thesis)
MTA-93-97	Hagen, Arnulf, MP	The Framework of a Design Process Language. (Dr.Ing. Thesis)
MTA-93-98	Nordrik, Rune, MM	Investigation of Spark Ignition and Autoignition in Methane and Air Using Computational Fluid Dynamics and Chemical Reaction Kinetics. A Numerical Study of Ignition Processes in Internal Combustion Engines. (Dr.Ing. Thesis)
MTA-94-99	Passano, Elizabeth, MK	Efficient Analysis of Nonlinear Slender Marine Structures. (Dr.Ing. Thesis)
MTA-94-100	Kvålsvold, Jan, MH	Hydroelastic Modelling of Wetdeck Slamming on Multihull Vessels. (Dr.Ing. Thesis)
MTA-94-102	Bech, Sidsel M., MK	Experimental and Numerical Determination of Stiffness and Strength of GRP/PVC Sandwich Structures. (Dr.Ing. Thesis)
MTA-95-103	Paulsen, Hallvard, MM	A Study of Transient Jet and Spray using a Schlieren Method and Digital Image Processing. (Dr.Ing. Thesis)
MTA-95-104	Hovde, Geir Olav, MK	Fatigue and Overload Reliability of Offshore Structural Systems, Considering the Effect of Inspection and Repair. (Dr.Ing. Thesis)
MTA-95-105	Wang, Xiaozhi, MK	Reliability Analysis of Production Ships with Emphasis on Load Combination and Ultimate Strength. (Dr.Ing. Thesis)
MTA-95-106	Ulstein, Tore, MH	Nonlinear Effects of a Flexible Stern Seal Bag on Cobblestone Oscillations of an SES. (Dr.Ing. Thesis)
MTA-95-107	Solaas, Frøydis, MH	Analytical and Numerical Studies of Sloshing in Tanks. (Dr.Ing. Thesis)
MTA-95-108	Hellan, Øyvind, MK	Nonlinear Pushover and Cyclic Analyses in Ultimate Limit State Design and Reassessment of Tubular Steel Offshore Structures. (Dr.Ing. Thesis)
MTA-95-109	Hermundstad, Ole A., MK	Theoretical and Experimental Hydroelastic Analysis of High Speed Vessels. (Dr.Ing. Thesis)
MTA-96-110	Bratland, Anne K., MH	Wave-Current Interaction Effects on Large-Volume Bodies in Water of Finite Depth. (Dr.Ing. Thesis)
MTA-96-111	Herfjord, Kjell, MH	A Study of Two-dimensional Separated Flow by a Combination of the Finite Element Method and

		Navier-Stokes Equations. (Dr.Ing. Thesis)
MTA-96-112	Æsøy, Vilmar, MM	Hot Surface Assisted Compression Ignition in a Direct Injection Natural Gas Engine. (Dr.Ing. Thesis)
MTA-96-113	Eknes, Monika L., MK	Escalation Scenarios Initiated by Gas Explosions on Offshore Installations. (Dr.Ing. Thesis)
MTA-96-114	Erikstad, Stein O., MP	A Decision Support Model for Preliminary Ship Design. (Dr.Ing. Thesis)
MTA-96-115	Pedersen, Egil, MH	A Nautical Study of Towed Marine Seismic Streamer Cable Configurations. (Dr.Ing. Thesis)
MTA-97-116	Moksnes, Paul O., MM	Modelling Two-Phase Thermo-Fluid Systems Using Bond Graphs. (Dr.Ing. Thesis)
MTA-97-117	Halse, Karl H., MK	On Vortex Shedding and Prediction of Vortex-Induced Vibrations of Circular Cylinders. (Dr.Ing. Thesis)
MTA-97-118	Igland, Ragnar T., MK	Reliability Analysis of Pipelines during Laying, considering Ultimate Strength under Combined Loads. (Dr.Ing. Thesis)
MTA-97-119	Pedersen, Hans-P., MP	Levendefiskteknologi for fiskefartøy. (Dr.Ing. Thesis)
MTA-98-120	Vikestad, Kyrre, MK	Multi-Frequency Response of a Cylinder Subjected to Vortex Shedding and Support Motions. (Dr.Ing. Thesis)
MTA-98-121	Azadi, Mohammad R. E., MK	Analysis of Static and Dynamic Pile-Soil-Jacket Behaviour. (Dr.Ing. Thesis)
MTA-98-122	Ulltang, Terje, MP	A Communication Model for Product Information. (Dr.Ing. Thesis)
MTA-98-123	Torbergsen, Erik, MM	Impeller/Diffuser Interaction Forces in Centrifugal Pumps. (Dr.Ing. Thesis)
MTA-98-124	Hansen, Edmond, MH	A Discrete Element Model to Study Marginal Ice Zone Dynamics and the Behaviour of Vessels Moored in Broken Ice. (Dr.Ing. Thesis)
MTA-98-125	Videiro, Paulo M., MK	Reliability Based Design of Marine Structures. (Dr.Ing. Thesis)
MTA-99-126	Mainçon, Philippe, MK	Fatigue Reliability of Long Welds Application to Titanium Risers. (Dr.Ing. Thesis)
MTA-99-127	Haugen, Elin M., MH	Hydroelastic Analysis of Slamming on Stiffened Plates with Application to Catamaran Wetdecks. (Dr.Ing. Thesis)
MTA-99-128	Langhelle, Nina K., MK	Experimental Validation and Calibration of Nonlinear Finite Element Models for Use in Design of Aluminium Structures Exposed to Fire. (Dr.Ing. Thesis)
MTA-99-	Berstad, Are J., MK	Calculation of Fatigue Damage in Ship Structures.

129		(Dr.Ing. Thesis)
MTA-99-130	Andersen, Trond M., MM	Short Term Maintenance Planning. (Dr.Ing. Thesis)
MTA-99-131	Tveiten, Bård Wathne, MK	Fatigue Assessment of Welded Aluminium Ship Details. (Dr.Ing. Thesis)
MTA-99-132	Søreide, Fredrik, MP	Applications of underwater technology in deep water archaeology. Principles and practice. (Dr.Ing. Thesis)
MTA-99-133	Tønnessen, Rune, MH	A Finite Element Method Applied to Unsteady Viscous Flow Around 2D Blunt Bodies With Sharp Corners. (Dr.Ing. Thesis)
MTA-99-134	Elvekrok, Dag R., MP	Engineering Integration in Field Development Projects in the Norwegian Oil and Gas Industry. The Supplier Management of Norne. (Dr.Ing. Thesis)
MTA-99-135	Fagerholt, Kjetil, MP	Optimeringsbaserte Metoder for Ruteplanlegging innen skipsfart. (Dr.Ing. Thesis)
MTA-99-136	Bysveen, Marie, MM	Visualization in Two Directions on a Dynamic Combustion Rig for Studies of Fuel Quality. (Dr.Ing. Thesis)
MTA-2000-137	Storteig, Eskild, MM	Dynamic characteristics and leakage performance of liquid annular seals in centrifugal pumps. (Dr.Ing. Thesis)
MTA-2000-138	Sagli, Gro, MK	Model uncertainty and simplified estimates of long term extremes of hull girder loads in ships. (Dr.Ing. Thesis)
MTA-2000-139	Tronstad, Harald, MK	Nonlinear analysis and design of cable net structures like fishing gear based on the finite element method. (Dr.Ing. Thesis)
MTA-2000-140	Kroneberg, André, MP	Innovation in shipping by using scenarios. (Dr.Ing. Thesis)
MTA-2000-141	Haslum, Herbjørn Alf, MH	Simplified methods applied to nonlinear motion of spar platforms. (Dr.Ing. Thesis)
MTA-2001-142	Samdal, Ole Johan, MM	Modelling of Degradation Mechanisms and Stressor Interaction on Static Mechanical Equipment Residual Lifetime. (Dr.Ing. Thesis)
MTA-2001-143	Baarholm, Rolf Jarle, MH	Theoretical and experimental studies of wave impact underneath decks of offshore platforms. (Dr.Ing. Thesis)
MTA-2001-144	Wang, Lihua, MK	Probabilistic Analysis of Nonlinear Wave-induced Loads on Ships. (Dr.Ing. Thesis)
MTA-2001-145	Kristensen, Odd H. Holt, MK	Ultimate Capacity of Aluminium Plates under Multiple Loads, Considering HAZ Properties. (Dr.Ing. Thesis)
MTA-2001-146	Greco, Marilena, MH	A Two-Dimensional Study of Green-Water Loading. (Dr.Ing. Thesis)

MTA-2001-147	Heggelund, Svein E., MK	Calculation of Global Design Loads and Load Effects in Large High Speed Catamarans. (Dr.Ing. Thesis)
MTA-2001-148	Babalola, Olusegun T., MK	Fatigue Strength of Titanium Risers – Defect Sensitivity. (Dr.Ing. Thesis)
MTA-2001-149	Mohammed, Abuu K., MK	Nonlinear Shell Finite Elements for Ultimate Strength and Collapse Analysis of Ship Structures. (Dr.Ing. Thesis)
MTA-2002-150	Holmedal, Lars E., MH	Wave-current interactions in the vicinity of the sea bed. (Dr.Ing. Thesis)
MTA-2002-151	Rognebakke, Olav F., MH	Sloshing in rectangular tanks and interaction with ship motions. (Dr.Ing. Thesis)
MTA-2002-152	Lader, Pål Furset, MH	Geometry and Kinematics of Breaking Waves. (Dr.Ing. Thesis)
MTA-2002-153	Yang, Qinzheng, MH	Wash and wave resistance of ships in finite water depth. (Dr.Ing. Thesis)
MTA-2002-154	Melhus, Øyvin, MM	Utilization of VOC in Diesel Engines. Ignition and combustion of VOC released by crude oil tankers. (Dr.Ing. Thesis)
MTA-2002-155	Ronæss, Marit, MH	Wave Induced Motions of Two Ships Advancing on Parallel Course. (Dr.Ing. Thesis)
MTA-2002-156	Økland, Ole D., MK	Numerical and experimental investigation of whipping in twin hull vessels exposed to severe wet deck slamming. (Dr.Ing. Thesis)
MTA-2002-157	Ge, Chunhua, MK	Global Hydroelastic Response of Catamarans due to Wet Deck Slamming. (Dr.Ing. Thesis)
MTA-2002-158	Byklum, Eirik, MK	Nonlinear Shell Finite Elements for Ultimate Strength and Collapse Analysis of Ship Structures. (Dr.Ing. Thesis)
IMT-2003-1	Chen, Haibo, MK	Probabilistic Evaluation of FPSO-Tanker Collision in Tandem Offloading Operation. (Dr.Ing. Thesis)
IMT-2003-2	Skaugset, Kjetil Bjørn, MK	On the Suppression of Vortex Induced Vibrations of Circular Cylinders by Radial Water Jets. (Dr.Ing. Thesis)
IMT-2003-3	Chezhian, Muthu	Three-Dimensional Analysis of Slamming. (Dr.Ing. Thesis)
IMT-2003-4	Buhaug, Øyvind	Deposit Formation on Cylinder Liner Surfaces in Medium Speed Engines. (Dr.Ing. Thesis)
IMT-2003-5	Tregde, Vidar	Aspects of Ship Design: Optimization of Aft Hull with Inverse Geometry Design. (Dr.Ing. Thesis)
IMT-2003-6	Wist, Hanne Therese	Statistical Properties of Successive Ocean Wave Parameters. (Dr.Ing. Thesis)

IMT-2004-7	Ransau, Samuel	Numerical Methods for Flows with Evolving Interfaces. (Dr.Ing. Thesis)
IMT-2004-8	Soma, Torkel	Blue-Chip or Sub-Standard. A data interrogation approach of identity safety characteristics of shipping organization. (Dr.Ing. Thesis)
IMT-2004-9	Ersdal, Svein	An experimental study of hydrodynamic forces on cylinders and cables in near axial flow. (Dr.Ing. Thesis)
IMT-2005-10	Brodtkorb, Per Andreas	The Probability of Occurrence of Dangerous Wave Situations at Sea. (Dr.Ing. Thesis)
IMT-2005-11	Yttervik, Rune	Ocean current variability in relation to offshore engineering. (Dr.Ing. Thesis)
IMT-2005-12	Fredheim, Arne	Current Forces on Net-Structures. (Dr.Ing. Thesis)
IMT-2005-13	Heggernes, Kjetil	Flow around marine structures. (Dr.Ing. Thesis
IMT-2005-14	Fouques, Sebastien	Lagrangian Modelling of Ocean Surface Waves and Synthetic Aperture Radar Wave Measurements. (Dr.Ing. Thesis)
IMT-2006-15	Holm, Håvard	Numerical calculation of viscous free surface flow around marine structures. (Dr.Ing. Thesis)
IMT-2006-16	Bjørheim, Lars G.	Failure Assessment of Long Through Thickness Fatigue Cracks in Ship Hulls. (Dr.Ing. Thesis)
IMT-2006-17	Hansson, Lisbeth	Safety Management for Prevention of Occupational Accidents. (Dr.Ing. Thesis)
IMT-2006-18	Zhu, Xinying	Application of the CIP Method to Strongly Nonlinear Wave-Body Interaction Problems. (Dr.Ing. Thesis)
IMT-2006-19	Reite, Karl Johan	Modelling and Control of Trawl Systems. (Dr.Ing. Thesis)
IMT-2006-20	Smogeli, Øyvind Notland	Control of Marine Propellers. From Normal to Extreme Conditions. (Dr.Ing. Thesis)
IMT-2007-21	Storhaug, Gaute	Experimental Investigation of Wave Induced Vibrations and Their Effect on the Fatigue Loading of Ships. (Dr.Ing. Thesis)
IMT-2007-22	Sun, Hui	A Boundary Element Method Applied to Strongly Nonlinear Wave-Body Interaction Problems. (PhD Thesis, CeSOS)
IMT-2007-23	Rustad, Anne Marthine	Modelling and Control of Top Tensioned Risers. (PhD Thesis, CeSOS)
IMT-2007-24	Johansen, Vegar	Modelling flexible slender system for real-time simulations and control applications
IMT-2007-25	Wroldsen, Anders Sunde	Modelling and control of tensegrity structures. (PhD Thesis, CeSOS)
IMT-	Aronsen, Kristoffer Høye	An experimental investigation of in-line and

2007-26		combined inline and cross flow vortex induced vibrations. (Dr. avhandling, IMT)
IMT-2007-27	Gao, Zhen	Stochastic Response Analysis of Mooring Systems with Emphasis on Frequency-domain Analysis of Fatigue due to Wide-band Response Processes (PhD Thesis, CeSOS)
IMT-2007-28	Thorstensen, Tom Anders	Lifetime Profit Modelling of Ageing Systems Utilizing Information about Technical Condition. (Dr.ing. thesis, IMT)
IMT-2008-29	Berntsen, Per Ivar B.	Structural Reliability Based Position Mooring. (PhD-Thesis, IMT)
IMT-2008-30	Ye, Naiquan	Fatigue Assessment of Aluminium Welded Box-stiffener Joints in Ships (Dr.ing. thesis, IMT)
IMT-2008-31	Radan, Damir	Integrated Control of Marine Electrical Power Systems. (PhD-Thesis, IMT)
IMT-2008-32	Thomassen, Paul	Methods for Dynamic Response Analysis and Fatigue Life Estimation of Floating Fish Cages. (Dr.ing. thesis, IMT)
IMT-2008-33	Pákozdi, Csaba	A Smoothed Particle Hydrodynamics Study of Two-dimensional Nonlinear Sloshing in Rectangular Tanks. (Dr.ing.thesis, IMT/ CeSOS)
IMT-2007-34	Grytøyr, Guttorm	A Higher-Order Boundary Element Method and Applications to Marine Hydrodynamics. (Dr.ing.thesis, IMT)
IMT-2008-35	Drummen, Ingo	Experimental and Numerical Investigation of Nonlinear Wave-Induced Load Effects in Containerships considering Hydroelasticity. (PhD thesis, CeSOS)
IMT-2008-36	Skejic, Renato	Maneuvering and Seakeeping of a Singel Ship and of Two Ships in Interaction. (PhD-Thesis, CeSOS)
IMT-2008-37	Harlem, Alf	An Age-Based Replacement Model for Repairable Systems with Attention to High-Speed Marine Diesel Engines. (PhD-Thesis, IMT)
IMT-2008-38	Alsos, Hagbart S.	Ship Grounding. Analysis of Ductile Fracture, Bottom Damage and Hull Girder Response. (PhD-thesis, IMT)
IMT-2008-39	Graczyk, Mateusz	Experimental Investigation of Sloshing Loading and Load Effects in Membrane LNG Tanks Subjected to Random Excitation. (PhD-thesis, CeSOS)
IMT-2008-40	Taghipour, Reza	Efficient Prediction of Dynamic Response for Flexible amd Multi-body Marine Structures. (PhD-thesis, CeSOS)
IMT-2008-41	Ruth, Eivind	Propulsion control and thrust allocation on marine vessels. (PhD thesis, CeSOS)
IMT-2008-42	Nystad, Bent Helge	Technical Condition Indexes and Remaining Useful Life of Aggregated Systems. PhD thesis, IMT

IMT-2008-43	Soni, Prashant Kumar	Hydrodynamic Coefficients for Vortex Induced Vibrations of Flexible Beams, PhD thesis, CeSOS
IMT-2009-43	Amlashi, Hadi K.K.	Ultimate Strength and Reliability-based Design of Ship Hulls with Emphasis on Combined Global and Local Loads. PhD Thesis, IMT
IMT-2009-44	Pedersen, Tom Arne	Bond Graph Modelling of Marine Power Systems. PhD Thesis, IMT
IMT-2009-45	Kristiansen, Trygve	Two-Dimensional Numerical and Experimental Studies of Piston-Mode Resonance. PhD-Thesis, CeSOS
IMT-2009-46	Ong, Muk Chen	Applications of a Standard High Reynolds Number Model and a Stochastic Scour Prediction Model for Marine Structures. PhD-thesis, IMT
IMT-2009-47	Hong, Lin	Simplified Analysis and Design of Ships subjected to Collision and Grounding. PhD-thesis, IMT
IMT-2009-48	Koushan, Kamran	Vortex Induced Vibrations of Free Span Pipelines, PhD thesis, IMT
IMT-2009-49	Korsvik, Jarl Eirik	Heuristic Methods for Ship Routing and Scheduling. PhD-thesis, IMT
IMT-2009-50	Lee, Jihoon	Experimental Investigation and Numerical in Analyzing the Ocean Current Displacement of Longlines. Ph.d.-Thesis, IMT.
IMT-2009-51	Vestbøstad, Tone Gran	A Numerical Study of Wave-in-Deck Impact usin a Two-Dimensional Constrained Interpolation Profile Method, Ph.d.thesis, CeSOS.
IMT-2009-52	Bruun, Kristine	Bond Graph Modelling of Fuel Cells for Marine Power Plants. Ph.d.-thesis, IMT
IMT 2009-53	Holstad, Anders	Numerical Investigation of Turbulence in a Sekwed Three-Dimensional Channel Flow, Ph.d.-thesis, IMT.
IMT 2009-54	Ayala-Uraga, Efren	Reliability-Based Assessment of Deteriorating Ship-shaped Offshore Structures, Ph.d.-thesis, IMT
IMT 2009-55	Kong, Xiangjun	A Numerical Study of a Damaged Ship in Beam Sea Waves. Ph.d.-thesis, IMT/CeSOS.
IMT 2010-56	Kristiansen, David	Wave Induced Effects on Floaters of Aquaculture Plants, Ph.d.-thesis, CeSOS.
IMT 2010-57	Ludvigsen, Martin	An ROV-Toolbox for Optical and Acoustic Scientific Seabed Investigation. Ph.d.-thesis IMT.
IMT 2010-58	Hals, Jørgen	Modelling and Phase Control of Wave-Energy Converters. Ph.d.thesis, CeSOS.
IMT 2010- 59	Shu, Zhi	Uncertainty Assessment of Wave Loads and Ultimate Strength of Tankers and Bulk Carriers in a

		Reliability Framework. Ph.d. Thesis, IMT/ CeSOS
IMT 2010-60	Shao, Yanlin	Numerical Potential-Flow Studies on Weakly-Nonlinear Wave-Body Interactions with/without Small Forward Speed, Ph.d.thesis,CeSOS.
IMT 2010-61	Califano, Andrea	Dynamic Loads on Marine Propellers due to Intermittent Ventilation. Ph.d.thesis, IMT.
IMT 2010-62	El Khoury, George	Numerical Simulations of Massively Separated Turbulent Flows, Ph.d.-thesis, IMT
IMT 2010-63	Seim, Knut Sponheim	Mixing Process in Dense Overflows with Emphasis on the Faroe Bank Channel Overflow. Ph.d.thesis, IMT
IMT 2010-64	Jia, Huirong	Structural Analysis of Intect and Damaged Ships in a Collission Risk Analysis Perspective. Ph.d.thesis CeSoS.
IMT 2010-65	Jiao, Linlin	Wave-Induced Effects on a Pontoon-type Very Large Floating Structures (VLFS). Ph.D.-thesis, CeSOS.
IMT 2010-66	Abrahamsen, Bjørn Christian	Sloshing Induced Tank Roof with Entrapped Air Pocket. Ph.d.thesis, CeSOS.
IMT 2011-67	Karimirad, Madjid	Stochastic Dynamic Response Analysis of Spar-Type Wind Turbines with Catenary or Taut Mooring Systems. Ph.d.-thesis, CeSOS.
IMT - 2011-68	Erlend Meland	Condition Monitoring of Safety Critical Valves. Ph.d.-thesis, IMT.
IMT – 2011-69	Yang, Limin	Stochastic Dynamic System Analysis of Wave Energy Converter with Hydraulic Power Take-Off, with Particular Reference to Wear Damage Analysis, Ph.d. Thesis, CeSOS.
IMT – 2011-70	Visscher, Jan	Application of Particla Image Velocimetry on Turbulent Marine Flows, Ph.d.Thesis, IMT.
IMT – 2011-71	Su, Biao	Numerical Predictions of Global and Local Ice Loads on Ships. Ph.d.Thesis, CeSOS.
IMT – 2011-72	Liu, Zhenhui	Analytical and Numerical Analysis of Iceberg Collision with Ship Structures. Ph.d.Thesis, IMT.
IMT – 2011-73	Aarsæther, Karl Gunnar	Modeling and Analysis of Ship Traffic by Observation and Numerical Simulation. Ph.d.Thesis, IMT.
Imt – 2011-74	Wu, Jie	Hydrodynamic Force Identification from Stochastic Vortex Induced Vibration Experiments with Slender Beams. Ph.d.Thesis, IMT.
Imt – 2011-75	Amini, Hamid	Azimuth Propulsors in Off-design Conditions. Ph.d.Thesis, IMT.
IMT – 2011-76	Nguyen, Tan-Hoi	Toward a System of Real-Time Prediction and Monitoring of Bottom Damage Conditions During

		Ship Grounding. Ph.d.thesis, IMT.
IMT-2011-77	Tavakoli, Mohammad T.	Assessment of Oil Spill in Ship Collision and Grounding, Ph.d.thesis, IMT.
IMT-2011-78	Guo, Bingjie	Numerical and Experimental Investigation of Added Resistance in Waves. Ph.d.Thesis, IMT.
IMT-2011-79	Chen, Qiaofeng	Ultimate Strength of Aluminium Panels, considering HAZ Effects, IMT
IMT-2012-80	Kota, Ravikiran S.	Wave Loads on Decks of Offshore Structures in Random Seas, CeSOS.
IMT-2012-81	Sten, Ronny	Dynamic Simulation of Deep Water Drilling Risers with Heave Compensating System, IMT.
IMT-2012-82	Berle, Øyvind	Risk and resilience in global maritime supply chains, IMT.
IMT-2012-83	Fang, Shaoji	Fault Tolerant Position Mooring Control Based on Structural Reliability, CeSOS.
IMT-2012-84	You, Jikun	Numerical studies on wave forces and moored ship motions in intermediate and shallow water, CeSOS.
IMT-2012-85	Xiang ,Xu	Maneuvering of two interacting ships in waves, CeSOS
IMT-2012-86	Dong, Wenbin	Time-domain fatigue response and reliability analysis of offshore wind turbines with emphasis on welded tubular joints and gear components, CeSOS
IMT-2012-87	Zhu, Suji	Investigation of Wave-Induced Nonlinear Load Effects in Open Ships considering Hull Girder Vibrations in Bending and Torsion, CeSOS
IMT-2012-88	Zhou, Li	Numerical and Experimental Investigation of Station-keeping in Level Ice, CeSOS
IMT-2012-90	Ushakov, Sergey	Particulate matter emission characteristics from diesel enignes operating on conventional and alternative marine fuels, IMT
IMT-2013-1	Yin, Decao	Experimental and Numerical Analysis of Combined In-line and Cross-flow Vortex Induced Vibrations, CeSOS
IMT-2013-2	Kurniawan, Adi	Modelling and geometry optimisation of wave energy converters, CeSOS
IMT-2013-3	Al Ryati, Nabil	Technical condition indexes doe auxiliary marine diesel engines, IMT
IMT-2013-4	Firoozkoohi, Reza	Experimental, numerical and analytical investigation of the effect of screens on sloshing, CeSOS
IMT-2013-5	Ommani, Babak	Potential-Flow Predictions of a Semi-Displacement Vessel Including Applications to Calm Water Broaching, CeSOS

IMT-2013-6	Xing, Yihan	Modelling and analysis of the gearbox in a floating spar-type wind turbine, CeSOS
IMT-7-2013	Balland, Océane	Optimization models for reducing air emissions from ships, IMT
IMT-8-2013	Yang, Dan	Transitional wake flow behind an inclined flat plate----Computation and analysis, IMT
IMT-9-2013	Abdillah, Suyuthi	Prediction of Extreme Loads and Fatigue Damage for a Ship Hull due to Ice Action, IMT
IMT-10-2013	Ramìrez, Pedro Agustìn Pèrez	Ageing management and life extension of technical systems- Concepts and methods applied to oil and gas facilities, IMT
IMT-11-2013	Chuang, Zhenju	Experimental and Numerical Investigation of Speed Loss due to Seakeeping and Maneuvering. IMT
IMT-12-2013	Etemaddar, Mahmoud	Load and Response Analysis of Wind Turbines under Atmospheric Icing and Controller System Faults with Emphasis on Spar Type Floating Wind Turbines, IMT
IMT-13-2013	Lindstad, Haakon	Strategies and measures for reducing maritime CO2 emissons, IMT
IMT-14-2013	Haris, Sabril	Damage interaction analysis of ship collisions, IMT
IMT-15-2013	Shainee, Mohamed	Conceptual Design, Numerical and Experimental Investigation of a SPM Cage Concept for Offshore Mariculture, IMT
IMT-16-2013	Gansel, Lars	Flow past porous cylinders and effects of biofouling and fish behavior on the flow in and around Atlantic salmon net cages, IMT
IMT-17-2013	Gaspar, Henrique	Handling Aspects of Complexity in Conceptual Ship Design, IMT
IMT-18-2013	Thys, Maxime	Theoretical and Experimental Investigation of a Free Running Fishing Vessel at Small Frequency of Encounter, CeSOS
IMT-19-2013	Aglen, Ida	VIV in Free Spanning Pipelines, CeSOS
IMT-1-2014	Song, An	Theoretical and experimental studies of wave diffraction and radiation loads on a horizontally submerged perforated plate, CeSOS
IMT-2-2014	Rogne, Øyvind Ygre	Numerical and Experimental Investigation of a Hinged 5-body Wave Energy Converter, CeSOS
IMT-3-2014	Dai, Lijuan	Safe and efficient operation and maintenance of offshore wind farms ,IMT
IMT-4-2014	Bachynski, Erin Elizabeth	Design and Dynamic Analysis of Tension Leg Platform Wind Turbines, CeSOS
IMT-5-2014	Wang, Jingbo	Water Entry of Freefall Wedged – Wedge motions

		and Cavity Dynamics, CeSOS
IMT-6-2014	Kim, Ekaterina	Experimental and numerical studies related to the coupled behavior of ice mass and steel structures during accidental collisions, IMT
IMT-7-2014	Tan, Xiang	Numerical investigation of ship's continuous- mode icebreaking in leverl ice, CeSOS
IMT-8-2014	Muliawan, Made Jaya	Design and Analysis of Combined Floating Wave and Wind Power Facilities, with Emphasis on Extreme Load Effects of the Mooring System, CeSOS
IMT-9-2014	Jiang, Zhiyu	Long-term response analysis of wind turbines with an emphasis on fault and shutdown conditions, IMT
IMT-10-2014	Dukan, Fredrik	ROV Motion Control Systems, IMT
IMT-11-2014	Grimsmo, Nils I.	Dynamic simulations of hydraulic cylinder for heave compensation of deep water drilling risers, IMT
IMT-12-2014	Kvittem, Marit I.	Modelling and response analysis for fatigue design of a semisubmersible wind turbine, CeSOS